# On the Design and Performance Analysis of mmWave-enabled Next generation of Wireless Networks

by

Zeeshan SATTAR

MANUSCRIPT-BASED THESIS PRESENTED TO ÉCOLE DE
TECHNOLOGIE SUPÉRIEURE IN PARTIAL FULFILLMENT FOR THE
DEGREE OF DOCTOR OF PHILOSOPHY
Ph.D.

MONTREAL, OCTOBER 29, 2020

ÉCOLE DE TECHNOLOGIE SUPÉRIEURE
UNIVERSITÉ DU QUÉBEC

## BOARD OF EXAMINERS

### THIS THESIS HAS BEEN EVALUATED

### BY THE FOLLOWING BOARD OF EXAMINERS

Mr. Georges Kaddoum, Thesis supervisor
Department of Electrical Engineering, École de Technologie Supérieure

Mr. Naïm Batani, Co-supervisor
Department of Electrical Engineering, École de Technologie Supérieure

Mr. Adel Francis, President of the board of examiners
Department of Construction Engineering, École de Technologie Supérieure

Mr. Dominic Deslandes, Member of the jury
Department of Electrical Engineering, École de Technologie Supérieure

Mr. Salama Ikki, External examiner
Department of Electrical Engineering, Lakehead University

### THIS THESIS  WAS PRESENTED AND DEFENDED

### IN THE PRESENCE OF A BOARD OF EXAMINERS AND THE PUBLIC

### ON "OCTOBER 26, 2020"

### AT ÉCOLE DE TECHNOLOGIE SUPÉRIEURE

## ACKNOWLEDGEMENTS

# À propos de la conception et de l'analyse des performances de la prochaine génération de réseaux sans fil compatibles à ondes millimétriques

Zeeshan SATTAR

## RÉSUMÉ

La prochaine génération de systèmes de communication (5G) à ondes millimétriques est en train de voir le jour. Comme pour toute nouvelle technologie, il y a inévitablement des problèmes de démarrage et des obstacles à surmonter avant de trouver sa véritable valeur commerciale. La technologie des ondes millimétriques a eu sa part de cynisme ces dernières années, avec des questions sur son efficacité pour la transmission sur de longues distances, sa capacité à traverser les murs, et même si la pluie ou la main d'un utilisateur pouvait bloquer le signal.

Ces questions sont valables, mais la plupart d'entre elles ont été abordées avec des solutions innovantes ces dernières années. En outre, les ondes millimétriques et la 5G sont souvent utilisées comme synonymes, mais il existe des différences essentielles entre les deux. Le spectre des ondes millimétriques n'est qu'une partie de la bande de fréquences disponible pour les futurs réseaux 5G. Les fréquences micro-ondes typiques ou le spectre inférieur à sous-6GHz feront également partie de la norme. Et la coexistence de ces deux spectres offrira, entre autres, une meilleure couverture et de meilleurs débits de données aux clients.

Puisque la technologie des ondes millimétriques est presque prête à faire ses débuts publics sur la scène du monde technologique commercial, le thème principal de notre projet de recherche est centré sur la conception et l'analyse des performances des principaux outils de la 5G, tels que les communications à ondes millimétriques, les systèmes massifs à entrées multiples et sorties multiples, et les réseaux hétérogènes. Plus spécifiquement, cette thèse se concentre sur (i) la coexistence des ondes millimétriques et des fréquences inférieures à sous-6 GHz dans un réseau hétérogène et (ii) les systèmes de communication à large bande et à bande ultra-large rendus possibles par les ondes millimétriques.

Dans ce contexte, le deuxième chapitre de cette thèse présente une analyse très détaillée et un modèle de simulation d'un réseau hétérogène à deux-tiers en semi-duplex utilisant différentes bandes de fréquences (c'est-à-dire sous-6GHz et ondes millimétriques). Les outils de la géométrie stochastique sont utilisés pour modéliser un environnement où les équipements des utilisateurs ont les moyens de choisir différentes stations de base pour les transmissions en liaison montante et descendante, appelées accès sans fil découplé. Les principales mesures de performance, telles que la probabilité d'association des équipements des utilisateurs, les distributions de distance entre les équipements des utilisateurs et leurs stations de base marquées, et l'efficacité spectrale sont analysées et évaluées pour les différents scénarios de déploiement pragmatiques.

Le troisième chapitre de cette thèse présente une analyse des performances d'un réseau hétérogène à deux tiers en duplex intégral avec accès découplé utilisant différentes bandes de fréquences (c'est-à-dire sous-6GHz et ondes millimétriques). La nouveauté du modèle

analytique dérivé est qu'il prend en compte des puissances d'émission variables, différents coefficients d'affaiblissement sur le trajet pour différents niveaux et tient compte des interférences dans les réseaux à ondes millimétriques. C'est le premier modèle analytique qui encapsule de manière exhaustive les caractéristiques des réseaux denses jusqu'aux réseaux ultra-denses. Par conséquent, la nature exhaustive du modèle analytique proposé peut nous aider à comprendre les limites de performance d'un réseau pour divers scénarios de déploiement.

Les quatrième et cinquième chapitres de cette thèse se concentrent sur la question de déviation des faisceaux (Beam Squinting) dans les systèmes de communication à large bande et à ultra large bande à entrées multiples et sorties multiples massives. La principale attraction de la bande des ondes millimétriques est sa grande largeur de bande disponible. Par conséquent, les systèmes de communication à large bande et à bande ultra-large deviendront bientôt une réalité inévitable. Bien que les systèmes de communication à large bande et à bande ultra-large aient le potentiel d'augmenter considérablement la capacité réalisable, cela soulève également un nouveau problème appelé la déviation des faisceaux qui limite la capacité réalisable. Jusqu'à récemment, la déviation des faisceaux n'avait pas pris suffisamment d'importance pour devenir le problème majeur de la communauté des chercheurs en communications mobiles. Cette négligence délibérée s'explique par le fait que, jusqu'à présent, presque tous les systèmes de communication mobile fonctionnent sur des signaux à bande étroite, ce qui, par nature, rend le problème de déviation des faisceaux négligeable. Dans ce chapitre, une nouvelle architecture d'émetteur-récepteur pour un système de communication à bande ultra-large à entrées multiples et sorties multiples est proposée afin d'atténuer les effets de la déviation des faisceaux. L'avantage de la conception proposée est qu'elle ne repose sur aucune compensation dans le domaine numérique. Elle convient donc aux applications à puissance de calcul limitée ou sensibles aux délais qui n'ont pas les moyens de calculer de grandes matrices de compensation dans le domaine numérique. De plus, le cinquième chapitre de cette thèse souligne l'utilisation potentielle d'hyper-surfaces qui peuvent être exploitées pour atténuer le problème de déviation des faisceaux dans un système de communication à bande ultra-large utilisant des ondes millimétriques.

**Mots-clés:** ondes millimétriques, 5G, réseaux hétérogènes et MIMO massifs

# On the Design and Performance Analysis of mmWave-enabled Next generation of Wireless Networks

Zeeshan SATTAR

## ABSTRACT

The hush of expectancy of a millimeter-wave enabled next generation (i.e., 5G) of communication systems are upon us. As with every new technology, there are inevitable teething issues and obstacles to overcome before finding its true commercial value. Millimeter-wave technology has had its fair share of cynics in the past few years, with questions arising about its efficacy for transmission over long distances, how well it can penetrate through walls, and even if rain or a user's hand might block the signal.

These issues are valid, but most of them have been tackled with innovative solutions in recent years. In addition, millimeter-wave and 5G are often used synonymously, but there are critical differences between the two. The millimeter-wave spectrum is just one part of the frequency band available to future 5G networks. The typical microwave frequencies or sub-6GHz spectrum will also be part of the standard. Among other benefits, the coexistence of these two spectra will offer better coverage and data speeds to customers.

Since the millimeter-wave technology is almost ready to make its public debut on the stage of the commercial tech-world, the main theme of our research project revolves around design and performance analysis of the key enablers of 5G, such as millimeter-wave communications, massive multiple-input multiple-output systems, and heterogeneous networks. More specifically, this thesis focuses on (i) the coexistence of millimeter-wave, and sub-6GHz frequencies in a heterogeneous network and (ii) millimeter-wave enabled wideband and ultra-wideband communication systems.

In this context, the second chapter of this thesis presents a detailed analysis and simulation model of a half-duplex two-tier heterogeneous network employing different frequency bands (i.e., sub-6GHz and millimeter wave). Tools from stochastic geometry are used to model an environment, where users' equipment have the liberty to choose different base stations for uplink and downlink transmissions, called decoupled wireless access. The key performance metrics, such as the probability of users' equipment association, the distribution of the distances between the users' equipment and their tagged base stations, and spectral efficiency are analyzed and evaluated for various pragmatic deployment scenarios.

The third chapter of this thesis presents a performance analysis of a full-duplex two-tier heterogeneous network with decoupled access employing different frequency bands (i.e., sub-6GHz and millimeter wave). The novelty of the derived analytical model is that it accommodates variable transmit powers and different path loss exponents for different tiers, and accounts for the interference in millimeter-wave networks. To the best of our knowledge, it is the first analytical model that comprehensively encapsulates the characteristics of dense to ultra-dense networks.

X

Hence, the comprehensive nature of the proposed analytical model can help us understand the performance limits of a network for diverse deployment scenarios.

The fourth and fifth chapters of this thesis focus on an issue in wideband and ultra-wideband massive multiple-input multiple-output communication systems, i.e., beam-squinting. The main attraction in the millimeter-wave band is its large available bandwidth. Therefore wideband and ultra-wideband communication systems will become an unavoidable reality soon. Though wideband and ultra-wideband communication systems have the potential to increase the achievable capacity significantly, such communication also raises a new issue called beam-squinting, limiting the achievable capacity. The beam-squinting did not get enough prominence to become the blue-eyed problem of the research community of mobile communications until recently. The reason for this deliberate neglect is the fact that, so far, almost all mobile communication systems work on narrowband signals, which by their very nature, make the beam-squinting issue negligible. In chapter four, a novel transceiver architecture for ultra-wideband massive multiple-input multiple-output communication is proposed to mitigate beam-squinting effects. The advantage of the proposed design is that it does not rely on any compensation in the digital domain. Therefore it is suitable for computational power-constrained or delay-sensitive applications that do not have the liberty to calculate large compensation matrices in the digital domain. Moreover, the fifth chapter of this thesis highlights the potential use of hypersurfaces that can be exploited to mitigate the beam-squinting issue in a millimeter-wave enabled ultra-wideband communication systems.

# TABLE OF CONTENTS

# LIST OF TABLES

# LIST OF FIGURES

## LIST OF ABBREVIATIONS

| | |
|---|---|
| 4G | The fourth generation |
| 5G | The fifth generation |
| ADC | Analog-to-digital |
| AWGN | Additive white Gaussian noise |
| | BPSK Binary phase shift keying |
| BS | Base station |
| CSI | Channel state information |
| EMF | Electromagnetic field |
| FBS | Femtocell base station |
| FCC | Federal communications commission |
| GSMA | Global Systems for Mobile Communications Association |
| HetNet | Heterogeneous network |
| i.i.d. | Independent and Identically Distributed |
| IoT | Internet of things |
| ITU | International telecommunication union |
| MBS | Macrocell base station |
| mmWave | Milimeter wave |
| MIMO | Multiple-input multiple-output |
| | OOK On-off-keying |

| | |
|---|---|
| PBS | Picocell base station |
| PDP | Power delay profile |
| PPP | Poisson point process |
| RF | Radio frequency |
| SBS | Small cell base station |
| SINR | Signal-to-interference-plus-noise ratio |
| SNR | Signal-to-noise ratio |
| TDD | Time division duplex |
| TDMA | Time division multiple access |
| UDN | Ultra dense network |
| UE | User equipment |
| $\mu$BS | microcell base station |

## LIST OF SYMBOLS AND UNITS OF MEASUREMENTS

| | |
|---|---|
| $\mathbf{a}$ | Vector |
| $\mathbf{A}$ | Matrix |
| $\mathbf{A}^T$ | The transpose of matrix $\mathbf{A}$ |
| $\mathbf{A}^H$ | The transpose conjugate of matrix $\mathbf{A}$ |
| $\exp(\cdot)$ | Exponential function |
| $\mathbb{E}[\cdot]$ | Expectation function |
| $\text{tr}(\mathbf{A})$ | Trace of a matrix $\mathbf{A}$ |
| $\text{diag}(\mathbf{A})$ | Diagonal of matrix $\mathbf{A}$ |
| $\|\mathbf{A}\|_F$ | Frobenius norm |
| $\Gamma(\cdot)$ | Gamma function |
| $\log_2$ | Logarithm with base 2 |
| $\ln$ | Natural logarithm |
| $\Re\{.\}$ | The real part |
| $\Im\{.\}$ | The imaginary part |
| $\Phi_k$ | PPP of $k$th tier of BSs |
| $\Phi_u$ | PPP of UEs |
| $\lambda_k$ | Density of BSs in $k$th tier |
| $\lambda_u$ | Density of UEs |
| $Q_k$ | Transmit power of UEs tagged to BS in $k$th tier |

$P_k$          Transmit power of BS in $k$th tier

$G_k$          Antenna gain of $k$th tier of BS

$\sigma_k^2$          Noise variance

$_2F_1[.,.,.;.]$          Gauss hypergeometric function

**INTRODUCTION**

**Motivations**

We are living in an era of virtual products, from virtual shopping stores to virtual reality, the cutting edge technology is changing the world, including the way we see and feel it. This ever-growing and ever-changing e-world places new requirements on how we connect and communicate and sets new constraints on the next generation, i.e., fifth-generation (5G), of wireless communication systems.

The 5G wireless communication network is becoming a hot research topic, and its evolution is a necessity to meet the exponential growth of data traffic in all forms. If 2G network was voice-centric, 3G provided combined circuit-switched, packet-switched data and voice services, 4G offered higher bit rates and many architectural improvements such as voice over IP, then 5G network can be seen as the orchestration of a number of different technologies allowing a higher density of mobile broadband users, and supporting device-to-device, ultra-reliable, massive machine communications. The main goal of 5G is to transform our society into a hyper-connected community in which mobile devices will play an even more critical role in shaping and improving the lives of human beings.

The data rate demands of 5G systems when met with the scarce resources in the microwave spectrum; the result was rather disappointing. Therefore, it forced the research community of both industry and academia to search for new horizons. It did not take them long to come up with the solution in the form of a huge unused spectrum of millimeter-wave (Rappaport, Sun, Mayzus, Zhao, Azar, Wang, Wong, Schulz, Samimi & Gutierrez, 2013). Though the idea of using millimeter-wave is new in wireless communications, its history goes back to the 1890s when J.C. Bose was experimenting with millimeter-wave signals and, just to have a good perspective about the time, it was the same era when Marconi was inventing radio communications. Therefore when it comes to the fundamental physics of millimeter-wave,

we already know almost everything about it. Since, by nature, millimeter-wave is extremely susceptible to blockages and bears huge path losses, hence, the idea of using a massive number of antennas on a base station (BS) to focus power in sharp beams towards a typical user came into existence (Hoydis, Ten Brink & Debbah, 2013). Now, formally, we name this idea *massive MIMO* or *large-scale MIMO*.

Millimeter-wave and massive multiple-input multiple-output (MIMO) are unavoidable needs rather than choices from an available pool of options. They are instrumental not only to obtain high spectral efficiencies but also to provide homogeneous quality of service to all the users in a cell. Since millimeter-wave networks are susceptible to blockages and huge pathloss, future millimeter-wave networks are envisioned to coexist with microwave or sub-6GHz networks where sub-6GHz BSs will provide an umbrella coverage to all user equipments (UEs), and millimeter-wave BSs will mainly focus on the high capacity links with individual UEs. Hence, one of the real challenges for the research community is to evaluate the performance of a two-tier heterogeneous network (HetNet) where one tier operates on millimeter-wave and the other on the microwave or sub-6GHz spectra.

In addition, one of the main attractions in the millimeter-wave band is its sizeable available bandwidth, which intuitively has the potential to make wideband and ultra-wideband communication systems a reality. Since, so far, almost all mobile communication systems work on narrowband signals, therefore it is worth investigating how typical conventions followed for narrowband transmissions will work with wideband and ultra-wideband communications.

**Problem Statement**

The two key ingredients that have the potential to shape the future of wireless networks are (i) multi-tier HetNets and (ii) millimeter-wave enabled wideband massive MIMO systems. It is envisaged that future wireless networks are to be multi-tier. Therefore, the transition from single-tier homogeneous cellular networks to multi-tier HetNets is inevitable (Andrews,

Claussen, Dohler, Rangan & Reed, 2012; Andrews, 2013). In HetNets, different tiers of BSs typically use different transmit powers, which result in significantly different interference levels. Therefore, the idea of whether the conventional way of cell association, i.e., coupled access, where a user connects to a single BS for both uplink and downlink transmission would be optimal in HetNets came under the scrutiny of the research community (Boccardi, Andrews, Elshaer, Dohler, Parkvall, Popovski & Singh, 2016).

Since the dawn of cellular communication systems, a single BS serves a UE for both uplink and downlink transmissions. Recently, this idea has been challenged in the form of decoupled wireless access (Elshaer, Boccardi, Dohler & Irmer, 2014; Elshaer, Kulkarni, Boccardi, Andrews & Dohler, 2016). The basic idea of decoupled wireless access challenges the optimality of connecting to the same BS for both uplink and downlink transmissions. It advocates for the UEs' liberty to simultaneously connect to two different BSs from any two different tiers of BSs for uplink and downlink transmissions. Hence, it is worth investigating the effects of decoupled access on a cellular communication system's performance metrics.

Moreover, as mentioned earlier, the millimeter-wave band's real potential lies in its unprecedented massive bandwidth, which can make wideband and ultra-wideband communications a reality. Therefore Wang *et al.* (Wang, Gao, Jin, Lin & Li, 2018a; Wang, Gao, Jin, Lin, Li, Sun & Rappaport, 2018b) revisited the typical conventions of cellular communication systems that can affect wideband and ultra-wideband communication systems. In their work, Wang *et al.* highlighted problems specific to wideband massive MIMO systems caused by beam-squinting. Therefore, recently the issue of beam-squinting got the traction and concentrated attention it deserves (Li, Zhao & Hui, 2018a; Liu & Qiao, 2019; Liu & Zhu, 2018).

**Research Objectives**

In this thesis, we focus on (i) the performance analysis of two-tier HetNet with decoupled access and (ii) the mitigation of beam-squinting in wideband and ultra-wideband communication

systems. To achieve the first goal, we considered two different HetNet models based on the type of communication style, i.e., half-duplex and full-duplex. Previous studies either did not consider two-tier HetNet employing millimeter-wave and microwave spectra separately in each tier or did not fully accommodate, in the analytical model , the differences these two spectra have in their characteristics. Therefore, there is a need for a robust analytical model, which comprehensively accommodates the characteristics of both millimeter-wave and microwave spectra and helps us evaluate the achievable performance of such HetNets. We developed robust analytical models for each case and further validated the analysis by providing rigorous simulation results. The novelty of the two analytical models developed in this thesis are their ability to encapsulate the attributes of both millimeter-wave and microwave spectra in their numerical expressions. This consequently results in a more robust analysis of key performance metrics of HetNets, such as probability of association, distance distribution, coverage, and spectral efficiency.

Since the beam-squinting issue is intrinsic to ultra-wideband signals' analog nature, any compensation in the digital domain can only result in minimal improvements with additional computational complexity. Therefore, the second goal of this thesis highlights the importance of the mitigation of beam-squinting in the analog domain and provides a solution for computational power constrained or delay-sensitive applications. In other words, it addresses the question in ultra-wideband mmWave-enabled massive MIMO systems: *"how to provide an order of magnitude capacity improvement without adding any computational complexity?"*. In this regard, previous studies either tried to compensate beam-squinting, which is a characteristic of wideband or an ultra-wideband communication systems, in the digital domain or proposed methods which are either specifically intended for a system employing hybrid precoding or require multiple radio frequency (RF) chains in the transceiver design. In contrast, our proposed solution does not have such constraints and can be tailored for the scenarios mentioned above. Moreover, a use case of hypersurfaces that can be exploited to mitigate the beam-squinting issue

in a millimeter-wave enabled ultra-wideband communication systems is also highlighted at the end of this thesis.

## Contributions and Outline

The dissertation is structured as shown in Fig. 0.1, and detailed as follows.
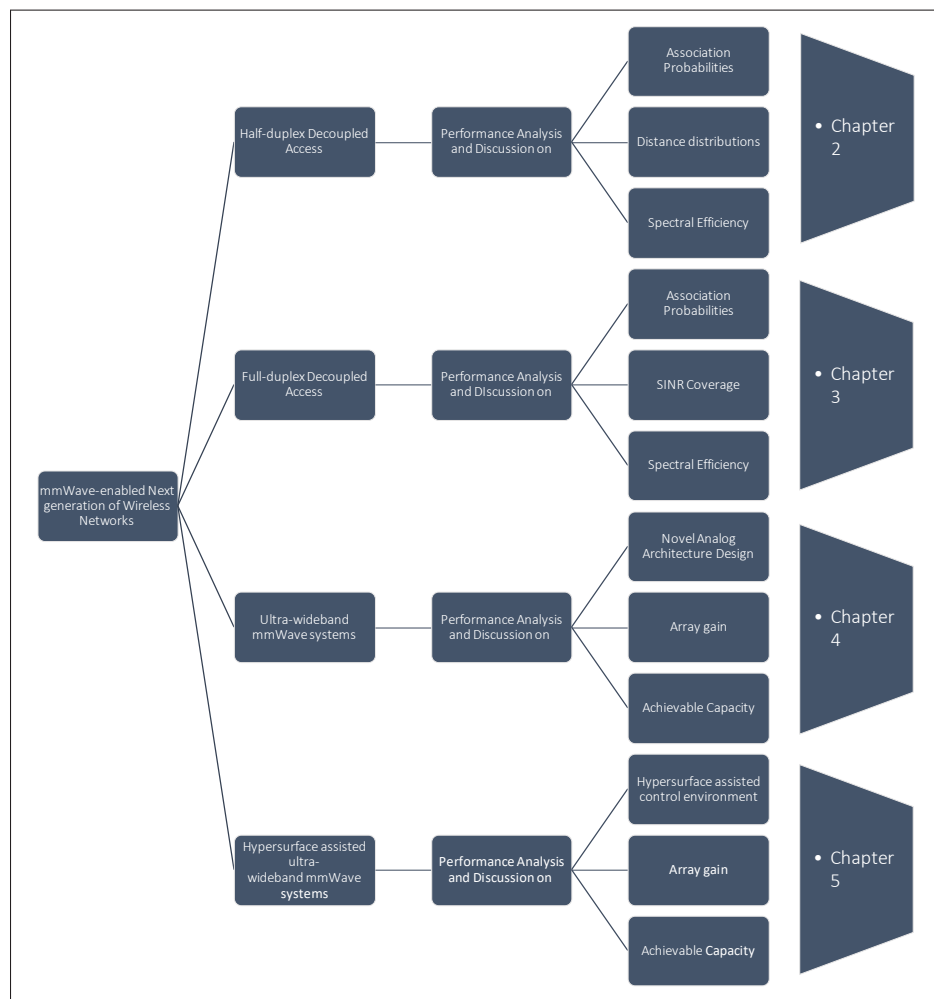


Figure 0.1    Paradigm of the thesis contributions

Chapter 1 presents a comprehensive literature review of 5G communication systems. It highlights the enabling technologies of 5G communication systems, such as massive MIMO, millimeter-wave, HetNets, and provides a brief description of recent related works. It also presents the

initial semi-analytical work on cell association of mobile devices in decoupled wireless access in a multi-tier network with a realistic blockage model. Here, an environment where a human body is considered as a blocker to millimeter-wave is emulated. Moreover, a detailed discussion on the intuitiveness and the mathematical tractability of the blockage model used is also provided in this chapter.

Chapter 2 presents a detailed performance analysis of decoupled wireless access in a half-duplex two-tier heterogeneous network. In this chapter, an in-depth analysis of its efficacy from the spectral efficiency perspective is provided. To achieve this task, the following three aspects are being developed: (i) new closed-form expressions for the probability of association of user equipment with different tiers employing different frequency bands (i.e., microwave and millimeter-wave) with different pathloss exponents are derived using univariate Fox's H-functions; (ii) distributions of the distance to the serving base stations are derived; (iii) exact expressions of the spectral efficiency for different association cases are further obtained using bivariate Fox's H-functions. In this context, rigorous simulation results are provided to validate the aforementioned analytical results. Furthermore, a detailed discussion on the decoupling gain of decoupled wireless access and its efficacy is also provided. Lastly, despite the improvement provided by decoupled wireless access, which is evident from the results presented in this chapter, few questions are raised on its practical value.

Chapter 3 presents a detailed performance analysis of decoupled wireless access in a full-duplex two-tier heterogeneous network. A typical point-to-point full-duplex transmission link can double the link rate by simultaneously using the same spectrum for bidirectional traffic. However, the characterization of full-duplex two-tier heterogeneous networks is not as straightforward as that of point-to-point full-duplex systems, especially when the different tiers of the heterogeneous network use different frequency bands (millimeter-wave and microwave) for their transmissions. This chapter characterizes a full-duplex two-tier heterogeneous network with decoupled access,

where both tiers operate on different frequency bands (millimeter-wave and microwave). To evaluate the achievable spectral efficiency and association behavior of users and base stations, a two-tier heterogeneous network model is proposed in which all users and base stations are modeled using Poisson point processes. First, a signal-to-interference-plus-noise-ratio optimal user association scheme is characterized. Based on the user association scheme, the spectral efficiencies of the uplink and downlink transmissions are derived. In addition, a thorough analysis of the signal-to-interference-plus-noise-ratio coverage is also provided. Moreover, to render the analytical model more comprehensive and robust, i.e., different from the convention of the noise-limited millimeter-wave network, the interference in millimeter-wave networks is also accounted for in the analytical model. Lastly, the pragmatic value of full-duplex heterogeneous networks and decoupled access is discussed in detail through numerous numerical and simulation results.

Chapter 4 presents a discussion on the issue of beam-squinting encountered in ultra-wideband millimeter wave mobile communication systems and provides a novel analog architecture to mitigate the beam-squinting. First, the beam-squinting effects on the antenna array gain, and the usable bandwidth of these systems are analyzed. The obtained results show that, in ultra-wideband communication systems, beam-squinting causes loss in array gain and limits the achievable capacity. A new analog architecture design that improves the array gain and the achievable capacity is proposed to mitigate these effects. The proposed architecture is most suitable for delay-sensitive or computational power-constrained applications and does not require any compensation matrix computation in the digital domain. In addition, the exact expression for the array gain of the proposed analog architecture is derived. To further simplify the evaluation of the system performance, an approximated closed-form expression for the array gain is obtained. Finally, to evaluate the performance of the proposed design, rigorous numerical results concerning different system parameters are provided in this chapter.

Chapter 5 highlights the use case of hypersurfaces that can be exploited to mitigate the beam-squinting issue in a millimeter-wave enabled ultra-wideband communication systems. A hypersurface is a software-controlled intelligent surface, which can manipulate impinging signals for the benefit of their intended receiver. Consequently, this chapter explores achievable capacity gains by minimizing beam-squinting in a unique programmable environment consisting of hypersurface coated walls and objects. The obtained results show that a transceiver in a hypersurface assisted controlled environment can achieve better performance compared to a more sophisticated transceiver, proposed in Chapter 4, in a typical environment, i.e., a conventional environment without any hypersurface assistance.

**Related Publications**

The author's PhD research contributed to the following published and submitted research articles. The journal publications and conference proceedings are denoted by "J" and "C", respectively

J1:  **Z. Sattar**, J. V. C. Evangelista, G. Kaddoum and N. Batani, "Spectral Efficiency Analysis of the Decoupled Access for Downlink and Uplink in Two-Tier Network," in *IEEE Transactions on Vehicular Technology*, vol. 68, no. 5, pp. 4871-4883, May 2019.

J2:  **Z. Sattar**, J. V. C. Evangelista, G. Kaddoum and N. Batani, "Full-Duplex Two-Tier Heterogeneous Network with Decoupled access: Cell Association, Coverage, and Spectral Efficiency Analysis," in *IEEE Access*, vol. 08, pp. 172982-172995, September 2020.

J3:  **Z. Sattar**, J. V. C. Evangelista, G. Kaddoum and N. Batani, "Antenna Array Gain and Capacity Improvements of Ultra-Wideband Millimeter Wave Systems Using a Novel Analog Architecture Design," in *IEEE Wireless Communications Letters*, vol. 9, no. 3, pp. 289-293, March 2020.

C1:  **Z. Sattar**, J. V. C. Evangelista, G. Kaddoum and N. Batani, "Analysis of the cell association for decoupled wireless access in a two tier network," *2017 IEEE 28th Annual International Symposium on Personal, Indoor, and Mobile Radio Communications (PIMRC)*, Montreal, QC, 2017, pp. 1-6.

C2: **Z. Sattar**, J. V. C. Evangelista, G. Kaddoum and N. Batani, "Antenna Array Gain and Capacity improvements in a Hypersurface assisted Controlled Environment," submitted to *IEEE ICC*, Montreal, QC, 2021.

Beside the above articles that contribute to the main contents of this thesis, full list of publications that the author was involved in and which are not included in this thesis is given at the end of this thesis.

# CHAPTER 1

# BACKGROUND AND LITERATURE REVIEW

## 1.1 What is 5G?

In telecommunications, 5G is the fifth generation technology standard for cellular networks. It can be best described as a hyper-connected network where mobile service providers would create a blend of technologies, where 2G, 3G, 4G, Wi-fi and others will coexist to allow higher coverage and availability on top of an addition of a next-generation of wireless access technology, i.e., massive MIMO and millimeter-wave. Furthermore, similar to previous generations, there are specific goals for 5G networks, for example, 100 billion connections, 1 ms of latency, 10 Gbps throughput.

The goal of 100 billion connections is to fulfill the vision of the internet of things (IoT). Here, from smart logistics to smart agriculture, all come under the umbrella of IoT, and their practical realization is not possible without a network that offers massive connectivity. Whereas, the requirement of 10 Gbps throughput is for use cases such as high-speed access to cloud storage and virtual reality. The requirement of 1ms of latency is the most crucial characteristic of 5G networks. Its importance can be understood by a simple self driving car example, with the latency of 4G network, i.e., 50ms, a car driving at 100 km/h will move 1.4 m between the time it finds an obstacle and the time the braking command is executed. On the other hand, under the same conditions, with the latency requirement of 5G network, i.e., 1ms, the car will move just 2.8 cm, which is comparable to the standard anti-lock braking system.

### 1.1.1 Potential 5G use cases

From an industry point of view, the rate of adoption of 5G solely depends on the use cases which can only be unlocked by this new technology. Therefore, from a mobile operator's perspective, there are two key questions which need to be addressed: (i) What would we be able to do on the

12

5G network which we cannot do with existing technologies? (ii) What makes these potential services profitable?

Some of the potential use cases of 5G are illustrated in Fig. 1.1. The figure shows the bandwidth and latency requirement of those use cases, which have been discussed in the context of 5G to date.
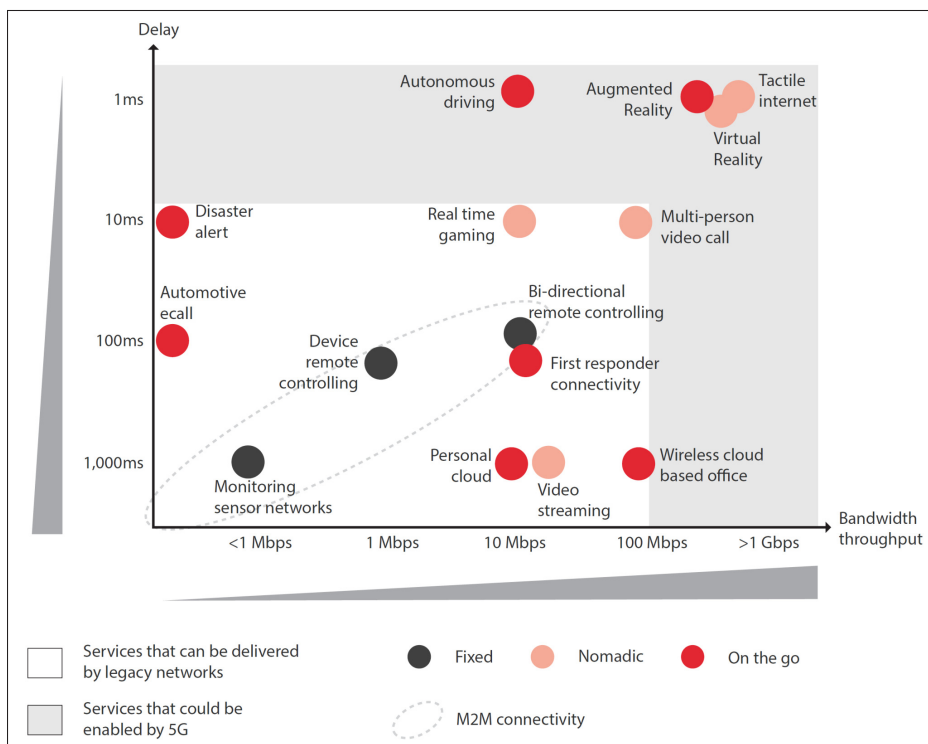


Figure 1.1 Potential 5G use cases and their bandwidth / latency requirements
Taken from Intelligence (2014)

## 1.2 Enabling technologies for 5G

As of today, 5G communication systems list the aforementioned set of goals that must be achieved for future wireless networks. However, despite its full standardization, few technologies are foreseen to accomplish those goals, such as massive MIMO, millimeter-wave, and ultra-dense

network. If we look into the question of what influences the rate experienced by a user? A partly intuitive and partly mathematical answer can be found in the following equation (1.1).

$$\underset{\text{(bits per second)}}{\text{Rate per user}} = \frac{\text{Bandwidth} \times \text{MIMO}}{\text{Number of users}} \times \text{Spectral efficiency} \tag{1.1}$$

Therefore, the concatenation of the unmatched bandwidth of the millimeter-wave band and the vast array gain of massive MIMO together seems to be a key enabler of the next generation of wireless network. Massive MIMO implies that the millimeter-wave communication links will have a very narrow footprint (i.e., sharp and narrow beams), which improves spectral efficiency by reducing the interference. Similarly, two-tier HetNet employing two different frequency bands in each tier, i.e., millimeter-wave and microwave, have the potential to improve the spectral efficiency by reducing the interference. Therefore, millimeter-wave, massive MIMO, and HetNets would be the key enablers of the next generation of wireless networks.

### 1.2.1   Massive MIMO and millimeter-wave

Network densification and the use of extremely high frequencies (EHF), commonly known as millimeter-wave band, are the two most promising candidates for the future wireless access to fulfill the ever-increasing capacity demands. It is the small wavelength of millimeter-wave that makes it possible to increase the density of BSs significantly by reducing the footprint of BSs' deployment sites. In addition, millimeter-wave is what made it possible to use massive MIMO in realistic scenarios.

Massive MIMO might sound reasonably new as a topic of research, but as a concept, it has been a hot topic of research since the inception of multiuser information theory. At a glance massive MIMO may sound like a fancy name of multiuser MIMO but the following four key characteristics make it distinct; (i) only the BS learns the channel matrix using uplink pilots; (ii) the number of antennas on a typical BS are greater than the number of users in a cell; (iii) simple

signal processing techniques; (iv) it serves multiple users (assuming mutual orthogonality in a practical sense) through spatial multiplexing in time-division duplex mode.

### 1.2.1.1   Massive MIMO and Millimeter-Wave: A Natural Wedlock

In this section, we want to highlight the strong dependence of massive MIMO and millimeter-wave on each other. Even though there is no direct relationship between these two technologies, significant amount of research has been done on massive MIMO mainly focused on conventional cellular frequency bands. While massive MIMO is an option at current cellular bands to provide array and multiplexing gain, it became an unavoidable need or prerequisite to gather enough energy at the millimeter-wave band. Since the area per antenna element is shrunk as the frequency is increased, therefore more antenna elements are required to gather the same amount of signal energy as before. Moreover, small wavelengths of frequencies in the millimeter-wave band made it easier to pack a large number of antenna elements in a compact form. For example, a carrier frequency $f_c$ = 30 GHz (i.e., $\lambda$ = 1 cm), and with $\lambda/2$ antenna spacing, more than 180 antennas can be placed on an area as large as a standard credit card as shown in Fig. 1.2. This number can reach up to 1300 at 80 GHz. Therefore both millimeter-wave and massive MIMO are key enablers of the next generation of high-speed wireless networks.

### 1.2.2   Ultra dense networks

The immense growth in data traffic requires a paradigm shift in all aspects of mobile networks. From the point of view of many experts and industrial consortia in this area, network densification is one of the leading ideas to tackle this challenge. A network can be considered as ultra-dense if there are more cells than active users (Ding, López-Pérez, Mao, Wang & Lin, 2015; López-Pérez, Ding, Claussen & Jafari, 2015). The basic idea is to get the access nodes as close as possible to the end-users. To yield a better idea of the dimension of this class of networks, Ding et al. provided a quantitative measure of the density at which a network can be considered ultra-dense. According to this study, a network is deemed dense if there are more than $10^3$cells/Km$^2$ for 600 active users/Km$^2$ (Ding *et al.*, 2015). The motivation behind this idea is to have access nodes

Figure 1.2    Example of compactness of millimeter-wave antenna elements. At a carrier frequency of $f_c$ = 30 GHz (i.e., $\lambda$ = 1 cm), and with $\lambda/2$ antenna spacing, more than 180 antennas can be placed on an area as large as a credit card

as close as possible to end-users. The practical implementation of network densification can be achieved by the dense deployment of small cells in the hotspots where immense traffic is generated. In general, small cells in ultra dense network (UDN) are fully-functioning BSs that are capable of performing all the functions of a macrocell with a lower power and a smaller coverage area.

### 1.2.3   Heterogeneous Networks

The key idea behind HetNets is to densely deploy different categories of BSs to increase the network coverage and the performance of cell-edge users. Traditional macrocell BSs (MBS), characterized by high power consumption and high infrastructure costs are added to small cell BS (SBS) comprising, microcell BSs ($\mu$BS), pico cell BSs (PBS) and femtocell BSs (FBS) requiring low power, little infrastructure, and low maintenance costs. The idea is that a small number of sparsely deployed MBSs provide umbrella coverage to the cell. In contrast, a high number of densely deployed SBSs, $\mu$BSs, PBSs, and FBSs, that are more closely located to the users, offload the traffic from the MBS increasing the coverage of the cell, the area spectral

efficiency and improving the quality of service (QoS) of cell edge users. SBS deployment, along with MBS, is already in the specifications of long term evolution (LTE) for 4G.

A key design parameter with respect to the performance of HetNets is the user association algorithm, which determines to which BS tier each user should connect. Common metrics to asses the performance of a HetNet are: the outage/coverage probability (Dhillon, Ganti, Baccelli & Andrews, 2012; Singh, Dhillon & Andrews, 2013), the spectral efficiency (Hu & Qian, 2014), the energy efficiency (Su, Yang, Xu & Molisch, 2013; Liu, Chen, Chai & Zhang, 2014a; Zhu, Wang & Chen, 2012; Chavarria-Reyes, Akyildiz & Fadel, 2015), QoS (Liu, Chen, Chai & Zhang, 2014b; Liu, Chen, Chai, Zhang & Elkashlan, 2014c), and the fairness (Liao, Hong & Luo, 2014; Bethanabhotla, Bursalioglu, Papadopoulos & Caire, 2016). Typical user association algorithms associate the user to the BS with maximum received power; however, this approach is not the optimal solution in a HetNet scenario, due to disparity between the transmitted power of different network tiers, which results in most of the users associating with the MBS, hence, making ineffective use of the other tiers. A big challenge while designing user association algorithms is that, due to the combinatorial nature of the association problem, the resulting optimization problem is generally NP-hard (Liu, Wang, Chen, Elkashlan, Wong, Schober & Hanzo, 2016), rendering it computationally prohibitive to solve. Furthermore, some of the objectives are conflicting, i.e., energy efficiency and QoS, resulting in performance tradeoffs.

HetNets also pose a great resource management challenge. Specially, due to the dense deployment of SBSs, $\mu$BSs, PBSs, and FBSs, the interference between different tiers and among the same tier can be a limiting factor to the overall network performance. In addition to the user association challenge discussed earlier, spectrum sharing strategies are of utmost importance to minimize the interferences.

## 1.3   Millimeter-wave communications: A technology overview

The millimeter-wave spectrum corresponds to some specific bands (i.e., spectrum around 38 GHz, 60 GHz, 70 GHz, 90 GHz, and 94 GHz) with wavelength between one and ten millimeters. However in the wireless communications context, generally, the term millimeter-wave corresponds to a rather broad spectrum between 30 GHz to 300 GHz (Adhikari, 2008).
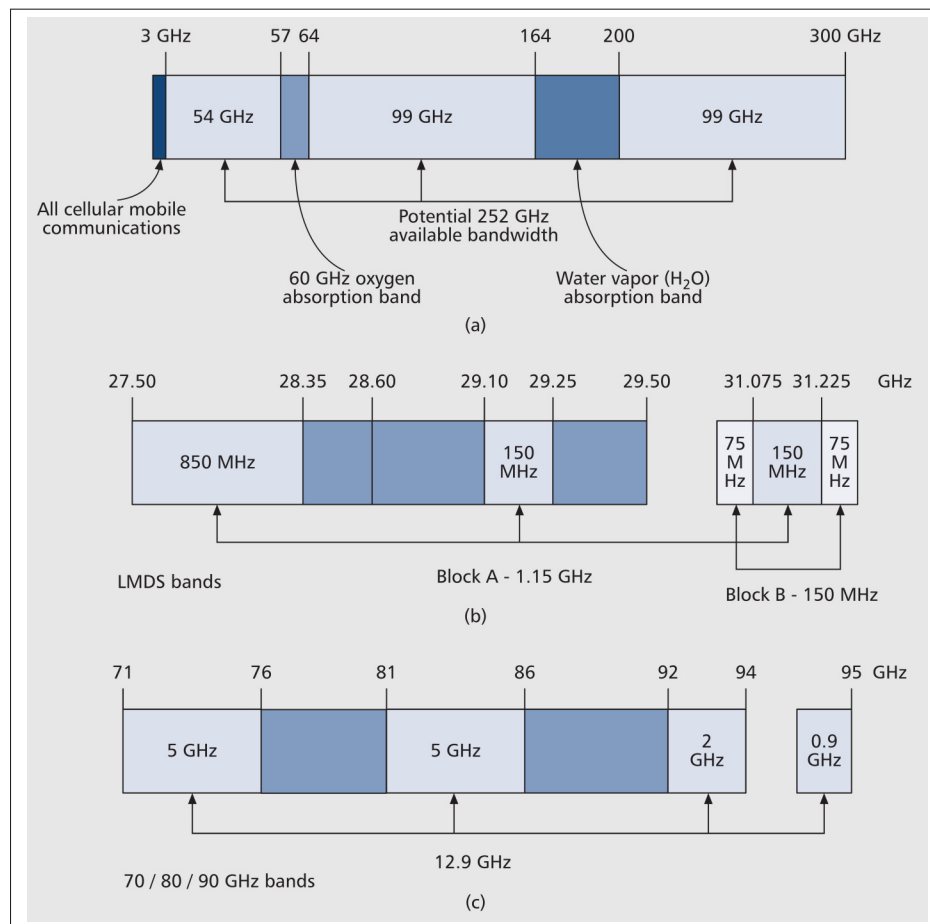


Figure 1.3   Millimeter-wave spectrum
Taken from Pi & Khan (2011)

### 1.3.1   The band and the bandwidth

There are four bands in the United States in the millimeter-wave spectrum that have been opened for commercial applications.

- The 59-64 GHz band, commonly known as V-band. It is governed by the FCC Part 15 for unlicensed operations.

- The 92-95 GHz band with the exception of the frequencies in the 94-94.1 GHz range, commonly known as W-band. It is also governed by the FCC Part 15 for unlicensed indoor applications only.

- The 71-76 GHz and 81-86 GHz bands, commonly known as E-band. They are governed by the FCC Part 101 for licensed operations.

In the E-band spectrum, the 5 GHz of available bandwidth in each sub-band can be used as a single, contiguous, transmission channel, as shown in Fig.1.3. This would result in the most efficient use of this expensive resource, i.e., spectrum, since no channelization would be required to use the entire band. A throughput of 1 to 3 Gbps can be readily achieved in each sub-band of the spectrum with simple modulation schemes such as OOK (On-Off-Keying) or BPSK (Binary Phase Shift Keying) (Adhikari, 2008), which is significantly more than what can be achieved by more complex modulation schemes in other bands of the licensed spectrum. Therefore, migrating to millimeter-wave bands would result in even higher throughputs when using higher-order modulation schemes.

### 1.3.2 Key challenges of millimeter-wave communications

Apart from the vast available bandwidth of millimeter-wave and its unprecedented theoretical performance in terms of achievable data rates, there are some key challenges associated to its use in the next generation of wireless networks. They are mainly related to the propagation characteristics of millimeter-wave, making its practical application relatively more challenging than its predecessor, i.e., microwave. A brief introduction to different aspects of the propagation characteristics of millimeter-wave is provided in the following subsection.

### 1.3.2.1 Propagation Characteristics

Radio signals of all types experience attenuation as they propagate through the atmosphere, primarily because of absorption or scattering. Therefore, how much of the transmitted signal actually makes it to a receiver significantly depends on the environment.

**Pathloss**

The received power of a radio signal that propagate in a free space, outside the Kirchhoff area, can be mathematically calculated as (Rappaport *et al.*, 2013)

$$P_r(d) = P_t G_t G_r \left(\frac{\lambda}{4\pi}\right)^2 d^{-n}. \tag{1.2}$$

This relationship is known as Friis transmission formula. Here, $P_r$ and $P_t$ denote the received power by the receiver and transmitted power by the transmitter, respectively. Whereas $G_t$ and $G_r$ are the antenna gains of transmitter and receiver, respectively, $\lambda$ is wavelength, $d$ is the transmission distance, and $n$ is the pathloss exponent (for free space $n = 2$).

Even though the expression in (1.2) is for the free space case, it can be altered to approximate the non-free space propagation by changing the value of the pathloss exponent $n$ with respect to channel measurements. In general, the value of the pathloss exponent $n$ remains between 2 to 6 in different propagation conditions.

Since the millimeter-wave band, as its name suggests, is characterized by very small wavelengths, the atmospheric oxygen, humidity, fog, and rain can represent significant impairment factors on a millimeter-wave communication link. However, among all the atmospheric conditions, rain causes the most significant loss. Table 1.1 illustrates the attenuation of E-band signals for different atmospheric conditions, whereas Fig. 1.4 shows the attenuation of millimeter-wave

signals for different rates of rain (Xiao, Mumtaz, Huang, Dai, Li, Matthaiou, Karagiannidis, Björnson, Yang, Chih-Lin et al., 2017).

Table 1.1    Signal loss through atmosphere

| Effects | Comments | Signal Loss (dB/km) |
|---|---|---|
| Oxygen | Sea level | 0.22 |
| Humidity | 100%, 30°C | 1.7 |
| Heavy Fog | 10°C, 1 $gm/m^3$, (50m visibility) | 3.2 |
| Cloud burst | 25mm/hr rain | 10.7 |
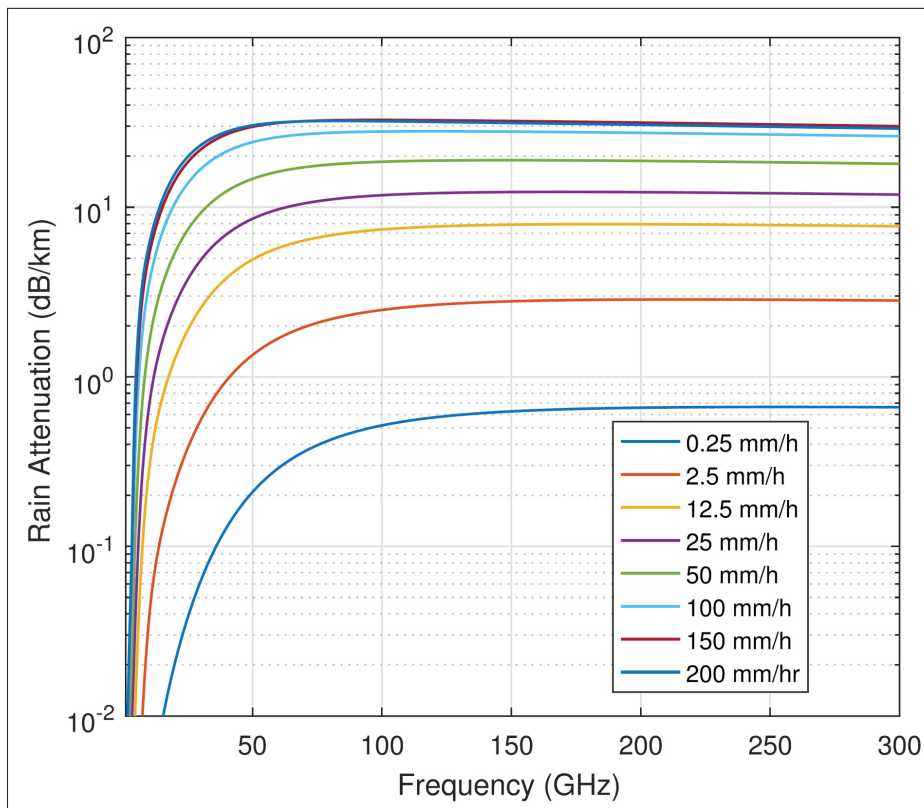


Figure 1.4    Rain attenuation in different frequency bands
Taken from Xiao *et al.* (2017)

**Penetration Loss**

Another critical challenge in the design of a millimeter-wave communication network is the susceptibility of millimeter-wave to penetration losses. The small wavelengths of millimeter-

waves makes them almost impossible to penetrate bricks and tinted glass (about 28 dB and 40 dB penetration loss at 28 GHz) (Ghosh, 2016; Haneda, Zhang, Tan, Liu, Zheng, Asplund, Li, Wang, Steer, Li et al., 2016). Though the penetration losses for drywalls and clear glass are relatively lower; however, the huge path loss combined with penetration losses make an indoor coverage by an outdoor deployed millimeter-wave BS almost impossible.

## High Power Consumption

Another challenge to make millimeter-wave communication a practical reality is its theoretical high power consumption. Precisely, to keep the signal-to-noise-ratio (SNR) intact for a higher bandwidth, the increase in transmit power is inevitable (Heath, Gonzalez-Prelcic, Rangan, Roh & Sayeed, 2016). An alternate method is to use directive antennas or MIMO beamforming to direct the signal power spatially, which not only leads to array gain but can also provide spatial multiplexing (Rusek, Persson, Lau, Larsson, Marzetta, Edfors & Tufvesson, 2013).

It is the small wavelength of millimeter-wave, that makes it possible to pack a large number of half-wavelength spaced antenna elements in a compact size. Therefore, large scale MIMO or massive MIMO is considered as an inevitable technology to make millimeter-wave communication systems a practical reality.

## Narrow Beamwidth and Side Lobes

The millimeter-wave communication link always envision in conjunction with massive MIMO to focus transmit power in sharp beams, which eventually results in a system with a high reuse factor of frequencies in a given geographical area. One of the main benefits of the sharp beams is the reuse factor of frequency resource due to marginalize cross-interference. Typically, the beam's directivity and the radiation pattern are modeled in an idealized fashion, i.e., without any side-lobes, as shown in Fig. 1.5. On the other hand, in reality, the side lobes can never be completely zeroed. The main lobe can not remain constant. Therefore, these idealized assumptions can deviate expected results far from reality and can eventually result in a completely
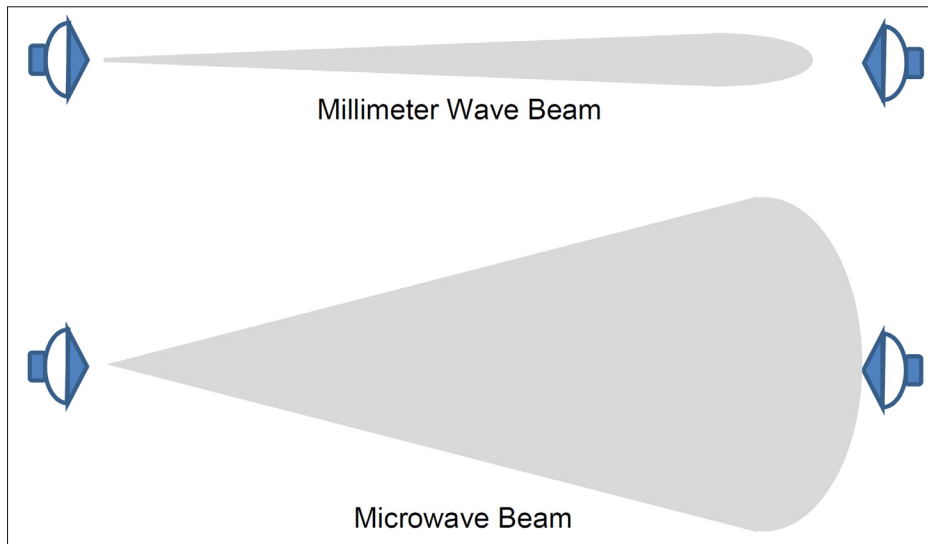
Figure 1.5    Illustration of millimeter-wave and microwave
beamwidths
Taken from Adhikari (2008)

misaligned beam. Hence, the ideal beamforming gain, which can only be achieved if the main lobes of the transmitter and receiver are perfectly aligned, is practically impossible to reach due to implementation constraints.

### 1.3.3   Key Benefits and Technical Potentials

In the previous section, we briefly discussed some of the key challenges faced by millimeter-wave communication technology. This section highlights some of the major benefits of millimeter-wave technology and its prospective potential for future wireless networks.

**Unmatched Bandwidth**

One of the key benefits of millimeter-wave communication technology is its large available pool of bandwidth, as shown in Fig. 1.3. Only in the E-band, there is a total of 12.9 GHz of bandwidth available for ultra-high-speed data communication, including point-to-point WLAN, mobile backhaul, and broadband Internet access, which is much more than the sum total of all other licensed spectra available for wireless communication in microwave spectrum.

**Narrow Beam with Highly Scalable Deployments**

As briefly discussed above, the small footprint of millimeter-wave made it easier to pack a large number of antenna elements into a compact space, which leads us to the massive MIMO technology. As a result, we get communication links with very narrow beamwidths, which result in high reuse factor, i.e., the spectrum can be reused frequently in space without causing any significant interference, as shown in Fig.1.6. In addition to that, the narrow beamwidth also provides better security against eavesdropping and jamming (Xiao *et al.*, 2017).
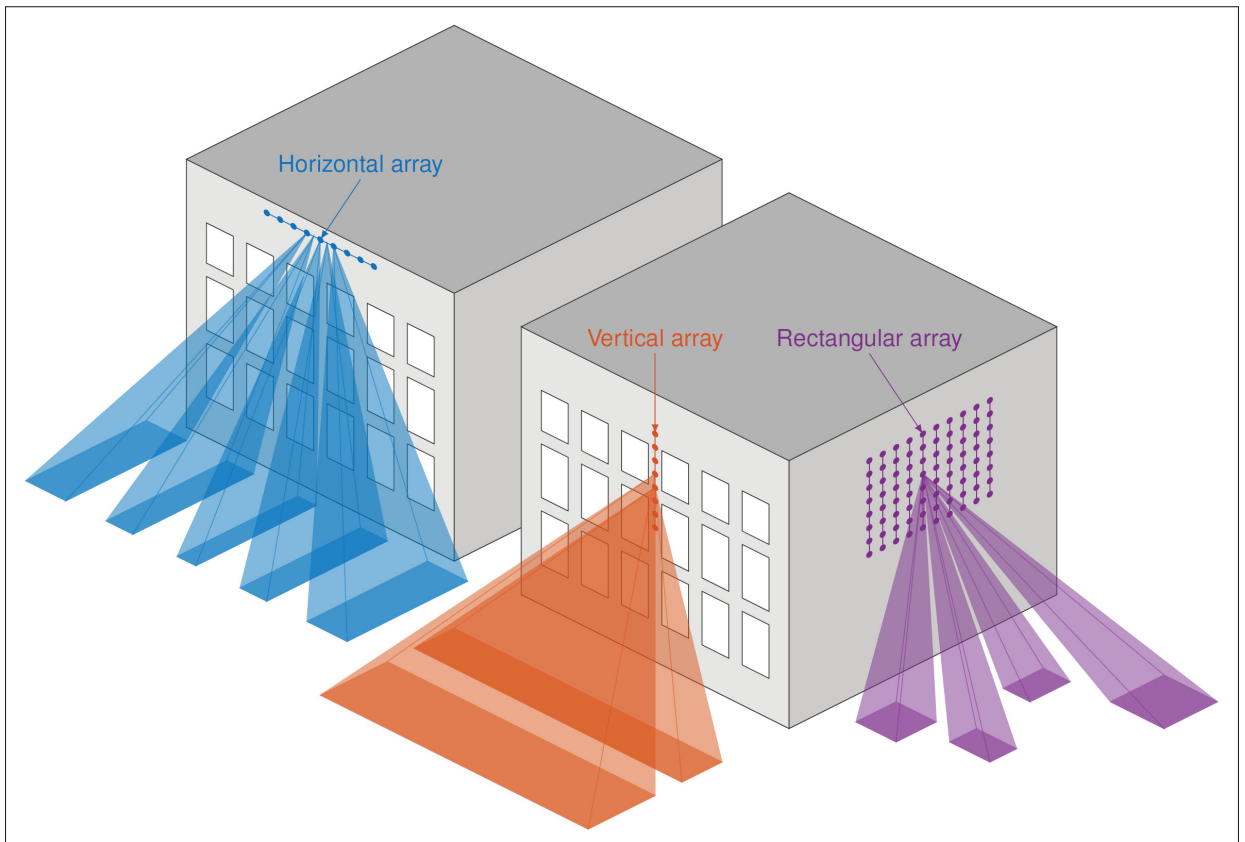


Figure 1.6    Examples of horizontal, vertical, and 3D beamforming
Taken from Ferrand, Amara, Valentin & Guillaud (2016)

## 1.4 MIMO Design for millimeter-wave Communications

In this section, we discuss the hardware architectures of MIMO for millimeter-wave communications and their respective advantages and disadvantages and highlight the implementation complexity.

### 1.4.1 MIMO Architectures

Typically, in conventional MIMO systems, signal processing happens in baseband, and therefore such systems are referred to as fully digital, as shown in Fig.1.7 (Rusek *et al.*, 2013). On the other hand, fully digital massive MIMO systems at least for now, do not sound like a practical idea since fully digital massive MIMO architecture requires a massive number of energy-intensive RF chains, resulting in a significant increase in the implementation cost. Therefore, different alternative massive MIMO architectures have been proposed recently. For example, a fully analog architecture employing only one RF chain, i.e., only one data stream, connected with a massive number of antenna elements using phase shifters to achieve an array gain was proposed (Kim & Lee, 2015) as shown in Fig.1.8. An extension to the fully analog architecture has been proposed recently to support multi-streams (Zhang, Molisch & Kung, 2005; Sudarshan, Mehta, Molisch & Zhang, 2006; Venkateswaran & van der Veen, 2010). This hybrid architecture divides the signal processing of very high dimension matrices into a dimension reduced digital part (i.e., requiring a small number of RF chains) and a large size analog part similar to the fully analog case, as shown in Fig.1.9.

One of the key advantages of the fully analog architecture is its low hardware cost and energy consumption. However, since its analog circuitry can not perfectly adjust the signals, it is not possible to adjust the beams precisely according to channel conditions. Hence, a significant performance loss could occur (Heath *et al.*, 2016), specifically for mobile users. Therefore, the hybrid architecture is a good balance between accuracy, hardware cost, and energy consumption. Moreover, since effective scatterers at millimeter-wave frequencies are always small in number, this leads to low-rank MIMO channel matrix (Rappaport *et al.*, 2013). Hence, typically the
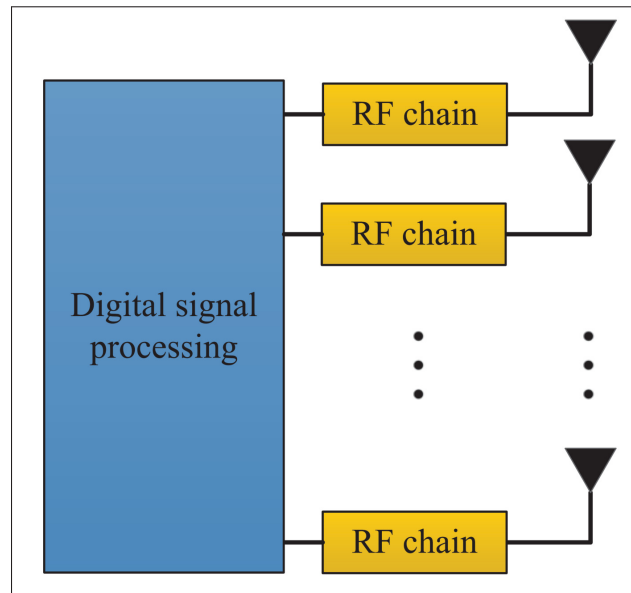
Figure 1.7    Fully digital MIMO architecture
Taken from Xiao *et al.* (2017)
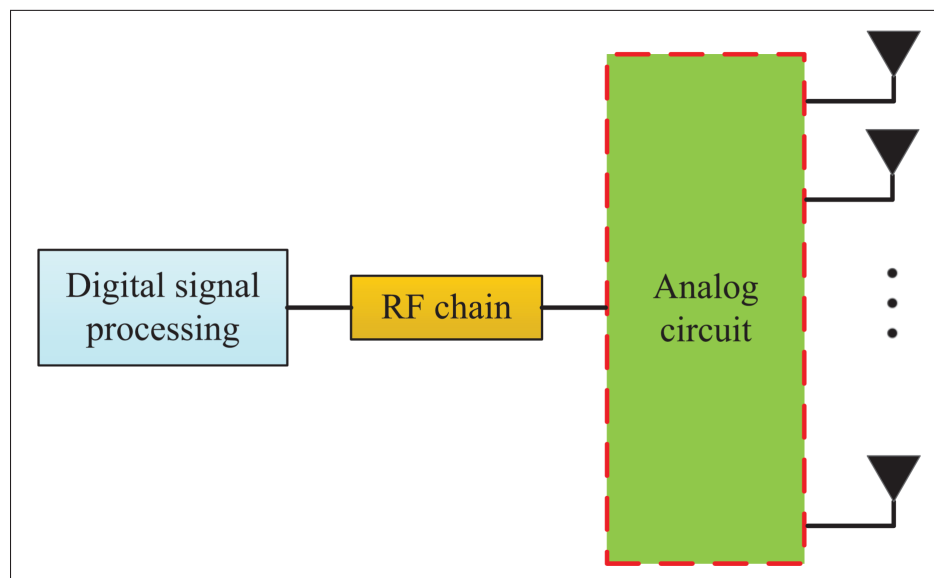


Figure 1.8    Fully analog MIMO architecture
Taken from Xiao *et al.* (2017)

number of independent data streams is less than the massive number of antennas. Since the
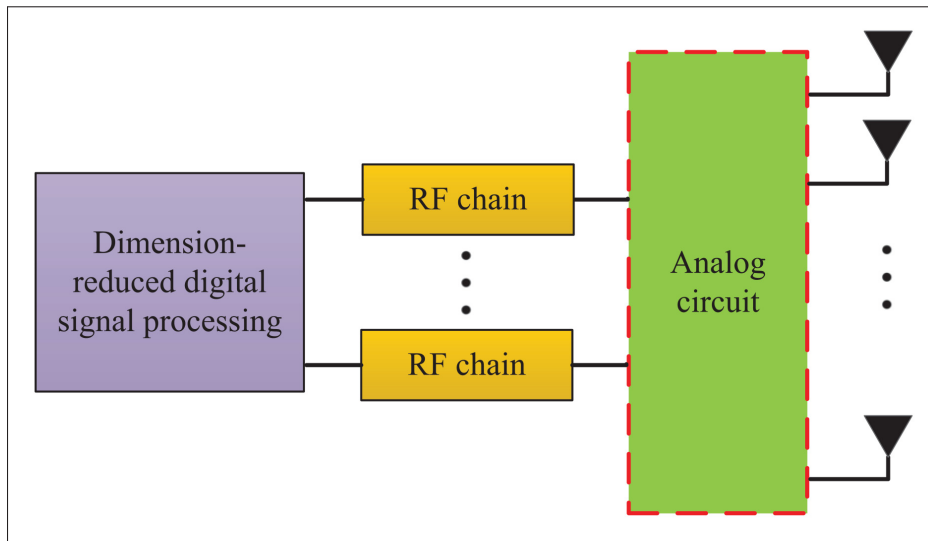
Figure 1.9   Hybrid MIMO architecture
Taken from Xiao *et al.* (2017)

number of data streams defines the minimum number of RF chains required for parallel data transmission, this makes hybrid architecture a much better fit.

The analog part of the hybrid architecture can be implemented in many different ways, each having its own constraints and limitations (Heath *et al.*, 2016; Méndez-Rial, Rusu, Alkhateeb, González-Prelcic & Heath, 2015; Méndez-Rial, Rusu, González-Prelcic, Alkhateeb & Heath, 2016). This difference in analog architectures affects not only the signal processing techniques but also the maximum theoretically achievable performance of massive MIMO systems. Following is a brief description of the two typical implementations of the analog part of the hybrid architecture.

1.  Fully-connected network with phase-shifters (El Ayach, Rajagopal, Abu-Surra, Pi & Heath, 2014)
    - Each RF chain connects to all antennas via phase-shifters.
    - Highly directive beams can be formed by adjusting the phases of the transmitted signals on all antennas.
    - Due to the finite resolution of phase-shifters, using a larger number of phase-shifters to form a beam would result in more phase noise which eventually degrades the performance.
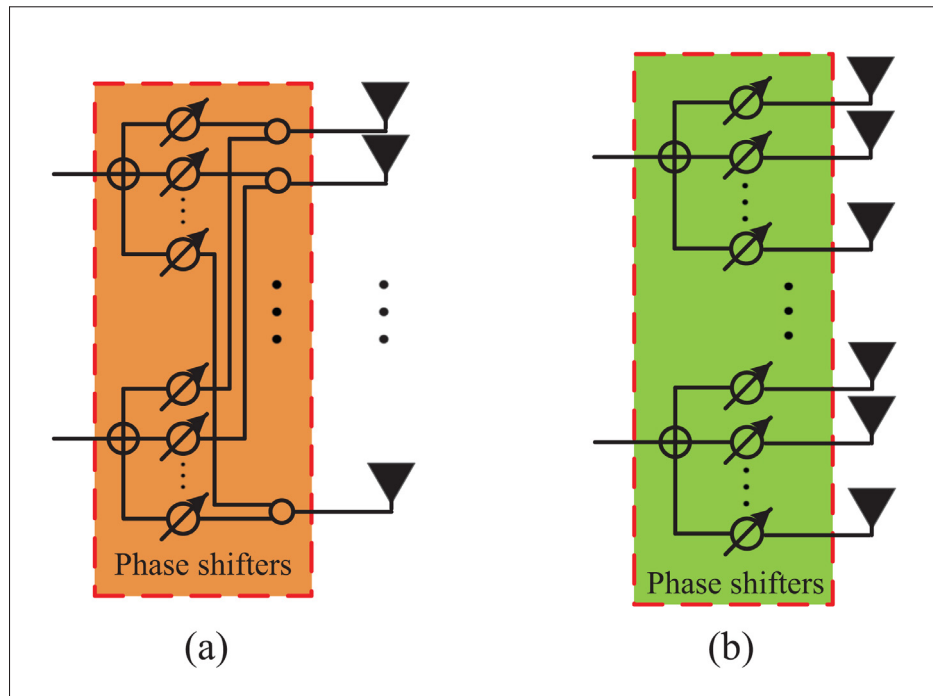
Figure 1.10    Analog circuits with different networks:
(a) Fully-connected network with Phase shifters; (b) Sub-connected
network with phase-shifters
Taken from Xiao *et al.* (2017)

- The most difficult factor with respect to the implementation is the sum of analog signals at each antenna element.

2.  Sub-connected network with phase-shifters (Han, Chih-Lin, Xu & Rowell, 2015; Gao, Dai, Han, Chih-Lin & Heath, 2016)

    - Each RF chain only connects to a subarray of antenna elements via phase-shifters.

    - For each RF chain, only a subset of the phase-shifters can be used to form a beam, which eventually results in relatively less array gain and directivity (i.e., proportional to the number of subarrays).

    - With respect to the implementation complexity, this network is simple to implement as there is no need to add analog signals at the input of antenna elements.

### 1.4.2 Beam-squinting

As discussed in section 1.4.1, phase-shifters play a vital role in the design of a communication system with fully analog MIMO architectures or hybrid MIMO architectures. Typically, these phase-shifters are configured at a particular frequency, usually the carrier frequency. Since it is impossible to configure phase-shifters for all the frequencies within the transmission band simultaneously, therefore same configuration (i.e., phase-shifter values for a carrier frequency) is applied to all the frequencies within the transmission band.

Phase-shifters are relatively good approximations to the ideal time shifters for narrowband communication systems. However, this approximation becomes invalid for wideband or ultra-wideband communication systems. Since the angle of arrival (AoA) of the received signal or the angle of departure (AoD) of the transmitted signal is far from the broadside, the required phase shifts become frequency-dependent. Consequently, a frequency component $f_0 + \Delta f$ points to $\theta_0 + \Delta\theta$ instead of $\theta_0$ , which was the beam direction at frequency $f_0$ (Cai, 2018; Mailloux, 2017). This squinting effect of frequency components other than the carrier frequency is called beam-squinting.

## 1.5 Mathematical tools and properties used

### 1.5.1 Fox's H-function

Fox's H-function is a generalization of a very well studied Meijer's G-function. Meijer introduced the G-function into mathematical analysis by using Mellin-Barnes integrals in 1946 (Mathai, Saxena & Haubold, 2009). In 1961, Charles Fox in his attempt to discover most generalized symmetrical Fourier kernel came up with the H-function (Fox, 1961). Three of the most important features of this mystical function are that: (i) many of the special functions in the same category of mathematical analysis are its special cases; (ii) the integral of the product of two H-functions is again a Fox's H-function (Mathai *et al.*, 2009; Kilbas, 2004); (iii) many

generalized channel models can be formulated in a compact form using H-functions (Kong, Kaddoum & da Costa, 2018a; Kong, Kaddoum & Vuppala, 2018b; Kong, 2019).

#### 1.5.1.1 The Univariate Fox's H-function

The univariate Fox's H-function is defined as follows (Mathai & Saxena, 1978)

$$H_{p,q}^{m,n}\left[x \left| \begin{array}{c} (a_i, A_i)_{i=1:p} \\ (b_l, B_l)_{l=1:q} \end{array} \right. \right] = \frac{1}{2\pi j} \int_{\mathcal{L}} \Theta(s) x^{-s} ds. \tag{1.3}$$

#### 1.5.1.2 The Bivariate Fox's H-function

Similarly, the bivariate Fox's $H$-function is defined as follows (Mathai & Saxena, 1978):

$$\begin{aligned} &H_{p,q;p_1,q_1;p_2,q_2}^{m,n;m_1,n_1;m_2,n_2}\left[x, y \left| \begin{array}{c|c|c} (a_i; \alpha_i, A_i)_{i=1:q} & (c_i, C_i)_{i=1:q_1} & (e_i, E_i)_{i=1:q_2} \\ (b_l; \beta_l, B_l)_{l=1:p} & (d_l, D_l)_{l=1:p_1} & (f_l, F_l)_{l=1:p_2} \end{array} \right. \right] \\ &= -\frac{1}{4\pi^2} \int_{\mathcal{L}_1} \int_{\mathcal{L}_2} \Theta(s, \xi)\Theta(\xi)\Theta_E(s) x^\xi y^s ds d\xi, \end{aligned} \tag{1.4}$$

where $\mathcal{L}_1$ and $\mathcal{L}_2$ are two suitable contours, $m, n, m_1, n_1, m_2, n_2, p, q, p_1, q_1, p_2, q_2$ are positive integers with constraints: $0 \le m \le q, 0 \le n \le p, 0 \le m_1 \le q_1, 0 \le n_1 \le p_1, 0 \le m_2 \le q_2,$ $0 \le n_2 \le p_2$. The sequence of parameters $\alpha_q, \beta_p, A_q, B_p, C_{q_1}, D_{p_1}, E_{q_2}$, and $F_{p_2}$ are real and positive numbers.

$$\Theta(s, \xi) = \frac{\prod\limits_{i=1}^{n_1} \Gamma(1 - a_i + \alpha_i s + A_i \xi) \prod\limits_{l=1}^{m_1} \Gamma(b_l - \beta_l s - B_l \xi)}{\prod\limits_{i=n_1+1}^{p_1} \Gamma(a_i - A_i s - A_i \xi) \prod\limits_{l=m_1+1}^{q_1} \Gamma(1 - b_l + B_l s + B_l \xi)}, \tag{1.5a}$$

$$\Theta(\xi) = \frac{\prod\limits_{i=1}^{m_1} \Gamma(d_l - D_l\xi) \prod\limits_{l=1}^{n_1} \Gamma(1 - c_i + A_i\xi)}{\prod\limits_{i=m_1+1}^{q_1} \Gamma(1 - d_l + D_l\xi) \prod\limits_{l=n_1+1}^{p_1} \Gamma(d_i - D_i\xi)}, \tag{1.5b}$$

$$\Theta(s) = \frac{\prod\limits_{i=1}^{m_1} \Gamma(f_l - F_l s) \prod\limits_{l=1}^{n_1} \Gamma(1 - e_i + E_i s)}{\prod\limits_{i=m_1+1}^{q_1} \Gamma(1 - f_l + F_l s) \prod\limits_{l=n_1+1}^{p_1} \Gamma(e_i - E_i s)}. \tag{1.5c}$$

### 1.5.1.3 Elementary properties of Fox's H-function

The two elementary properties of fox's H-function, which are repeatedly used in Chapter 2 are as follows.

$$H_{1,1}^{1,1}\left[ z \left| \begin{array}{c} -- \\ (b, \beta) \end{array} \right. \right] = \frac{1}{\beta} z^{b/\beta} \exp\left(-z^{1/\beta}\right). \tag{1.6}$$

$$\int_0^\infty t^{\eta-1} H_{p,q}^{m,n}\left[ zt^\sigma \left| \begin{array}{c} (a_i, \alpha_i)_{1,p} \\ (b_j, \beta_j)_{1,q} \end{array} \right. \right] H_{P,Q}^{M,N}\left[ wt^\sigma \left| \begin{array}{c} (c_i, \gamma_i)_{1,P} \\ (d_j, \delta_j)_{1,Q} \end{array} \right. \right] dt$$

$$= w^{-\eta} H_{p+Q,q+P}^{m+N,n+M}\left[ zw^{-\sigma} \left| \begin{array}{c} (a_i, \alpha_i)_{1,n}, (1 - d_j - \eta\delta_j, \sigma\delta_j)_{1,Q}, (a_i, \alpha_i)_{n+1,p} \\ (b_j, \beta_j)_{1,m}, (1 - c_i - \eta\gamma_i, \sigma\gamma_i)_{1,P}, (b_j, \beta_j)_{m+1,q} \end{array} \right. \right]. \tag{1.7}$$

## 1.6 Analysis of the Cell Association for Decoupled Wireless Access in a Two Tier Network

In this section we present an initial semi-analytical work on the decoupled wireless access. This work was published in the proceedings of IEEE 28th Annual International Symposium on Personal, Indoor, and Mobile Radio Communications (PIMRC), Montreal, QC, October, 2017 (Sattar, Evangelista, Kaddoum & Batani, 2017).

### 1.6.1 Abstract

In this paper, we analyze the association of a user terminal in a two-tier network (i.e., macrocells and millimeter wave small cells). We assumed a decoupled wireless access where a user terminal has the liberty to choose different base stations (BSs) for uplink and downlink based on the received power and the channel quality. A practical blockage model where a human body is a blocker to millimeter wave (mmWave) signals is considered. An in-depth simulation study is done to explore the effectiveness of decoupled wireless access in a crowded environment. In addition to that, a detailed analysis on the intuitiveness and the mathematical tractability of the blockage model used is also provided. In the end, few research questions on the efficacy of decoupled wireless access are raised in this paper.

### 1.6.2 Introduction and motivation

The network densification and the use of extremely high frequencies (EHF), commonly known as millimeter wave (mmWave) band, are the two most promising candidates for the future wireless access to fulfill the ever increasing demand of capacity. It is the small wavelength of mmWave which made it practical to increase the density of BSs significantly without any increase in the absurdly large footprint of conventional BSs (Andrews, Buzzi, Choi, Hanly, Lozano, Soong & Zhang, 2014). Although intuitively network densification in a heterogeneous network would sound a straight forward way to increase the capacity of the overall system, it also forces us to revisit some of the conventional techniques in cell planning and deployment of a communication system (Andrews, 2013; Boccardi, Heath, Lozano, Marzetta & Popovski, 2014).

Recently an idea to decouple the downlink (DL) and uplink (UL) BSs has been proposed (Boccardi *et al.*, 2016; Elshaer *et al.*, 2016). This idea not only flips the convention of coupled BSs (since the inception of mobile technology) but indirectly also questions the way we do channel estimation as it breaks the channel reciprocity by its very design. In (Boccardi *et al.*, 2016), Boccardi *et al.* argues on the efficacy of decoupled wireless access in hyper-dense heterogeneous networks. Though they also pointed out that without channel reciprocity in decoupled wireless access, the problem of channel estimation would become a bit more challenging, especially in the case of mmWave.

The susceptibility to blockage of mmWave makes it significantly different from all other standard wireless technologies. Since, electromagnetic waves cannot travel around any obstacle that exceeds their wavelength, various objects which had never been considered as blockers for microwave cause significant propagation losses for mmWave (Adhikari, 2008). Therefore to analyze the heterogeneous network with mmWave BSs, it is necessary to assume a blockage model which emulates the practical scenario mmWave faces. In the past couple of years, there has been some progress in blockage modeling for mmWave wireless access (Bai, Vaze & Heath, 2014; Singh, Kulkarni, Ghosh & Andrews, 2015; Kulkarni, Singh & Andrews, 2014). In this paper, we are using a very recently proposed blockage model which quantifies the effect of the human body on mmWave (Gapeyenko, Samuylov, Gerasimenko, Moltchanov, Singh, Aryafar, Yeh, Himayat, Andreev & Koucheryavy, 2016) to analyze the cell association in a decoupled wireless access.

The proposal of decoupled wireless access is getting considerable attention since its inception (Elshaer *et al.*, 2014) and authors in (Boccardi *et al.*, 2016; Elshaer *et al.*, 2016) made quite reasonable arguments in its favor. In this paper, we explore the efficacy of decoupled wireless access in an environment where the human body is considered as a blocker to mmWave wireless links. Since highly populated areas would be the one which will attract the deployment of mmWave networks to fulfill the ever increasing demand of wireless traffic, it is very important to study the effects of the human body on the decoupled wireless access.

The rest of the paper is organized as follows. In Section 1.6.3, we describe the system model in detail, which includes the propagation assumptions and a precise description of the blockage model used. In Section 1.6.4, a commentary on the mathematical feasibility of the considered blockage model is provided. In Section 1.6.5, discussion on the obtained simulation results is provided and Section 1.6.6 concludes the paper.

### 1.6.3 System Model

The system model consists of a two-tier heterogeneous cellular network, where sub-6GHz (i.e., conventional microwave or *mcell*) BSs and mmWave (i.e., *scell*) BSs are modeled using independent homogeneous Poisson point process (PPP) as shown in Fig.1.11. All the BSs are uniformly distributed in an area of concern (a circular area with radius $\mu$ ). We use $\Phi_k$ to denote the set of points obtained through PPP with density $\lambda_k$, which can be explicitly written as

$$\Phi_k \triangleq \{x_{k,i} \in \mathbb{R}^2 : i \in \mathbb{N}_+\}, \quad k \in \mathcal{K},$$

where the set $\mathcal{K} \triangleq \{scell, mcell\}$. All the user equipments (UEs) are assumed to form an independent PPP with density $\lambda_u$ and they are denoted by a set $\Phi_u$ given as

$$\Phi_u \triangleq \{u_j \in \mathbb{R}^2 : j \in \mathbb{N}_+\}.$$

Since the distribution of a point process is completely indifferent to the addition of a node at the origin, thanks to Slivnyak's theorem (Chiu, Stoyan, Kendall & Mecke, 2013), the analysis is done for a typical UE located at origin $u_j = (0, 0)$.

The summary of parameters and notations used in the rest of this paper is presented in Table 1.2.

Table 1.2  System parameters and their definitions

| Notation | Description |
|---|---|
| $P_{uk}$ | UE transmit power to BS in $k^{th}$ tier, where $k \in \{scell, mcell\}$ |
| $P_k$ | Transmit power of BS in $k^{th}$ tier, where $k \in \{scell, mcell\}$ |
| $T_k, T_k'$ | DL and UL association bias for $k \in \{scell, mcell\}$ |
| $\psi_k$ | The combination of antenna gain and near-field pathloss for $k \in \{scell, mcell\}$ |
| $L_{\min,k}$ | The minimum pathloss $||x||^{\alpha_k}$ of the typical UE from the $k^{th}$ tier |
| $\alpha_k$ | The pathloss exponent, for macrocell i.e., when $k = mcell$ its value remains constant. On the other hand for $k = scell$, pathloss exponent becomes a function of the distance between the transmitter and the receiver, and its value switches between line of sight (LOS) and non line of sight (NLOS) exponent values with the probability $P_{LOS}$ and $P_{NLOS}$, respectively |
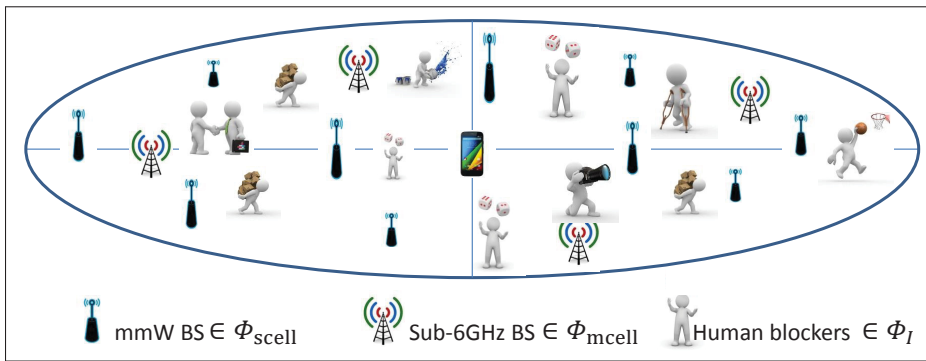


Figure 1.11  System Model

### 1.6.3.1  Propagation assumptions and cell association criteria

In our system model it is assumed that all the UEs and sub-6GHz BSs have omni directional antennas and antenna gains from a massive array of antenna elements are only accounted for the mmWave BSs. This is a realistic assumption in a sense that in such hybrid BSs' deployment, the sub-6GHz BSs will provide an umbrella coverage to all the UEs to guarantee a consistent service, whereas the mmWave BSs will mainly focus on high capacity links with individual UEs. Therefore the antenna gain is only considered with mmWave BS.

It is assumed that in both UL and DL, a typical UE associates with a BS based on the received power. The typical UE associates with a BS in UL at $x* \in \Phi_l$, where $l \in \{scell, mcell\}$ if and

only if

$$P_{ul}T'_l\psi_l L_l(x*)^{-1} \geq P_{uk}T'_k\psi_k L^{-1}_{\min,k}, \quad \forall k \in \{scell, mcell\}. \tag{1.8}$$

Similarly, a typical UE associates with a BS in DL at $x* \in \Phi_l$ if and only if

$$P_l T'_l\psi_l L_l(x*)^{-1} \geq P_k T'_k\psi_k L^{-1}_{\min,k}, \quad \forall k \in \{scell, mcell\}. \tag{1.9}$$

### 1.6.3.2 Blockage Model

In this paper, we use a very intuitive blockage model (Gapeyenko *et al.*, 2016), where a human body is considered as a blocker to mmWave. The potential blockers are generated using an independent homogeneous PPP $\Phi_I$ over the area of concern with intensity $\lambda_I$ as shown in Fig. 1.11. Each blocker is modeled as a cylinder with a certain height $H$ and a width $W$. Here, both the height and the width are generated randomly using the well researched statistical data (Ogden, Fryar, Carroll & Flegal, 2004).

Moreover, it is obvious from Fig. 1.12 that not all blockers can affect the LOS link between the transmitter and receiver. Therefore, we can model the PPP of blockers whose height can cause the LOS link to break by thinning the $\Phi_I$ with probability $Pr(H > h_m(x))$. The thinned PPP is denoted as $\Phi_{IB}$ with density $\lambda_{IB}$,

$$\lambda_{IB}(x) = \lambda_I Pr(H > h_m(x)), \quad x \in (0, r), \tag{1.10}$$

where $h_m(x)$ is a function describing the distance between the LOS link and the ground at $x$

$$h_m(x) = -\frac{h_T - h_R}{r}x + h_T. \tag{1.11}$$
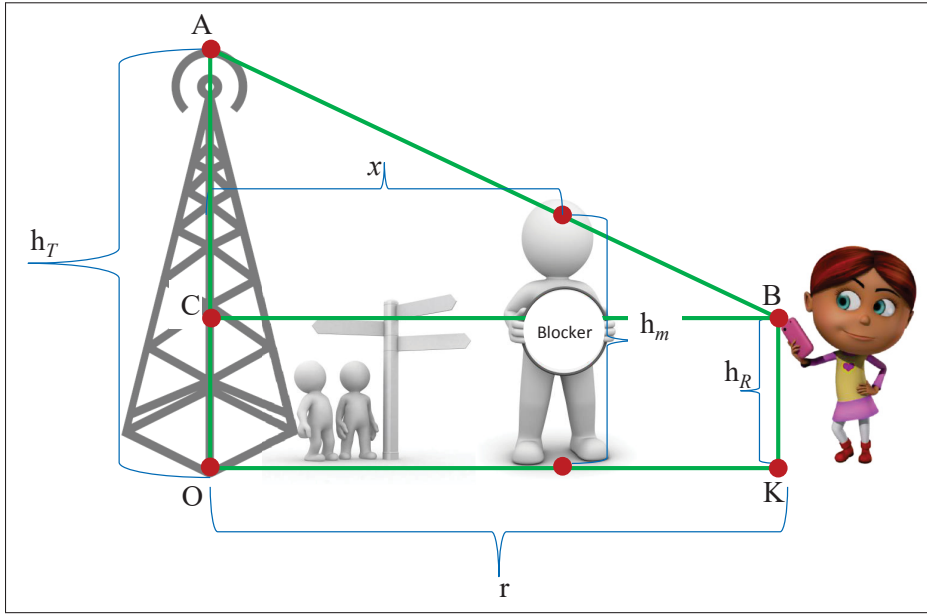
Figure 1.12    Blockage Scenario

And as shown in Fig. 1.12, $h_T$ and $h_R$ are the Tx and Rx heights, respectively. The aforementioned process $\Phi_{IB}$ is non-homogeneous but still remains Poisson with thinned density $\lambda_{IB}(x)$, which increases non-linearly as $x$ grows (Chiu *et al.*, 2013). The probability $Pr(H > h_m(x))$ is a complementary cumulative distribution function (CCDF) of $H$. Since, $H$ follows a Normal distribution (Ogden *et al.*, 2004), The probability $Pr(H > h_m(x))$ takes the following form

$$Pr\left(H > h_m\left(x\right)\right) = 1 - \frac{1}{2}\left[1 + \mathrm{erf}\left(\frac{h_m\left(x\right) - \mu_H}{\sigma_H\sqrt{2}}\right)\right], \tag{1.12}$$

where erf(.) is the error function, and $\mu_H, \sigma_H$ are mean and variance of $H$, respectively.

For the mathematical formulation of the probability of LOS ($P_{\mathrm{LOS}}$) we have to determine the probability of few events described in Table 1.3.

Having defined all the events and probabilities, $P_{\mathrm{LOS}}$ can be formulated as follows:
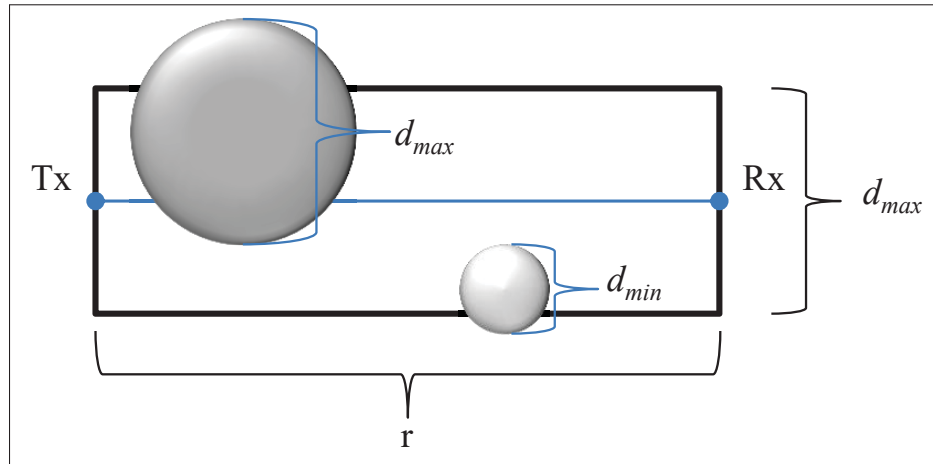
Figure 1.13    Top view of the blockage scenario

Table 1.3    Probabilistic events and their definitions

| Events | Description |
|--------|-------------|
| $A_i$ | There are $i$ blockers in the area of interest |
| $B_0$ | Diameter of the blocker is not large enough to cross the LOS link |
| $B_1$ | Complementary to $B_0$ |
| $C_0$ | Blocker's height is not large enough to block the LOS link |
| $C1$ | Complementary to $C_0$ |

$$P_{\text{LOS}} = Pr\{A_0\} + \sum_{i=1}^{\infty} Pr\{A_i\} \cdot [Pr\{B_0\} + Pr\{B_1\}Pr\{C_0\}]^i, \qquad (1.13)$$

where the first part of the equation $Pr\{A_0\}$ is the probability that there are no blockers in the area of interest and the second part of the equation sums the probability in the event that there are $i$ blockers in the area of interest, but their width and height are not enough to block the LOS link. A rectangular area shown in Fig. 1.13 is considered where the widths of all blockers are uniformly distributed between $d_{min}$ and $d_{max}$, therefore, the width of this area is bounded by $d_{max}$. As mentioned in the start of this section, the number of blockers follow a Poisson distribution, hence, the number of blockers in the area of concern follows a Poisson distribution with intensity

$\lambda_I r d_{max}$. Having defined all the necessary assumptions, the mathematical expressions of the aforementioned events can be easily formulated as in (Gapeyenko *et al.*, 2016).

Even though this blockage model is intuitive in nature, and it can accurately emulate a crowded environment (Gapeyenko *et al.*, 2016), and so far, there is no closed-form expression for this model. To the best of our knowledge, it is mathematically intractable to provide a closed-form expression of $P_{LOS}$, as its expression contains a double integral of an erf function. Since, it is a well known fact that, mathematically, it is extremely difficult to approximate an integral of erf over a wide range of values (which is the case here); hence, further discussion on the efficacy, intuitiveness, and mathematical intractability of this blockage model in calculating the association probabilities is provided in the following section.

### 1.6.4 Analytical Analysis

In this section expressions for the association probability for a typical user in the human blockage model scenario are derived. In the association scenario under analysis there are two random variables to be considered; these are the associated tier for uplink $\mathcal{A}_{UL}$ and the associated tier for downlink $\mathcal{A}_{DL}$. Considering the model proposed in Section 1.6.3 with two tiers there are four possible outcomes:

- $\mathcal{A}_{UL} = mcell, \mathcal{A}_{DL} = mcell$
- $\mathcal{A}_{UL} = mcell, \mathcal{A}_{DL} = scell$
- $\mathcal{A}_{UL} = scell, \mathcal{A}_{DL} = mcell$
- $\mathcal{A}_{UL} = scell, \mathcal{A}_{DL} = scell$

Since the events $\mathcal{A}_{UL}$ and $\mathcal{A}_{DL}$ are independent, the derivation of the probabilities $Pr(\mathcal{A}_{UL} = mcell)$, $Pr(\mathcal{A}_{UL} = scell)$, $Pr(\mathcal{A}_{DL} = mcell)$ and $Pr(\mathcal{A}_{DL} = scell)$ are enough to calculate the probabilities of the four possible outcomes. Furthermore, the user only associates to one base station for uplink and one for downlink, therefore

$$Pr(\mathcal{A}_{UL} = mcell) \quad = \quad 1 - Pr(\mathcal{A}_{UL} = scell), \tag{1.14}$$

and

$$Pr(\mathcal{A}_{\text{DL}} = mcell) \quad = \quad 1 - Pr(\mathcal{A}_{\text{DL}} = scell). \tag{1.15}$$

As seen in equations (1.8) and (1.9) the base station to which the user associates depends on the minimum path loss of the typical UE from the $k^{th}$ tier, thus, in order to derive the probabilities of association, the point process obtained from the path loss between the typical user and each base station must be characterized. Following a similar approach to (Elshaer *et al.*, 2016), the path loss point process is defined as

$$\mathcal{P}_k : \{L_k(x) = \|x\|^{\alpha_k(\|x\|)}\}_{x \in \Phi_k} \text{ , for } k \in \{scell, mcell\}. \tag{1.16}$$

From the displacement theorem (Błaszczyszyn, Karray & Keeler, 2013), $\mathcal{P}_k$ is a Poisson point process with intensity measure $\Lambda_k(\cdot)$ and CCDF

$$\bar{F}_{L_k}(t) = Pr(L_k(x) \geq t) = \exp(-\Lambda_k([0, t])). \tag{1.17}$$

**Lemma 1.1.** *The intensity measure of the path loss process of the tagged BS for tiers* 1 *and* 2 *are given by*

$$\Lambda_m([0, t]) \quad = \quad \pi \lambda_m t^{\frac{2}{\alpha_m}}, \tag{1.18}$$

$$\Lambda_s([0, t]) \quad = \quad 2\pi \lambda_s \left[ \int_0^{t^{\frac{1}{\alpha_{LOS}}}} r P_{LOS}(r) dr + \int_0^{t^{\frac{1}{\alpha_{NLOS}}}} r(1 - P_{LOS}(r)) dr \right]. \tag{1.19}$$

*Proof.* The proof for the macro cell case (1.18) is available on (Elshaer *et al.*, 2016). For the scell (mmWave) we have that the intensity of the path loss process $\mathcal{P}_s : \{L_s(x) = \|x\|^{\alpha_s(\|x\|)}\}_{x \in \Phi_s}$ is given by

$$\Lambda_s([0,t]) \;=\; \lambda_s \int_{R^2} Pr(L_s(x) < t)dx.$$

Switching to polar coordinates leads to

$$\Lambda_s([0,t]) \;=\; 2\pi\lambda_s \int_0^\infty Pr(r^{\alpha_2(r)} < t)r\,dr.$$

As described in Section 1.6.3 $\alpha_s(r)$ is equal to $\alpha_{\text{LOS}}$ with probability $P_{\text{LOS}}$ and $\alpha_{\text{NLOS}}$ with probability $1 - P_{\text{LOS}}$. Thus, we have

$$\begin{aligned}
\Lambda_s([0,t]) \;=\; 2\pi\lambda_s \Bigg[ &\int_0^\infty r P_{\text{LOS}}(r)1(r < t^{\frac{1}{\alpha_{\text{LOS}}}})dr \\
&+ \int_0^\infty r(1 - P_{\text{LOS}}(r))1(r < t^{\frac{1}{\alpha_{\text{NLOS}}}})dr \Bigg],
\end{aligned} \tag{1.20}$$

which leads to (1.19). ∎

From (1.18) and (1.17) it is possible to obtain the probability density function (PDF) as

$$f_{L_m}(t) = -\frac{d\bar{F}_m(t)}{dt} = \frac{2\pi\lambda_m t^{\frac{2}{\alpha_m}-1}}{\alpha_m} \exp(-\pi\lambda_m t^{\frac{2}{\alpha_m}}). \tag{1.21}$$

For the millimeter wave scell tier the CCDF is given by

$$\bar{F}_{L_s}(t) = \exp\left[-2\pi\lambda_s\left(\int_0^{t^{\frac{1}{\alpha_{\text{LOS}}}}} rP_{\text{LOS}}(r)dr + \int_0^{t^{\frac{1}{\alpha_{\text{NLOS}}}}} r(1 - P_{\text{LOS}}(r))dr\right)\right]. \qquad (1.22)$$

By manipulating (1.8) and (1.9) it is possible to obtain an expression for the probability of associating to the macro cell in the uplink and in the downlink as

$$\begin{aligned} Pr(\mathcal{A}_{\text{UL}} = mcell) &= Pr(L_{\min,scell} > a_{\text{UL}}L_{\min,mcell}) \\ &= \frac{1}{a_{\text{UL}}}\int_0^\infty \bar{F}_{L_s}(l)f_{L_m}\left(\frac{l}{a_{\text{UL}}}\right)dl, \end{aligned} \qquad (1.23)$$

and

$$\begin{aligned} Pr(\mathcal{A}_{\text{DL}} = mcell) &= Pr(L_{\min,scell} > a_{\text{DL}}L_{\min,mcell}) \\ &= \frac{1}{a_{\text{DL}}}\int_0^\infty \bar{F}_{L_s}(l)f_{L_m}\left(\frac{l}{a_{\text{DL}}}\right)dl, \end{aligned} \qquad (1.24)$$

where

$$a_{\text{UL}} = \frac{P_{u,scell}T'_{scell}\psi_{scell}}{P_{u,mcell}T'_{mcell}\psi_{mcell}},$$

and

$$a_{\text{DL}} = \frac{P_{scell}T_{scell}\psi_{scell}}{P_{mcell}T_{mcell}\psi_{mcell}}.$$

As the calculation of $P_{\text{LOS}}(r)$ is not obtained in closed-form and involves the numerical evaluation of three integrals, it is not feasible to obtain a closed-form expression for $\bar{F}_{L_s}(t)$ as well. Considering the intractability of calculating $\bar{F}_{L_s}(l)$ due to the blockage model, a simulation approach is taken to characterize the probabilities of association under this blockage model.

### 1.6.5   Simulation results

#### 1.6.5.1   Simulation setup

A system-level simulation model is developed to mimic the real scenario of association between a UE and its tagged BS(s) in a decoupled wireless access environment. The simulation model not only provides the association probabilities of a particular UE with its tagged BS(s) but it also gives an insight on the portability of having a decoupled wireless access.

We generated the blockers, the mmWave BSs, and the sub-6GHz BSs in a circular area of radius $\mu$ as described in Section 1.6.3. In case of mmWave wireless access, for the sake of consistency with previous published work (Gapeyenko *et al.*, 2016) the height of the transmitter and the receiver are assumed to be 4m and 1.3m, respectively. As described in section 1.6.3.2, each generated blocker has a random height and width, following (Gapeyenko *et al.*, 2016), the height and width of the blockers are generated using a normal $\mathcal{N}(\mu_H, \sigma_H)$ and uniform $\mathcal{U}(d_{min}, d_{max})$ distributions, respectively. Here, $\mu_H, \sigma_H, d_{min}$, and $d_{max}$ are assumed to be 1.7m, 0.1m, 0.2m, and 0.8m, respectively. The rest of the parameters used in the simulation are similar to what was used in (Elshaer *et al.*, 2016).

#### 1.6.5.2   Discussion

As already mentioned in section 1.6.4, the blockage model under consideration has no closed-form expression which made further analytical analysis mathematically intractable. Nevertheless, its practical nature is still very useful. For example, it is obvious that the average distance between the transmitter and the receiver is a function of the intensity of blockers $\lambda_I$. This implies that the optimal height of the Tx of *scell* BS to minimize the average pathloss is also a function of $\lambda_I$, as the optimal height of the Tx depends on the average distance between Tx and Rx. Using this blockage model we can easily predict the optimal height of the Tx of *scell* BSs for different urban environments as shown in Fig. 1.14. The dashed curve in Fig. 1.14, which is intersecting all the other curves shows the optimal height of the Tx for different values of
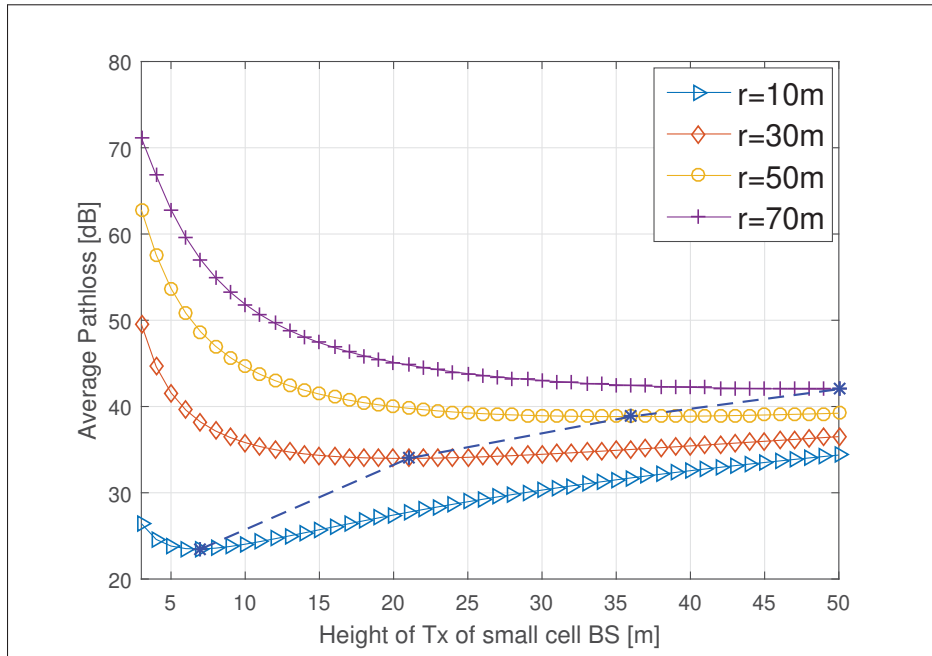
Figure 1.14    Average pathloss vs optimal Tx height for different r
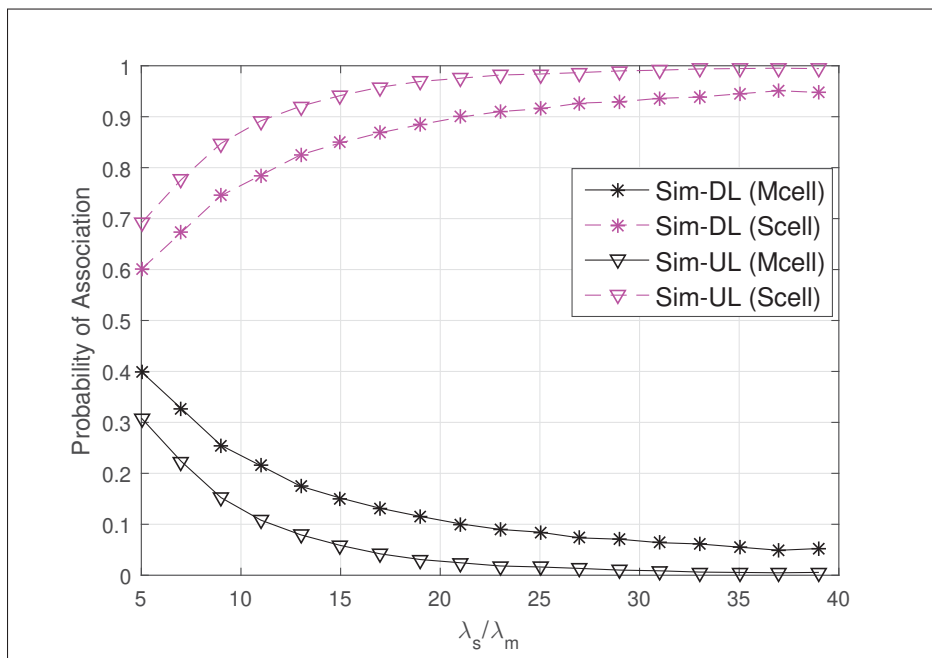


Figure 1.15    Association probability for antenna gain = 30dBi, and
blockers intensity $\lambda_I = 0.3$ blockers/$m^2$
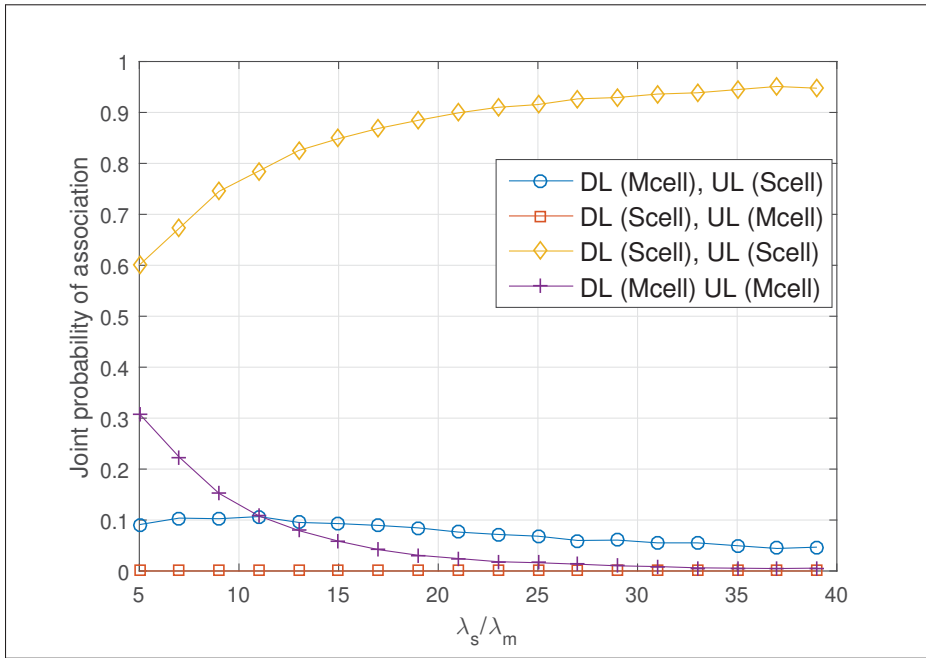
Figure 1.16 Joint association probability for antenna gain = 30dBi, and blockers intensity $\lambda_I = 0.3$ blockers/$m^2$

the distance $r$. Here, we want to emphasize on the fact that choosing the optimal height of the Tx in *scell* is extremely important because it makes a huge difference in the average pathloss. Therefore, any arbitrary height of the Tx can make or break the connection completely. Hence, in our opinion Txs for the next generation of wireless access should be designed to adjust their heights in real-time according to the density of blockers $\lambda_I$.

The association probabilities of a UE with two tiers of BSs are shown in Fig. 1.15 and Fig. 1.17. Meanwhile Fig. 1.16 and Fig. 1.18 show the joint probabilities of four possible association scenarios of a particular UE as mentioned in Section 1.6.4. It is obvious from the simulation results in Fig. 1.15, Fig. 1.16, Fig. 1.17, and Fig. 1.18 that the antenna gain has a significant impact on the efficacy of decoupled wireless access. A higher antenna gain (which would be the case in future mmWave BSs) significantly reduces the decoupling gain (i.e., when a UE chooses to select two different types of BSs in DL and UL).
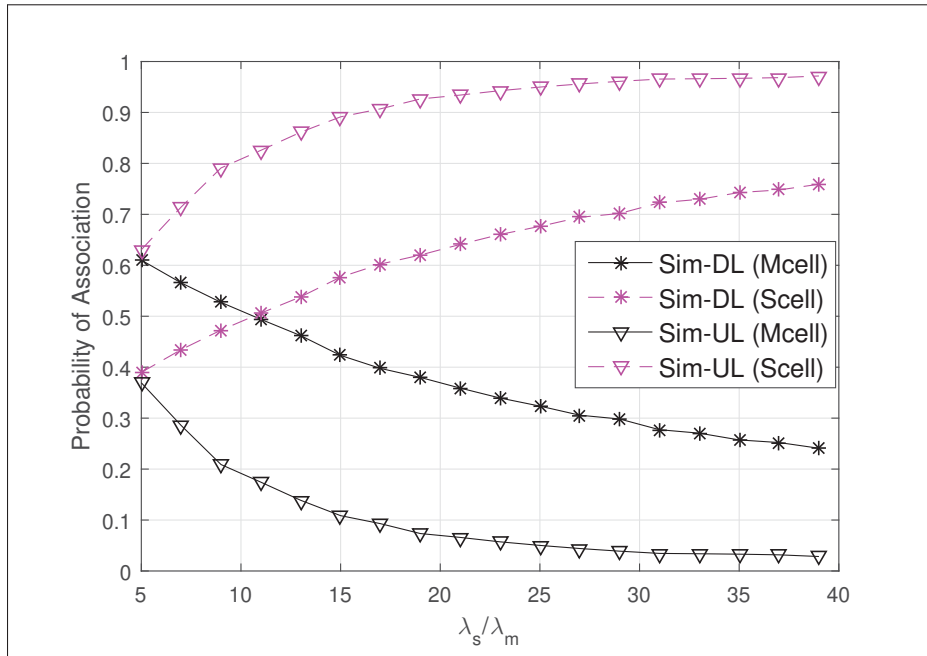
Figure 1.17   Association probability for antenna gain = 18dBi, and
blockers intensity $\lambda_I = 0.3$ blockers/$m^2$

Moreover, an interesting observation that we can be made from Fig. 1.16 and Fig. 1.18 is that
the joint association probability of an event when a particular UE connects to scell in DL and
mcell in UL is zero. This contradicts the argument made in (Boccardi *et al.*, 2016) in support to
decoupled wireless access; which is that for future generation of wireless network, more UEs
will connect with scell in DL for higher data rate and mcell will provide an umbrella coverage as
well as UL connection to decoupled UEs. Although, their argument was based on the difference
between the allowed transmit power for mmWave and microwave UEs, this difference would
not be enough to make the joint probability of aforementioned event to non-zero (Colombi,
Thors & Törnevik). Mathematically, using equations (1.23) and (1.24), we can formulate the
joint probability of the aforementioned event as $Pr(L_{\min,s} < a_{DL}L_{\min,m}; L_{\min,s} > a_{UL}L_{\min,m})$.
Since, in general $a_{UL} > a_{DL}$, the joint association probability of that event will remain zero.

Even though power biasing can be used to change the inequality $a_{UL} > a_{DL}$ and also to do load
balancing between the two tiers of network, which would definitely increase the decoupling
gain, it would also result in a decrease in the sum-capacity of the overall network. Besides that,
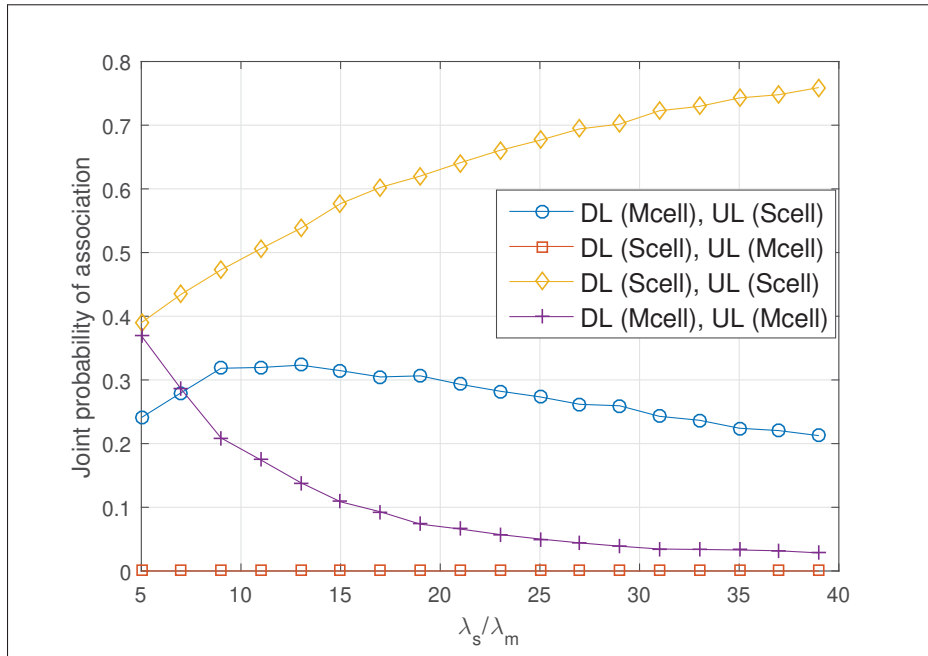
Figure 1.18    Joint association probability for antenna gain =
18dBi, and blockers intensity $\lambda_I = 0.3$ blockers/$m^2$

decoupled wireless access kills the channel reciprocity by its very design, which would force the network to bear the additional cost of control signals. Therefore, the answer to the question of how much pragmatic this idea can be for future wireless networks will solely depend on an in depth cost analysis of additional control signals. Furthermore, if the industry decides to stick with the time division duplexing (TDD), we believe that the future of decoupled wireless access will remain ambiguous.

### 1.6.6    Conclusion

We derive the following conclusions from this study. Firstly, despite the fact that the considered blockage model is mathematically intractable, which makes it infeasible for stochastic geometric analysis of wireless networks, still its practical nature provides some interesting insights. For example, tuning of Tx height with respect to the density of blockers or association biasing for load balancing. Secondly, the decoupling gain in our studied scenario is not very significant. Therefore, whether we should bear the cost of extra control signaling for decoupled wireless

access solely depends on a cost analysis of additional control signals, and only then anything on its pragmatism can be said. Lastly, if TDD becomes a standard for next generation wireless networks, then the future of decoupled wireless access is certainly very bleak.

# CHAPTER 2

# SPECTRAL EFFICIENCY ANALYSIS OF THE DECOUPLED ACCESS FOR DOWNLINK AND UPLINK IN TWO TIER NETWORK

Zeeshan Sattar[a] , Joao V.C. Evangelista[b] , Georges Kaddoum[c] , Naïm Batani[d]

[a,b,c,d]Department of Electrical Engineering, École de Technologie Supérieure, 1100 Notre-Dame Ouest, Montréal, Québec, Canada H3C 1K3

## 2.1   Abstract

This paper analyzes the efficacy of decoupled wireless access in a two-tier heterogeneous network. The decoupled wireless access and its performance benefits have been studied in different scenarios recently. In this paper, an in-depth analysis on its efficacy from spectral efficiency perspective is provided. To achieve this task, (i) new closed form expressions for probability of association of user equipment with different tiers employing different frequency bands (i.e., microwave and millimeter wave) with different pathloss exponents are derived using univariate Fox's H-functions; (ii) Distributions of the distance to the serving base stations are also derived; (iii) Exact expressions of spectral efficiency for different association cases are further obtained using bivariate Fox's H-functions. Furthermore, rigorous simulation results are provided which validate the aforementioned analytical results. In addition to that, a detailed discussion on the decoupling gain of decoupled wireless access and its efficacy is also provided. Lastly, despite the improvement provided by the decoupled wireless access, which is evident from the results presented in this paper, few questions are raised on its pragmatic value.

## 2.2   Introduction

What shape the next generation of communication systems will take is a question which can not be answered in one line or in other words there can never be just one answer to this question. The evolution of technology and recent advancement in the available computing power gave

us plenty of room to think out of the box. Therefore, when the research community brought fifth generation (5G) of communication systems on the table, lots of innovative ideas came into existence (Ge, Tu, Mao, Wang & Han, 2016). Few of them will definitely see the light of the practical world and many of them will get lost somewhere inside the research laboratories of academia only to be found again on a later date for another generation of communication systems. The main quest of 5G is to provide seamless coverage, hot-spot high capacity, low end to end latency, and massive connections (Andrews *et al.*, 2014; Yang, Mao, Ding, Ge & Tao, 2018). To meet these requirements two of the most promising candidates are the network densification and the use of extremely high frequencies (EHF) which are commonly known as millimeter wave (mmWave) band. Here, the network densification refers to the paradigm shift of single-tier homogeneous cellular networks towards multi-tier heterogeneous cellular networks (HetNets) (Andrews *et al.*, 2012). In HetNets, different tiers of base stations (BSs) typically use different transmit powers which result in significantly different interference levels (Andrews, 2013). Therefore whether the conventional way of cell association i.e., coupled access, where a user connects to a single BS for both uplink and downlink transmission would be optimal in HetNets came under scrutiny of the research community.

Since the inception of cellular communication systems, coupled access is the only way for any user equipment (UE) to connect to a BS. This conventional way of association to a BS recently has been challenged in form of decoupled wireless access (Elshaer *et al.*, 2014; Boccardi *et al.*, 2016; Elshaer *et al.*, 2016). The concept of decoupled wireless access argues on the optimality of choosing the same BS for both uplink and downlink transmissions, and proposes to give the liberty to UEs to simultaneously connect to two different BSs from any two different tiers of BSs for uplink and downlink transmissions. Though, both intuition and probability theory supports this idea for a simple fact that if we increase the size of the set of BSs to choose from, it would definitely result in a better performance in terms of coverage and spectral efficiency. In addition, the decoupled wireless access also breaks the channel reciprocity by its very design, so indirectly it also raises questions on the way we typically estimate the channel. Therefore, despite the potential benefits of the decoupled wireless access as it is evident in theory, its pragmatic value

is still in question (Sattar *et al.*, 2017). This inspires us to scrutinize the potential benefits of the decoupled wireless access and compare it to the conventional coupled access. To make things mathematically simple and tractable yet robust, we didn't employ any blockage model but used different pathloss exponents and transmit powers to emulate the characteristics of two different kinds of BSs (i.e., microwave BSs and mmWave BSs) operating in different tiers.

The rationale behind omitting the blockage model is depicted in (Sattar *et al.*, 2017) which is an early study for this work, where a very practical blockage model was used as described in (Gapeyenko *et al.*, 2016). We reached to the conclusion that though it does add the pragmatic value to the analytical model, it does not significantly affect the analysis of the average spectral efficiency. More detailed discussion on this assumption is given in section 2.3.1.

### 2.2.1   Related Work

The idea of multi-tier cellular system is not new and it has been under the lens of both academia and industry for a long time. For example, authors in (Chandrasekhar, Kountouris & Andrews, 2009) investigated the case of two-tier cellular systems with universal frequency reuse. They study the case of single user (SU) and multi-user (MU) multiple antenna methods to mitigate cross-tier interference and the 'near-far' deadspot coverage in a two tier network. They further provided location-assisted power control scheme for regulating femtocell BSs transmit powers.

Even though a lot of work has been done on the performance analysis of cellular systems, the scientific community is still working on new theoretical tools to evaluate the network performance of cellular systems. For example, authors in (Ge, Yang, Ye, Mao, Wang & Han, 2015) proposed new spatial spectrum and energy efficiency models for Poisson-Voronoi tessellation (PVT) random cellular networks. In (Di Renzo, 2015), the author provided a very detailed mathematical framework based on stochastic geometry to model multi-tier millimeter wave cellular network. An exact analytical model to derive coverage probability and average rate in form of numerical integrations are derived. Furthermore, to provide results in closed-form, approximated analytical

models are also derived. In addition to that, a detailed discussion on the noise-limited approximation for typical millimeter wave network deployments is also provided.

Recently there has been significant amount of progress on the analysis of the decoupled wireless access (Zhang, Nie, Feng, Zheng & Qin, 2017; Li, Luo, Jiang & Jin, 2018b; Shi, Yang, Xing & Fan, 2018; Aravanis, Pascual-Iserte & Munoz-Medina, 2018). Right after its proposal in (Elshaer *et al.*, 2014), the first analytical analysis of the decoupled wireless access has been done by Smiljkovikj *et al.* in (Smiljkovikj, Popovski & Gavrilovska, 2015b; Smiljkovikj, Gavrilovska & Popovski, 2015a).

In (Smiljkovikj *et al.*, 2015b), Smiljkovikj *et al.* analyzed a two-tier network with macro cells and small cells. They provided analytical expressions for probability of associations of UEs to different tiers and average throughput of UEs associated to different tiers. In (Smiljkovikj *et al.*, 2015a), the authors provided a deeper analysis on the benefits of the decoupled wireless access by analyzing its spectral and energy efficiencies.

In a more recent work (Zhang *et al.*, 2017), the authors provided a comparative analysis of the decoupled and the coupled wireless access for two kinds of UE's distributions, namely uniform and clustered distributions, which are modeled as Poisson point and Neyman–Scott cluster processes, respectively. They borrowed analytical expressions of probability of cell association and distance distribution of a UE and its serving BS from (Jo, Sang, Xia & Andrews, 2012) and derived new analytical expressions for average user rate for two UE's distributions.

In (Li *et al.*, 2018b), the authors analyzed the decoupled wireless access in multiuser multiple-input multiple-output (MIMO) HetNet scenario. They derived cell association probabilities with respect to the load balancing in BSs. They also compared the decoupled and coupled wireless access based on the load balancing in BSs and provided new analytical expressions for uplink spectral efficiency. Moreover, they also derived the lower bounds on the uplink spectral efficiency where interference is shown to be suppressed by multiple antennas at BSs.

In (Shi *et al.*, 2018), the authors provided a theoretical work on the impact of decoupled access in multi-tier HetNet. Using tools from stochastic geometry they derived general expression of association probability to a particular tier of BSs. Furthermore, a detailed analytical work on the impact of decoupled access on the coverage probability is also provided.

In (Aravanis *et al.*, 2018), the authors derived analytical bounds in closed form for the uplink ergodic capacity as a function of the density of BSs of different tiers for the decoupled access scenario. The novelty of their work is to accommodate the backbone network congestion and the synchronization of the acknowledgments of the decoupled channels into their analytical expression.

A semi-analytical analysis of the decoupled wireless access is provided in (Sattar *et al.*, 2017). The decoupled and coupled wireless access are compared for two-tier network employing a realistic blockage model proposed in (Gapeyenko *et al.*, 2016), where human body is considered as a blockage to a tier of BSs operating on mmWave frequencies. Despite the practical nature of the blockage model used, authors came to this conclusion that it made the analytical analysis intractable. Therefore authors in (Elshaer *et al.*, 2016) used a rather simple blockage model proposed in (Singh *et al.*, 2015) to develop a general analytical model to characterize and derive the uplink and downlink cell associations. Even for that simple blockage model, there analytical expressions for the cell association are too complicated for further analysis. For example, to study the distance distribution of a UE to its serving BS and to derive the expressions for spectral efficiency based on the analytical model in (Elshaer *et al.*, 2016), the only option is to solve a plethora of nested numerical integrations.

### 2.2.2 Novelty and Contributions

The main goal of this paper is to investigate the spectral efficiency gain of the decoupled wireless access over its coupled counterpart. Additionally it provides more compact and robust analytical model. The novelty of our analytical analysis is the fact that it accommodates variable transmit powers and different pathloss exponents for different tiers in its formulation. Moreover, instead of

a plethora of numerical integrations, Fox's H-function and its integration properties are used to solve numerical integrations into compact form. We believe that the proposed analytical model provides valuable insights into the mathematical analysis of the problem under consideration and several other related work. Furthermore, one can easily compute the first and second order derivatives of Fox's H-function, which are often used in numerical optimization methods (Kilbas, 2004). The insights obtained from the outcome of this paper, regarding the solution of complex numerical integrations into Fox's H-function form would inspire researchers to provide compact analytical models. The key contributions of this paper are listed as follows.

- New closed form expressions of joint probability of uplink and downlink cell associations are derived for a two-tier network.

- Univariate Fox's H-function is used in our analytical closed form expression to accommodate different pathloss exponents and variable transmit powers for different tiers (i.e., conventional mircowave BSs and mmWave BSs).

- The distance distributions of a UE to its serving BSs are also derived for three possible cases of the cell associations.

- Finally exact expressions of spectral efficiencies for three possible cases of cell association are derived using bivariate Fox's H-function. The motivation to use Fox's H-function is to formulate analytical expressions in compact and modular form[1]. In addition to that, three of the most important features of this function are: (i) many of the special functions in similar category of mathematical analysis are its special cases; (ii) the integral of the product of two H-functions is again a Fox's H-function (Mathai *et al.*, 2009; Kilbas, 2004); (iii) many generalized channel models can be formulated in a compact form using H-functions (Kong *et al.*, 2018a,b; Jeong, Shin & Win, 2015).

### 2.2.3  Organization

The rest of the paper is organized as follows.

---

[1]  The univariate Fox's H-function is implemented for Mathematica in (Yilmaz & Alouini, 2009; Ansari, Yilmaz & Alouini, 2013), and for MATLAB in (Peppas, Lazarakis, Alexandridis & Dangakis, 2012), whereas the implementation of the bivariate Fox's H-function is given for MATLAB in (Peppas, 2012).

In Section 2.3, the system model is described in detail, which includes the propagation assumptions and cell association criteria. In Section 2.4, the joint association probabilities, distance distributions of a typical UE and its serving BSs are derived. Furthermore, analytical expressions for average user rates and spectral efficiencies are also provided in this section. In Section 2.5, discussion on the obtained numerical and simulation results is provided and Section 2.6 concludes the paper.

## 2.3 System Model
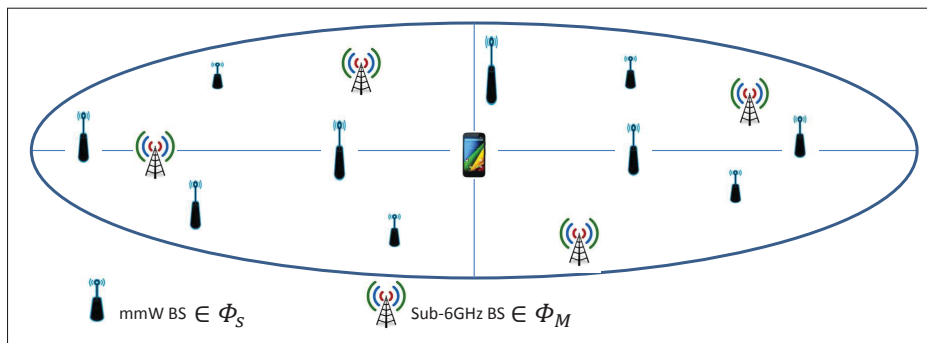


Figure 2.1    System Model

We consider a two-tier HetNet, where sub-6GHz (i.e., conventional microwave or $Mcell$) BSs and mmWave (i.e., $Scell$) BSs are modeled using independent homogeneous Poisson point process (PPP) as shown in Fig. 2.1. All the BSs are uniformly distributed in a circular area with radius $\mu$. We use $\Phi_k$ to denote the set of points obtained through PPP with density $\lambda_k$, that can be explicitly written as

$$\Phi_k \overset{\Delta}{=} \{x_{k,i} \in \mathbb{R}^2 : i \in \mathbb{N}_+\},$$

where the index $k \in \{M, S\}$) for $Mcell$ and $Scell$ BSs, respectively. Moreover, all the UEs are also assumed to form an independent PPP with density $\lambda_u$ and they are denoted by a set $\Phi_u$ given as

$$\Phi_u \overset{\Delta}{=} \{u_j \in \mathbb{R}^2 : j \in \mathbb{N}_+\}.$$

The transmit powers for downlink and uplink transmissions are $P_M$ and $Q_M$, respectively, for the tier of *Mcell* BSs. Similarly, for the tier of *Scell* BSs, $P_S$ and $Q_S$, respectively, are the transmit powers for downlink and uplink transmissions. Besides that, since the distribution of a point process is completely indifferent to the addition of a node at the origin, allowed by Slivnyak's theorem (Chiu *et al.*, 2013), the analysis is done for a typical UE located at $u_j = (0,0)$.

### 2.3.1 Propagation Assumptions

In this subsection all the major assumptions critical to the analytical analysis are listed.

- As mentioned in section 2.2, the rationale behind the assumption about blockage model is that for the higher values of $\lambda_S/\lambda_M$ the probability of association curves takes the same shape with and without any blockage model (Sattar *et al.*, 2017). In addition to that, even for the smaller values of $\lambda_S/\lambda_M$, the probability of association curves shows that the inclusion of blockage model decreases the probability of the case where UEs choose to decouple (Sattar *et al.*, 2017). Hence, the inclusion of blockage model will not significantly affect our results in anyway. Therefore, in the literature, the use of blockage model has been done for the cases when either the study is primarily about the channel modeling or just probability of associations.

- With regards to the effect of shadowing in our analysis, it should be mentioned that the authors in (Andrews, Baccelli & Ganti, 2011) pointed out that even a simplified model that only considers Rayleigh fading can closely track an actual base station deployment with lognormal shadowing. Therefore as far as the sub-6GHz networks are concerned, the randomness of the PPP BS locations emulates the shadowing effect, hence shadowing is ignored in the sub-6GHz model. On the other hand in mmWave networks, a blockage model introduces similar effect to shadowing. Since in our work we omitted blockage model, and explained in

detail the rationale behind this assumption, shadowing is ignored for mmWave networks too. Moreover, to further demonstrate the negligible effect of shadowing in decoupled wireless access, a detailed discussion along with related results are provided in section 2.5.

- It is assumed that $P_M > P_S$, as $Mcell$ BSs suppose to have more transmit power to provide coverage to all the UE in its cell. It is also assumed that $Q_M \geq Q_S$, which is not only an intuitive assumption as UEs need more power to transmit to far BSs but also based on the difference between the maximum allowed transmit power for mmWave and sub-6GHz UEs (Colombi *et al.*).

- In our system model beamforming gains from massive array of antenna elements are only accounted for $Scell$ BSs. Though, even in sub-6GHz domain, antenna pattern has certain shape, it is assumed that all UEs and $Mcell$ BSs have omni directional antennas. The rationale behind this assumption is that in hybrid BSs' deployment, the $Mcell$ BSs will provide an umbrella coverage to all UEs, on the other hand $Scell$ BSs will mainly focus on the high capacity links with individual UEs.

- It is assumed that in both uplink and downlink, a typical UE associates with a BS based on the received power.

- Another assumption that mmWave networks are noise-limited and sub-6GHz networks are interference limited is also considered. Additionally, from the perspective of medium access control (MAC), authors in (Singh, Mudumbai & Madhow, 2011) provides a detailed interference analysis, which shows that highly directional links can indeed be modeled as pseudowired. On the other hand, authors in (Shokri-Ghadikolaei & Fischione, 2016) discussed that mmWave networks may exhibit non-negligible transitional behavior from a noise-limited regime to an interference-limited. The practical aspect of the noise-limited mmWave networks is motivated by the work in (Di Renzo, 2015; Andrews, Bai, Kulkarni, Alkhateeb, Gupta & Heath, 2017) where the authors discuss in detail the pragmatic value of this assumption which also simplifies the mathematical analysis. Furthermore, the authors in (Rangan, Rappaport & Erkip, 2014; Akdeniz, Liu, Samimi, Sun, Rangan, Rappaport & Erkip, 2014) did simulation based studies on a measurement-based mmWave channel model. It

was observed that the impact of thermal noise on coverage dominates that of out of cell interference in mmWave networks.

The case of noise-limited mmWave networks has been considered and motivated in (Singh *et al.*, 2015) and later validated by (Elshaer *et al.*, 2016) even for high densities of mmWave *Scells*. Moreover, due to the orthogonality of both sub-6GHz and mmWave networks, no interference is assumed between the two tiers.

### 2.3.2   Cell Association Criteria

The typical UE associates with a BS in uplink at $x* \in \Phi_l$, where $l \in \{S, M\}$ if and only if

$$Q_l G_l ||x * ||^{-\alpha_l} \geq Q_k G_k ||x_{k,i}||^{-\alpha_k}, \quad \forall k \in \{S, M\}. \tag{2.1}$$

Similarly, a typical UE associates with a BS in downlink at $x* \in \Phi_l$ if and only if

$$P_l G_l ||x * ||^{-\alpha_l} \geq P_k G_k ||x_{k,i}||^{-\alpha_k}, \quad \forall k \in \{S, M\}, \tag{2.2}$$

where $G_k$ and $\alpha_k$ are antenna gain and path loss exponent for the communication link UE-$kcell$ BS, respectively.

Moreover, based on the assumption of noise-limited mmWave network and interference limited sub-6Ghz networks, the uplink/downlink mmWave signal-to-noise-ratios (SNRs) and sub-6GHz signal-to-interference and noise ratios (SINRs) take the following form

$$\text{SINR}_{\text{UL},M} = \frac{Q_M G_M h_{0,x*}||x*||^{-\alpha_M}}{I_{\text{UL},M} + \sigma_M^2}$$

$$\text{SINR}_{\text{DL},M} = \frac{P_M G_M h_{x*,0}||x*||^{-\alpha_M}}{I_{\text{DL},M} + \sigma_M^2}$$

$$\text{SNR}_{\text{UL},S} = \frac{Q_S G_S h_{0,x*}||x*||^{-\alpha_S}}{\sigma_S^2}$$

$$\text{SNR}_{\text{DL},S} = \frac{P_S G_S h_{x*,0}||x*||^{-\alpha_S}}{\sigma_S^2}, \tag{2.3}$$

where $\sigma_k^2$ and $h$ are the noise variance for the communication link UE-$kcell$ BS and small scale fading power gain, respectively. For the rest of the paper we denote $\bar{P}_k = P_k G_k$ and $\bar{Q}_k = Q_k G_k$.

## 2.4 Analytical Analysis

In the quest of deriving the analytical expressions for the spectral efficiency in different association scenarios, the first step is to derive the analytical expressions for the joint probability of association. The second step is to derive the distance distributions to the serving BSs for different association scenarios.

### 2.4.1 Joint Association Probabilities

Considering the model proposed in Section 2.3, if a typical UE has a liberty to choose at most two different BSs for uplink and downlink transmissions from two different tier of BSs, then the association process can lead to one of the following four cases:

- **Case 1**: Uplink BS = Downlink BS = $Mcell$ BS
- **Case 2**: Uplink BS = $Scell$ BS, Downlink BS = $Mcell$ BS
- **Case 3**: Uplink BS = $Mcell$ BS, Downlink BS = $Scell$ BS
- **Case 4**: Uplink BS = Downlink BS = $Scell$ BS

The joint association probabilities for homogeneous (i.e., all UEs communicate with the same transmit power) and heterogeneous user domain (i.e., UEs vary their transmit power levels

with respect to the BS's tier they are connected to ) are already elaborated in (Smiljkovikj *et al.*, 2015b) and (Smiljkovikj *et al.*, 2015a), respectively. Since, in the two-tier network under consideration, both tiers which are operating on significantly different frequency bands (sub-6GHz and mmWave) possess drastically different propagation characteristics. Hence, the novelty of this work is to accommodate different pathloss exponents in the closed form expressions of joint association probabilities, which further leads to robust expressions for spectral efficiency of the association cases under consideration.

Let $\{X_k\}_{k \in \{M,S\}}$ denotes the distance from the nearest BS in the $k^{th}$ tier to the typical UE located at $u_j = (0,0)$. We can derive the probability density function (pdf) of $X_k$ and cumulative distribution function (cdf) by the null probability of a 2D PPP (Chiu *et al.*, 2013) as follows:

$$f_{X_k}(x) = 2\pi\lambda_k x \exp(-\pi\lambda_k x^2), \quad x \geq 0, \tag{2.4}$$

$$F_{X_k}(x) = 1 - \exp(-\pi\lambda_k x^2), \quad x \geq 0. \tag{2.5}$$

Based on the cell association rules given by (2.1) and (2.2) we can derive the joint cell association probabilities for the four cases under consideration as follows:

### 2.4.1.1 Case 1: Uplink BS = Downlink BS = $Mcell$ BS

The probability that a UE associates to $Mcell$ BS for both uplink and downlink transmissions is given by

$$\Pr(\text{Case1}) = \Pr\left(X_M^{-\alpha_M} > \frac{\bar{P}_S}{\bar{P}_M}X_S^{-\alpha_S}; \ X_M^{-\alpha_M} > \frac{\bar{Q}_S}{\bar{Q}_M}X_S^{-\alpha_S}\right). \tag{2.6}$$

Based on the discussion on different power levels, $\frac{\bar{Q}_S}{\bar{Q}_M} > \frac{\bar{P}_S}{\bar{P}_M}$, therefore the joint probability reduces to the following form

$$
\begin{aligned}
\text{Pr(Case1)} &= \left( X_M^{-\alpha_M} > \frac{\bar{Q}_S}{\bar{Q}_M} X_S^{-\alpha_S} \right) \\
&= \left( X_M < \left( \frac{\bar{Q}_M}{\bar{Q}_S} \right)^{\frac{1}{\alpha_M}} X_S^{\frac{\alpha_S}{\alpha_M}} \right).
\end{aligned}
\tag{2.7}
$$

**Lemma 2.1.** *The joint probability of association of a typical UE for the association case 1 in closed form can be formulated as*

$$
\text{Pr(Case1)} = 1 - \frac{1}{2} \frac{\alpha_M}{\alpha_S} H_{1,1}^{1,1} \left[ z_1 \middle| \begin{array}{c} (0, \frac{1}{2}) \\ (0, \frac{1}{2} \frac{\alpha_M}{\alpha_S}) \end{array} \right],
\tag{2.8}
$$

*where* $z_1 = \left( \sqrt{\pi \lambda_M} \right)^{\frac{\alpha_M}{\alpha_S}} \left( \frac{\bar{Q}_M}{\bar{Q}_S} \right)^{\frac{1}{\alpha_S}} \left( \sqrt{\pi \lambda_S} \right)^{-1}.$

*Proof.* The development and proof are shown in Appendix I.1. ∎

### 2.4.1.2 Case 2: Uplink BS = *Scell* BS, Downlink BS = *Mcell* BS

The probability that a UE associates to *Scell* BS for uplink and *Mcell* BS for downlink transmission is given by

$$
\text{Pr(Case2)} = \text{Pr} \left( X_M^{-\alpha_M} > \frac{\bar{P}_S}{\bar{P}_M} X_S^{-\alpha_S}; \ X_M^{-\alpha_M} \leq \frac{\bar{Q}_S}{\bar{Q}_M} X_S^{-\alpha_S} \right).
\tag{2.9}
$$

Since, (2.9) is defined over an intersection of two regions, it can be written as

$$\Pr(\text{Case2}) \quad = \quad \Pr\left(X_M^{-\alpha_M} > \frac{\bar{P}_S}{\bar{P}_M}X_S^{-\alpha_S}\right) - \Pr\left(X_M^{-\alpha_M} > \frac{\bar{Q}_S}{\bar{Q}_M}X_S^{-\alpha_S}\right) \qquad (2.10)$$

**Lemma 2.2.** *The joint probability of association of a typical UE for the association case 2 in closed form can be formulated as*

$$\Pr(\text{Case2}) \quad = \quad \frac{1}{2}\frac{\alpha_M}{\alpha_S}\left(H_{1,1}^{1,1}\left[z_1 \,\middle|\, \begin{matrix}(0,\frac{1}{2})\\(0,\frac{1}{2}\frac{\alpha_M}{\alpha_S})\end{matrix}\right] - H_{1,1}^{1,1}\left[z_2 \,\middle|\, \begin{matrix}(0,\frac{1}{2})\\(0,\frac{1}{2}\frac{\alpha_M}{\alpha_S})\end{matrix}\right]\right), \qquad (2.11)$$

*where* $z_2 = \left(\sqrt{\pi\lambda_M}\right)^{\frac{\alpha_M}{\alpha_S}}\left(\frac{\bar{P}_M}{\bar{P}_S}\right)^{\frac{1}{\alpha_S}}\left(\sqrt{\pi\lambda_S}\right)^{-1}$.

*Proof.* Similar to the proof of Lemma 2.1 provided in Appendix I.1. ∎

### 2.4.1.3 Case 3: Uplink BS = $Mcell$ BS, Downlink BS = $Scell$ BS

The probability that a UE associates to $Mcell$ BS for uplink and $Scell$ BS for downlink transmission is given by

$$\Pr(\text{Case3}) \quad = \quad \Pr\left(X_M^{-\alpha_M} \le \frac{\bar{P}_S}{\bar{P}_M}X_S^{-\alpha_S}; \; X_M^{-\alpha_M} > \frac{\bar{Q}_S}{\bar{Q}_M}X_S^{-\alpha_S}\right). \qquad (2.12)$$

Since, there is no region which satisfies the domain of joint probability in (2.12), the $\Pr(\text{Case3}) = 0$.

#### 2.4.1.4 Case 4: Uplink BS = Downlink BS = *Scell* BS

The probability that a UE associates to *Scell* BS for both uplink and downlink transmissions is given by

$$\Pr(\text{Case4}) \;=\; \Pr\left(X_S^{-\alpha_S} \geq \frac{\bar{P}_M}{\bar{P}_S}X_M^{-\alpha_M}; \; X_S^{-\alpha_S} > \frac{\bar{Q}_M}{\bar{Q}_S}X_M^{-\alpha_M}\right). \tag{2.13}$$

Since, we are assuming that $\frac{\bar{Q}_S}{\bar{Q}_M} > \frac{\bar{P}_S}{\bar{P}_M}$, the joint probability of (2.13) reduces to the following form

$$\Pr(\text{Case4}) \;=\; \Pr\left(X_S^{-\alpha_S} \geq \frac{\bar{P}_M}{\bar{P}_S}X_M^{-\alpha_M}\right). \tag{2.14}$$

**Lemma 2.3.** *The joint probability of association of a typical UE for the association case 4 in closed form can be formulated as*

$$\Pr(\text{Case4}) \;=\; \frac{1}{2}\frac{\alpha_M}{\alpha_S}\mathrm{H}_{1,1}^{1,1}\left[z_2 \;\middle|\; \begin{array}{c} (0,\frac{1}{2}) \\ (0,\frac{1}{2}\frac{\alpha_M}{\alpha_S}) \end{array}\right]. \tag{2.15}$$

*Proof.* Similar to the proof of Lemma 2.1 provided in Appendix I.1. ∎

#### 2.4.2 Distance distributions of a typical UE to its Serving BSs

In this sub-section we derive the distance distributions of a typical UE to its serving BSs for all the three cases discussed in section 2.4.1. It is important to emphasize here that the serving BS may not be the nearest one to UE.

**Lemma 2.4.** *The distance distribution of a typical UE to its serving BS for the association case 1 is formulated as*

$$f_{X_M|\text{Case1}} = \frac{\left(\exp\left(-\pi\lambda_S\left(\frac{\bar{Q}_S}{\bar{Q}_M}\right)^{\frac{2}{\alpha_S}} x^{\frac{2\alpha_M}{\alpha_S}}\right)\right) \cdot f_{X_M}}{\text{Pr}(\text{Case1})}. \tag{2.16}$$

*Proof.* The development and proof are shown in Appendix I.2 ∎

**Lemma 2.5.** *The distance distributions of a typical UE to its serving BSs for the association case 2 is formulated as given in (2.17a) and (2.17b).*

$$f_{X_M|\text{Case2}} = \frac{\left(\exp\left(-\pi\lambda_S\left(\frac{\bar{P}_S}{\bar{P}_M}\right)^{\frac{2}{\alpha_S}} x^{\frac{2\alpha_M}{\alpha_S}}\right) - \exp\left(-\pi\lambda_S\left(\frac{\bar{Q}_S}{\bar{Q}_M}\right)^{\frac{2}{\alpha_S}} x^{\frac{2\alpha_M}{\alpha_S}}\right)\right) \cdot f_{X_M}}{\text{Pr}(\text{Case2})} \tag{2.17a}$$

$$f_{X_S|\text{Case2}} = \frac{\left(\exp\left(-\pi\lambda_M\left(\frac{\bar{P}_M}{\bar{P}_S}\right)^{\frac{2}{\alpha_M}} x^{\frac{2\alpha_S}{\alpha_M}}\right) - \exp\left(-\pi\lambda_M\left(\frac{\bar{Q}_M}{\bar{Q}_S}\right)^{\frac{2}{\alpha_M}} x^{\frac{2\alpha_S}{\alpha_M}}\right)\right) \cdot f_{X_S}}{\text{Pr}(\text{Case2})} \tag{2.17b}$$

*Proof.* Similar to the proof of Lemma 2.4 provided in Appendix I.2. ∎

**Lemma 2.6.** *The distance distribution of a typical UE to its serving BS for the association case 4 is formulated as*

$$f_{X_S|\text{Case4}} = \frac{\left(\exp\left(-\pi\lambda_M\left(\frac{\bar{P}_M}{\bar{P}_S}\right)^{\frac{2}{\alpha_M}} x^{\frac{2\alpha_S}{\alpha_M}}\right)\right) \cdot f_{X_S}}{\text{Pr}(\text{Case4})}. \tag{2.18}$$

*Proof.* Similar to the proof of Lemma 2.4 provided in Appendix I.2. ∎

### 2.4.3 Spectral Efficiency

In this sub-section we derive analytical expressions of spectral efficiency for each association case separately. Results from Lemma 2.1 to 2.6 are used to achieve this task.

The average system spectral efficiency can be formulated as

$$
\begin{aligned}
\text{SE} &= \sum_{i=1}^{4} \text{SE}(\text{Case}\,i)\,\text{Pr}(\text{Case}\,i) \\
&= \sum_{i=1}^{4} \frac{\tau_i}{W_k}\,\text{Pr}(\text{Case}\,i)),
\end{aligned}
\tag{2.19}
$$

where $\tau_i$ is the average UE rate of association case $i$ and $W_k$ is the system bandwidth, here $k \in \{M, S\}$. First the average UE rate for each association case is derived separately, then the average system spectral efficiency is derived.

**Theorem 2.1.** *Based on the distance distributions derived in Lemma 2.4, 2.5, 2.6, the average user rate for each association case i can be formulated as given in equations (2.20) to (2.25). The definitions of the variables therein are given in Table 2.1 and the structure of the bivariate Fox's H-function is defined in Appendix I.4.*

$$
\tau_{\text{UL,Case1}} = \frac{W_M 2\pi \lambda_M \beta_1 \beta_2 \beta_3}{\text{Pr}(\text{Case1})} \cdot \int\limits_{t>0} \xi_{\text{UL},M}^{-2} \hat{\text{H}}\left(1; \frac{\xi_6}{\xi_{\text{UL},M}}, \frac{\xi_5}{\xi_{\text{UL},M}}\right) dt.
\tag{2.20}
$$

$$
\tau_{\text{DL,Case1}} = \frac{W_M 2\pi \lambda_M \beta_1 \beta_2 \beta_3}{\text{Pr}(\text{Case1})} \cdot \int\limits_{t>0} \xi_{\text{DL},M}^{-2} \hat{\text{H}}\left(1; \frac{\xi_6}{\xi_{\text{DL},S}}, \frac{\xi_5}{\xi_{\text{DL},S}}\right) dt.
\tag{2.21}
$$

$$\tau_{\text{UL,Case2}} = \frac{W_S 2\pi \lambda_S \beta_4 \beta_5 \beta_6}{\text{Pr(Case2)}} \int\limits_{t>0} \xi_{\text{UL},S}^{-2} \left( \hat{H}\left(4; \frac{\xi_1}{\xi_{\text{UL},S}}, \frac{\xi_2}{\xi_{\text{UL},S}}\right) - \hat{H}\left(4; \frac{\xi_3}{\xi_{\text{UL},S}}, \frac{\xi_2}{\xi_{\text{UL},S}}\right) \right) dt. \quad (2.22)$$

$$\tau_{\text{DL,Case2}} = \frac{W_M 2\pi \lambda_M \beta_1 \beta_2 \beta_3}{\text{Pr(Case2)}} \int\limits_{t>0} \xi_{\text{DL},M}^{-2} \left( \hat{H}\left(1; \frac{\xi_4}{\xi_{\text{DL},M}}, \frac{\xi_5}{\xi_{\text{DL},M}}\right) - \hat{H}\left(1; \frac{\xi_6}{\xi_{\text{DL},M}}, \frac{\xi_5}{\xi_{\text{DL},M}}\right) \right) dt \quad (2.23)$$

$$\tau_{\text{UL,Case4}} = \frac{W_S 2\pi \lambda_S \beta_4 \beta_5 \beta_6}{\text{Pr(Case4)}} \cdot \int\limits_{t>0} \xi_{\text{UL},S}^{-2} \hat{H}\left(4; \frac{\xi_3}{\xi_{\text{UL},S}}, \frac{\xi_2}{\xi_{\text{UL},S}}\right) dt. \quad (2.24)$$

$$\tau_{\text{DL,Case4}} = \frac{W_S 2\pi \lambda_S \beta_4 \beta_5 \beta_6}{\text{Pr(Case4)}} \cdot \int\limits_{t>0} \xi_{\text{DL},S}^{-2} \hat{H}\left(4; \frac{\xi_3}{\xi_{\text{DL},S}}, \frac{\xi_2}{\xi_{\text{DL},S}}\right) dt. \quad (2.25)$$

*Proof.* The development and the proof are shown in Appendix I.3. ■

**Corollary 2.1.** *Following (2.19), the average uplink and downlink spectral efficiencies for the decoupled access modes can be, respectively, given by*

$$\text{SE}_{\text{UL}}^D = \sum_{i=1}^{4} \frac{\tau_{\text{UL,Case}\,i}}{W_k} \Pr(\text{Case}\,i). \quad (2.26)$$

$$\text{SE}_{\text{DL}}^D = \sum_{i=1}^{4} \frac{\tau_{\text{DL,Case}\,i}}{W_k} \Pr(\text{Case}\,i). \quad (2.27)$$

Table 2.1 Definitions of variables/parameters used in the expressions of Fox's H-function

| Variables | Definitions | Variables | Definitions |
|---|---|---|---|
| $\xi_{\text{UL},M}$ | $\dfrac{(\exp(t)-1)^{\frac{1}{\alpha_M}}}{\bar{Q}_M^{\frac{1}{\alpha_M}}}$ | $\xi_{\text{DL},M}$ | $\dfrac{(\exp(t)-1)^{\frac{1}{\alpha_M}}}{\bar{P}_M^{\frac{1}{\alpha_M}}}$ |
| $\xi_{\text{UL},S}$ | $\dfrac{(\exp(t)-1)^{\frac{1}{\alpha_S}}}{\bar{Q}_S^{\frac{1}{\alpha_S}}}$ | $\xi_{\text{DL},S}$ | $\dfrac{(\exp(t)-1)^{\frac{1}{\alpha_S}}}{\bar{P}_S^{\frac{1}{\alpha_S}}}$ |
| $\xi_1$ | $\left(\sqrt{\pi\lambda_M}\right)^{\frac{\alpha_M}{\alpha_S}}\left(\dfrac{\bar{Q}_M}{\bar{Q}_S}\right)^{\frac{1}{\alpha_S}}$ | $\xi_2$ | $\sqrt{\pi\lambda_S}$ |
| $\xi_3$ | $\left(\sqrt{\pi\lambda_M}\right)^{\frac{\alpha_M}{\alpha_S}}\left(\dfrac{\bar{P}_M}{\bar{P}_S}\right)^{\frac{1}{\alpha_S}}$ | $\xi_4$ | $\left(\sqrt{\pi\lambda_S}\right)^{\frac{\alpha_S}{\alpha_M}}\left(\dfrac{\bar{P}_S}{\bar{P}_M}\right)^{\frac{1}{\alpha_M}}$ |
| $\xi_5$ | $\sqrt{\pi\left(\lambda_M+\lambda_{\text{IU}}G(t)\right)}$ | $\xi_6$ | $\left(\sqrt{\pi\lambda_S}\right)^{\frac{\alpha_S}{\alpha_M}}\left(\dfrac{\bar{Q}_S}{\bar{Q}_M}\right)^{\frac{1}{\alpha_M}}$ |
| $\beta_1$ | $\dfrac{1}{\alpha_M}$ | $\beta_2$ | $\dfrac{\alpha_S}{2\alpha_M}$ |
| $\beta_3$ | $\dfrac{1}{2}$ | $\beta_4$ | $\dfrac{1}{\alpha_S}$ |
| $\beta_5$ | $\dfrac{\alpha_M}{2\alpha_S}$ | $\beta_6$ | $\beta_3$ |

**Corollary 2.2.** *Similar to Theorem 2.1, the average user rate for the coupled access mode for the two conventional association cases (i.e., either a UE connects to a Mcell BS or Scell BS ) can be formulated easily following the same steps as adopted in the proof of Theorem 2.1 in Appendix 3. When UEs connect to Scell BSs, in coupled access mode, this association case will be exactly*

*equal to the association case 4 of decoupled access mode. Therefore the average uplink UE rate $\tau_{UL,S}^C$ and the average downlink UE rate $\tau_{DL,S}^C$ in coupled access mode, respectively, are equal to $\tau_{UL,Case4}$ and $\tau_{DL,Case4}$. When UEs connect to Mcell BSs in coupled access mode, the average user rate of this association case can be formulated by simple mathematical manipulation of expressions of association case 1 and 2, given in Theorem 2.1.*

$$\tau_{UL,M}^C \quad = \quad \frac{W_M 2\pi\lambda_M\beta_1\beta_2\beta_3}{\Pr(Mcell)} \cdot \int_{t>0} \xi_{UL,M}^{-2}\hat{H}\left(1;\frac{\xi_4}{\xi_{UL,M}},\frac{\xi_5}{\xi_{UL,M}}\right)dt, \qquad (2.28)$$

$$\tau_{DL,M}^C \quad = \quad \frac{W_M 2\pi\lambda_M\beta_1\beta_2\beta_3}{\Pr(Mcell)} \cdot \int_{t>0} \xi_{DL,M}^{-2}\hat{H}\left(1;\frac{\xi_4}{\xi_{DL,M}},\frac{\xi_5}{\xi_{DL,M}}\right)dt, \qquad (2.29)$$

*where*

$$\Pr(Mcell) = \Pr(X_M^{-\alpha_M}\bar{P}_M > X_S^{-\alpha_S}\bar{P}_S)$$

$$= 1 - \frac{\alpha_M}{2\alpha_S}H_{1,1}^{1,1}\left[z_2 \left| \begin{array}{c} (0,\frac{1}{2}) \\ (0,\frac{1}{2}\frac{\alpha_M}{\alpha_S}) \end{array} \right. \right] \qquad (2.30)$$

*is the association probability of a UE to Mcell BS. Rest of the variables used in equations (2.28) to (2.30) are defined in Table 2.1.*

**Corollary 2.3.** *Similar to the decoupled access mode, following (2.19),the average uplink and downlink spectral efficiencies for the coupled access modes can be, respectively, given by*

$$SE_{UL}^C = \frac{\tau_{UL,M}^C}{W_M} \cdot \Pr(Mcell) + \frac{\tau_{UL,S}^C}{W_S} \cdot \Pr(Scell), \qquad (2.31)$$

$$\text{SE}_{\text{DL}}^{C} = \frac{\tau_{\text{DL},M}^{C}}{W_M} \cdot \text{Pr}(Mcell) + \frac{\tau_{\text{DL},S}^{C}}{W_S} \cdot \text{Pr}(Scell), \tag{2.32}$$

*where the* $\text{Pr}(Scell) = \text{Pr}(\text{Case 4})$.

## 2.5   Numerical and Simulation Results

Table 2.2   System Parameters

| Parameters | Value |
|---|---|
| $Mcell$ BS transmit power $P_M$ (dBm) | 46 |
| $Scell$ BS transmit power $P_S$ (dBm) | 20 |
| Antenna Gain for $Mcell$ BS $G_M$ (dBi) | 0 |
| Antenna Gain for $Scell$ BS $G_S$ (dBi) | 18 |
| UE's transmit power to $Mcell$ BS $Q_M$ (dBm) | 20 |
| UE's transmit power to $Scell$ BS $Q_S$ (dBm) | 20 |
| Pathloss exponent for sub-6GHz tier $\alpha_M$ | 3 |
| Pathloss exponent for millimeter wave tier $\alpha_S$ (LOS) | 2 |
| Pathloss exponent for millimeter wave tier $\alpha_S$ (NLOS) | 4 |
| Noise power $\sigma_S^2 = \sigma_M^2$ (dBm) | 0 |

In this section a comprehensive performance comparison between coupled and decoupled access modes is presented using numerical and simulation results. As presented in section 2.3, we consider two-tier HetNet, which consists of sub-6Ghz $Mcell$ BSs and millimeter wave $Scell$ BSs are modeled using independent homogeneous PPP. We assume that the tier of $Mcell$ BSs is interference limited whereas the tier of $Scell$ BSs in only noise limited (Singh *et al.*, 2015; Elshaer *et al.*, 2016). The simulation model simply consists of uniformly distributed BSs of both tiers and a UE located in the center of a circular area. The default system parameters are selected based on the 3GPP specifications (3GPP TR 36.942, 2009) and existing research work (Smiljkovikj *et al.*, 2015b,a; Elshaer *et al.*, 2016), their values are listed in Table 2.2. Without any loss of generality the noise power is normalised to 1mW. To validate the analytical model formulated in this paper, we perform Monte Carlo simulations for all the association cases

under consideration. The simulation results are obtained by averaging over 100,000 independent realizations in MATLAB. We investigate the potential gain of decoupled access in terms of spectral efficiency and discuss its efficacy from a pragmatic perspective. Moreover, we also discuss the joint association probabilities and distance distributions of a typical UE to its serving BSs for line of sight (LOS) and non line of sight (NLOS) cases.

### 2.5.1  Joint Association Probabilities

We first analyze the joint association probabilities of three possible association cases as shown in Fig. 2.2a and 2.2b, for NLOS and LOS scenarios, respectively. In LOS scenario i.e., when UEs have access to unobstructed link to mmWave BSs, UEs choose to connect with *Scell* BSs in both uplink and downlink with very high probability. The rationale behind this trend is obvious, the antenna gain along with high quality of LOS link of *Scell* BS becomes an attractive choice with respect to the received power. On the other hand, for NLOS scenario, Fig. 2.2a shows that the probability of UEs who choose to decouple are higher only for the lower values of $\lambda_S/\lambda_M$ and it decreases significantly at the cost of increase in association case 4 i.e., when UEs choose to connect with *Scell* BSs in both uplink and downlink, as we increase the density of *Scell* BSs. Similarly, in the case when LOS links to *Scell* BSs are available, which would be the case in less dense urban environments, the probability of UEs who choose to decouple goes to almost zero quite rapidly as we increase the density of BSs $\lambda_S/\lambda_M$ .

The effect of shadowing is analysed by performing simulations based on the shadowing parameters given in (Akdeniz *et al.*, 2014). In these simulations a lognormal shadowing parameter $\xi \sim \mathcal{N}(0, \sigma_\xi^2)$ is added in the pathloss. The results demonstrate that the effect of shadowing, as shown in Fig. 2.2a and Fig. 2.2b, does not modify in a measurable way the association curves. Without the loss of generality it can be stated that the effect of shadowing has a minimal impact on the association curves and therefore can be ignored in the rest of the work.

Moreover, to understand the impact of pathloss exponents in the association phase, we plotted the probabilities of three possible association cases against different values of the pathloss exponent

$\alpha_S$ in Fig. 2.3. It gives us an insight into the effect of BSs' density $\lambda_S/\lambda_M$ on the probability of association case 1 and the impact of *Scell* BSs link quality on the probability of association case 2 and 4. It is evident from Fig. 2.3 that as the link quality of *Scell* BSs decreases (i.e., higher values of $\alpha_S$), the probability of association case 2 increases at the cost of decrease in association case 4. Furthermore, it also shows that the higher density of *Scell* BSs makes them an attractive choice even for the higher values of $\alpha_S$.

These results indicate three important things, (i) without any power biasing the number of UEs who chose to decouple are not significant from a system level point of view; (ii) power biasing can certainly be used for load balancing which forces UEs to decouple at the cost of decrease in achievable rate and spectral efficiency; (iii) in a less dense urban environment (i.e., LOS scenario), where load balancing would not be an issue, the feasibility of the implementation of decoupled access is very bleak.

### 2.5.2 Distance Distributions

Fig. 2.4a and 2.4b shows the distance distributions of a typical UE to its serving BSs for NLOS and LOS cases, respectively. An interesting observation from these results is that even though the change in the quality of links (i.e., NLOS and LOS) is only accounted for the millimeter wave or *Scell* BSs' links, it still affects the distance distribution of a typical UE to the *Mcell* BS for the association case 2. It is observed that in NLOS scenario, for the association case 2, the PDF of the distance between the *Mcell* BS and a typical UE is spread over the range from 0 to 160 meters whereas this range shrinks to 0 to 35 meters for LOS scenario. The rationale behind this change in the distribution is that due to the high quality LOS links of *Scell* BSs, UEs with very high probability choose to associate with *Scell* BSs in both uplink and downlink. Therefore, in this scenario decoupling only happens when sub-6GHz or *Mcell* BSs' link quality is superior to its counterpart and it would only happen if the distance between a typical UE and *Mcell* BS is significantly less than its counterpart.

a) NLOS

b) LOS
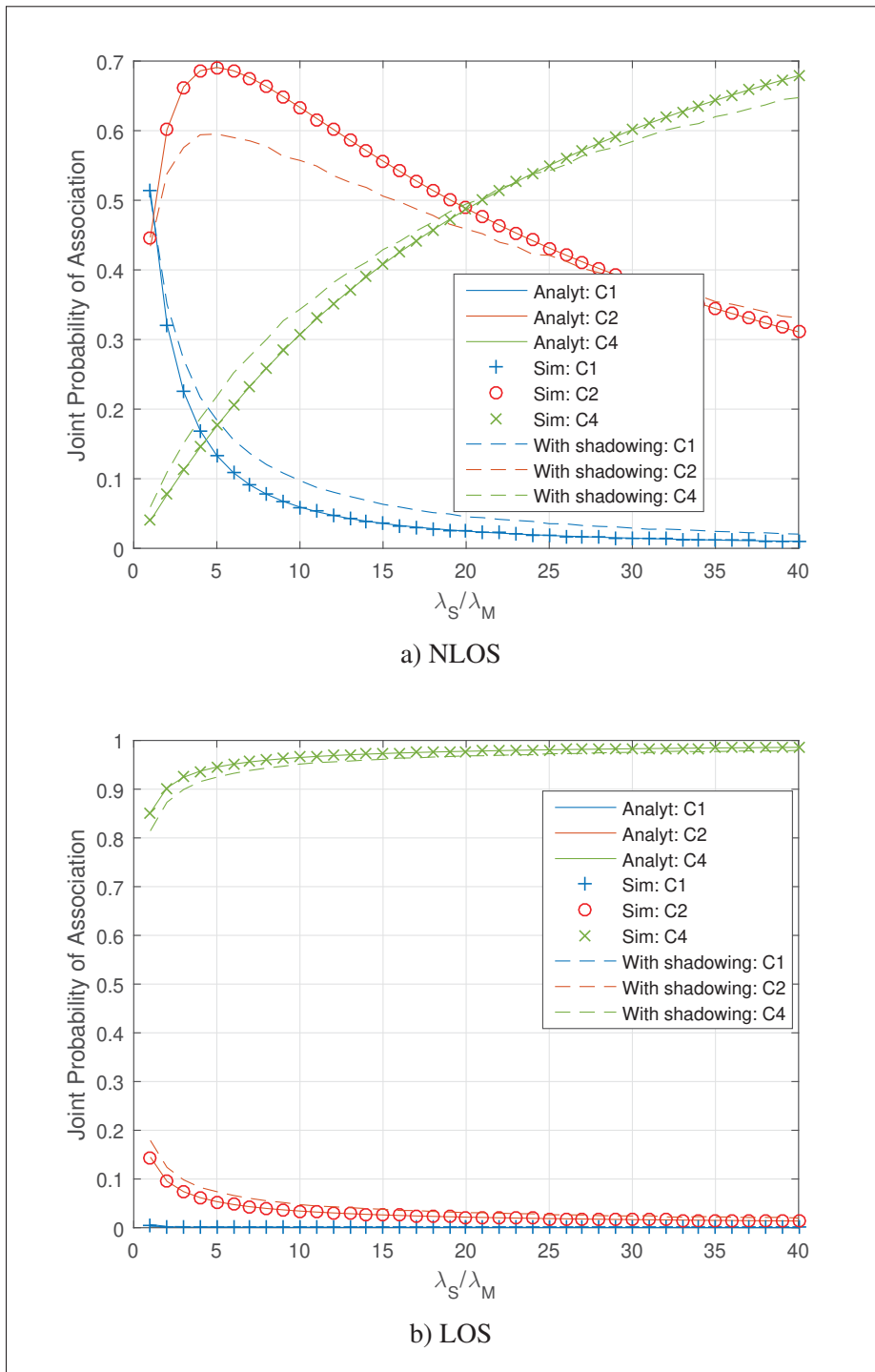
Figure 2.2    Joint association probabilities of all three possible
association cases
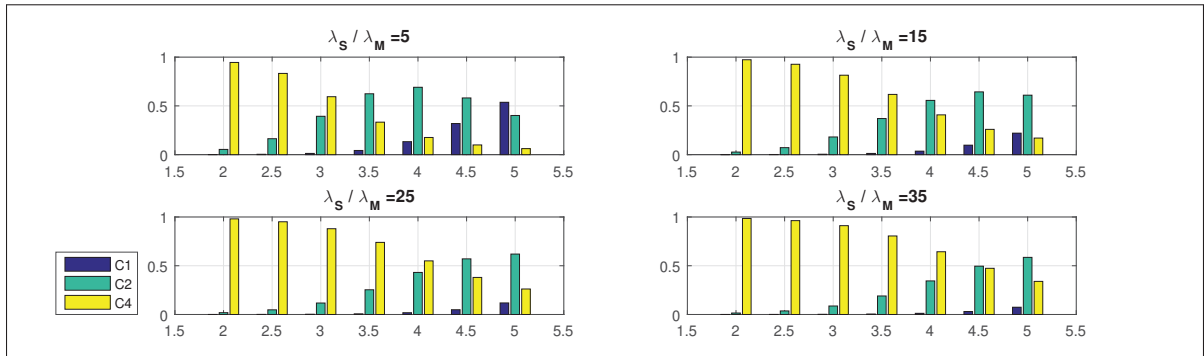
Figure 2.3    Joint association probabilities of all three possible
association cases (y-axis) versus $\alpha_S$ (x-axis) for different densities
$\lambda_S/\lambda_M$ of BSs

### 2.5.3    Spectral Efficiency

Now we examine the main result i.e., the comparison of spectral efficiency of decoupled and coupled access. It should be obvious that the only difference between the decoupled and coupled access modes are those UEs who choose *Scell* BSs for uplink in association case 2. Therefore, we only plot and compare the average uplink spectral efficiency of decoupled and coupled access modes. Fig. 2.5a compares the average spectral efficiencies of both coupled and decoupled access modes for the NLOS scenario whereas, 2.5b shows the same comparison for LOS scenario. Even though for the NLOS scenario in Fig. 2.5a, a considerable improvement in spectral efficiency can be observed but whether this gain is good enough from pragmatic point of view is still an open question.

### 2.5.4    Discussion

There is no doubt that in theory the decoupled access outperforms its coupled counterpart but whether the cost it comes with (i.e., control signals overhead ) makes it viable or not is not a trivial question to answer. From a pragmatic point of view, any proposal for a disruptive change in a system configuration as radical as the decoupled access should be seen from a very critical lens. Therefore following are the key critical insights we can take from this study.

- Decoupled access does not look a viable option to improve spectral efficiency of an overall system.

- As previous studies (Elshaer *et al.*, 2016; Zhang *et al.*, 2017) suggested that with the help of power biasing, decoupled access would be a viable option for load balancing in the next generation of communication systems. But as we know that the next generation of communication systems are envisioned as part of a dense or an ultra dense network where the density of access points would be greater than the density of UEs(Kamel, Hamouda & Youssef, 2016), hence, whether would there be any need of load balancing in such network settings is a question worth investigating.

- Decoupled access breaks the channel reciprocity by its very design, therefore, a big challenge is to come up with an cost effective channel estimation scheme. Since at the end it would be the control signals overhead which concretely defines the viability of decoupled access mode.

## 2.6 Conclusion

In this paper, we did a comparative analysis of decoupled and coupled access modes based on the stochastic geometry. We constructed a two-tier HetNet (i.e., sub-6Ghz and millimeter wave) where BSs of both tiers are modeled as independent PPP. In our analytical model, we accommodated two different pathloss exponents for two radically different tiers of BSs with respect to their frequency bands. Therefore, we used Fox's H-function to derive joint probability of associations in closed form, which eventually results in a rather simple, compact and modular expressions for spectral efficiency. Our analytical and simulation results validate each other and illustrate the effect of decoupled access on distance distributions of serving BSs and average spectral efficiency. We observed that though decoupling can improve the uplink spectral efficiency but still that improvement is rather small from a system level point of view. Therefore, whether the decoupled access is a viable option for the next generation of communication systems depends only on a comprehensive cost analysis of control signals overhead.
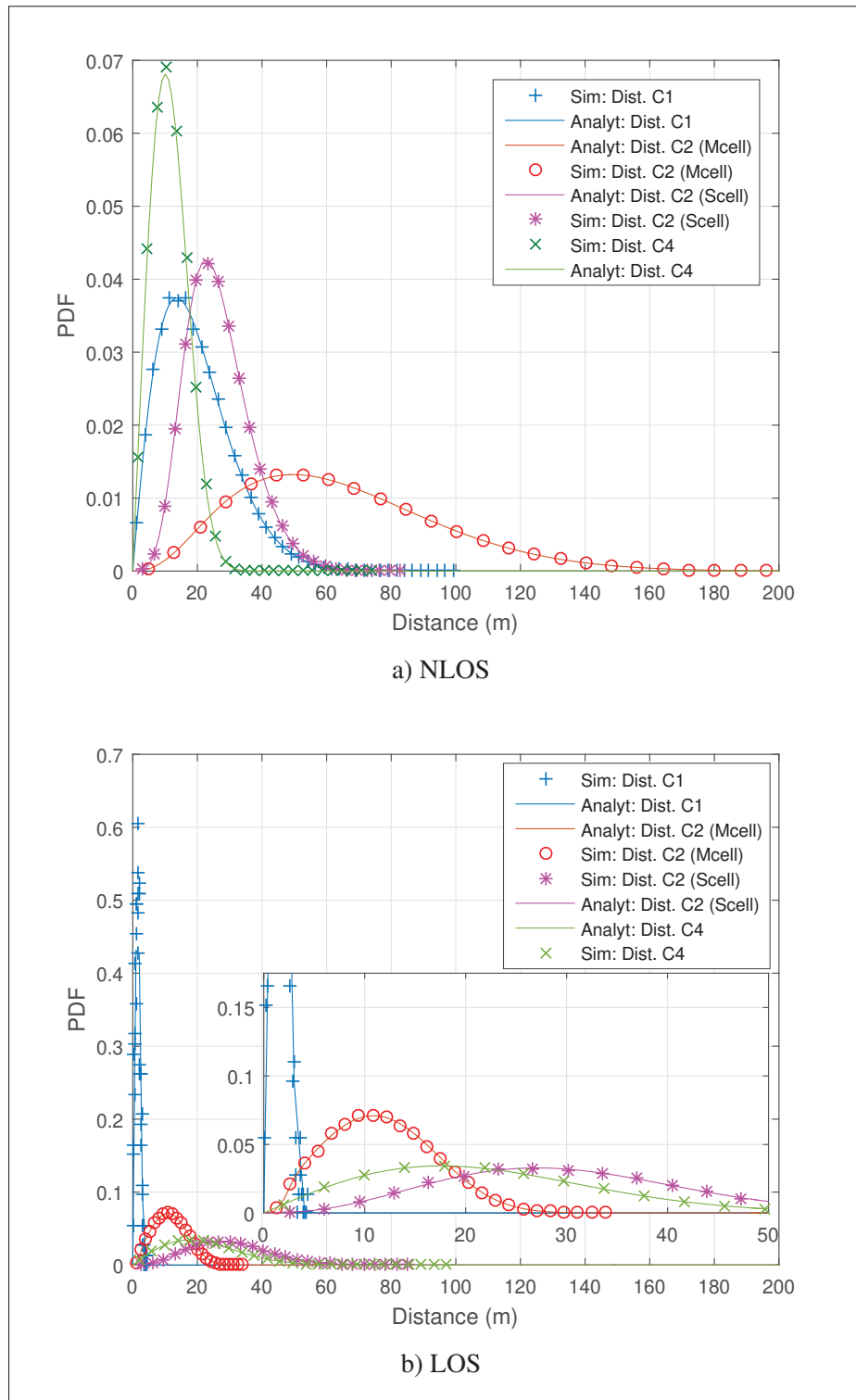
Figure 2.4    Distance distributions of a typical UE to its serving BSs
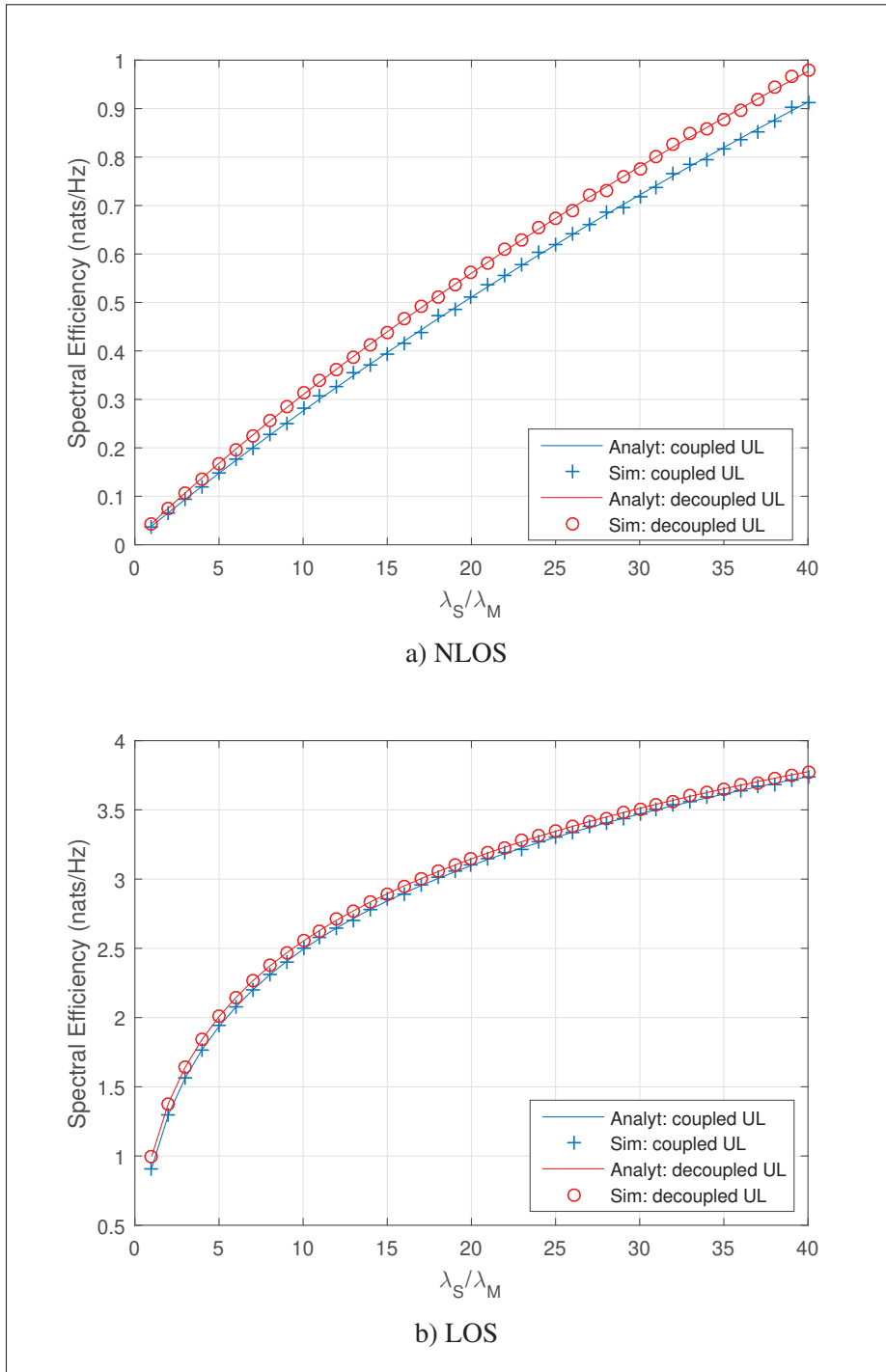
Figure 2.5    Comparison of average uplink spectral efficiency of
coupled and decoupled access modes

# CHAPTER 3

## FULL-DUPLEX TWO-TIER HETEROGENEOUS NETWORK WITH DECOUPLED ACCESS: CELL ASSOCIATION, COVERAGE, AND SPECTRAL EFFICIENCY ANALYSIS

Zeeshan Sattar[a] , Joao V.C. Evangelista[b] , Georges Kaddoum[c] , Naïm Batani[d]

[a,b,c,d]Department of Electrical Engineering, École de Technologie Supérieure, 1100 Notre-Dame Ouest, Montréal, Québec, Canada H3C 1K3

## 3.1 Abstract

The ever increasing thirst for the higher capacity demands radical changes in the design of cellular networks, such as a leap from single-tier homogeneous networks to multi-tier heterogeneous networks and the use of millimeter wave frequency band. A typical point-to-point full-duplex transmission link can double the link rate by simultaneously using the same spectrum for bidirectional traffic. However, the characterization of full-duplex two-tier heterogeneous networks is not as straightforward as that of point-to-point full-duplex systems, specially when the different tiers of the heterogeneous network use different frequency bands (millimeter wave and microwave) for their transmissions. This paper characterizes a full-duplex two-tier heterogeneous network with decoupled access, where both tiers operate on different frequency bands (millimeter wave and microwave). To evaluate the achievable spectral efficiency and association behavior of users and base stations, a two-tier heterogeneous network model is proposed in which all users and base stations are modeled using Poisson point processes. First a signal-to-interference-plus-noise-ratio optimal user association scheme is characterized. Based on the user association scheme, the spectral efficiencies of the uplink and downlink transmission links are derived. In addition, a thorough analysis of the signal-to-interference-plus-noise-ratio coverage is also provided. Moreover to render the analytical model more comprehensive and robust, i.e., different from the convention of noise-limited millimeter wave network, the interference in millimeter wave networks is also accounted for in the analytical model. Lastly,

the pragmatic value of full-duplex heterogeneous networks and decoupled access is discussed in detail through numerous numerical and simulation results.

## 3.2 Introduction

Whenever the hush of expectancy of a new generation of communication systems falls upon their predecessor, lots of ideas silently take birth in the research laboratories of both academia and industry. Some of these ideas scream their way out to commercial use and some of them remain on the dissecting table of researchers, only to be found again on a later date. The recent advancement in available computing power and the evolution in signal processing provide ample room for innovative and out of the box ideas for the fifth-generation (5G) of communication systems. Some of the main requirements imposed on 5G are seamless coverage, hotspot high capacity, low end-to-end latency, and massive connections (Andrews *et al.*, 2014; Yang *et al.*, 2018). To address these requirements, network densification and the use of extremely high frequencies (EHF) are two promising solutions. In this context, EHF, commonly known as the millimeter wave (mmWave) band, provides an unprecedented large bandwidth, while the network densification pushes for the paradigm shift of single-tier homogeneous cellular networks towards multi-tier heterogeneous cellular networks (HetNets) (Andrews *et al.*, 2012). In HetNets the typical transmit power of a base station (BS) varies with respect to its tier resulting in significantly different interference levels (Andrews, 2013). Therefore the optimality of the conventional way of cell association i.e., coupled access, where a user connects to a single BS for both uplink and downlink transmission came under scrutiny.

The authors in (Elshaer *et al.*, 2014, 2016; Boccardi *et al.*, 2016) revisited the conventional way of cell association and proposed a decoupled wireless access. The decoupled wireless access grants liberty to user equipment (UE) to choose different BSs for their uplink and downlink transmissions. In a two-tier HetNet that employs significantly different frequency bands in each tier, decoupled access can potentially be more effective due to zero inter-tier interference. After the initial analytical analysis in (Smiljkovikj *et al.*, 2015b,a), the decoupled access has been studied and analyzed against its coupled counterpart in detail for different network scenarios

in (Sattar *et al.*, 2017; Sattar, Evangelista, Kaddoum & Batani, 2019; Zhang *et al.*, 2017; Li *et al.*, 2018b; Shi *et al.*, 2018). On the other hand, its performance analysis against a coupled full-duplex system, which should have been the more intuitive choice due to the parallel it has with the simultaneous uplink and downlink transmissions of full-duplex system, has not been addressed in the literature. In this paper, a full-duplex two-tier HetNet, which employs decoupled access is analytically modeled and discussed. The resulting performance is compared against its coupled counterpart.

### 3.2.1  Related Work

The topic of multi-tier HetNets, more specifically two-tier HetNets, is not new to the research community. It has been under a critical lens of both academia and industry for a significantly long time. For example, a thorough analysis of two-tier cellular systems with universal frequency reuse has been undertaken in (Chandrasekhar *et al.*, 2009). The authors investigated the cross-tier interference and the 'near-far' deadspot coverage in a two-tier network. In addition, they also provided a location-assisted power control scheme to regulate transmit powers of femtocell BSs. A detailed mathematical framework based on stochastic geometry to model a multi-tier mmWave cellular networks is provided in (Di Renzo, 2015). The author provided an exact analytical model to derive the coverage probability and the average rate in the form of numerical integration. To further simplify the analytical model, approximated results were derived in closed-form. In addition, the author provided a detailed and in-depth discussion on the noise-limited approximation for typical millimeter-wave network deployments.

As mentioned earlier, there has been a significant amount of progress on the analysis of decoupled access (Smiljkovikj *et al.*, 2015b,a; Sattar *et al.*, 2017; Zhang *et al.*, 2017; Li *et al.*, 2018b; Shi *et al.*, 2018; Sattar *et al.*, 2019). After the initial proposal of decoupled access in (Elshaer *et al.*, 2014), Smiljkovik *et al* in (Smiljkovikj *et al.*, 2015b,a) provided an analysis of decoupled access. In (Smiljkovikj *et al.*, 2015b), they derived analytical expressions for the probability of associations of UEs to different tiers and average throughput of UEs associated with different

tiers, whereas in (Smiljkovikj *et al.*, 2015a), they provided a discussion on the efficacy of decoupled access by analyzing its spectral and energy efficiencies.

In (Zhang *et al.*, 2017), the authors derived new analytical results for the average user rate in decoupled access for two different types of UE's distributions, namely uniform and clustered distributions, modeled as Poisson point process and Neyman–Scott cluster process, respectively. In (Li *et al.*, 2018b), the authors derived cell association probabilities with respect to the load balancing in BSs for a multi-user multiple-input multiple-output (MIMO) HetNet with decoupled access. In addition, they also analytically showed the suppression of interference by multiple antennas at BSs and its effect on the spectral efficiency.

In (Shi *et al.*, 2018), the authors used tools from stochastic geometry and provided a rather generalized theoretical framework on the impact of decoupled access in multi-tier HetNet. In our previous work (Sattar *et al.*, 2017), we provided a semi-analytical analysis on the efficacy of decoupled access for a two-tier HetNet employing mmWave and microwave frequency bands. Later, this work was extended in (Sattar *et al.*, 2019) and new closed-form results'were derived for the probability of associations, distance distributions of UEs to their tagged BSs, and the average spectral efficiency using Fox's H-function.

A recent work explored the full-duplex HetNet with decoupled access (Liu & Hu, 2018) where the authors provided an analysis of the average link rate performance and proposed full-duplex scheduling algorithms to maximize the bidirectional traffic. In (Sekander, Tabassum & Hossain, 2016), the authors formulated the association problem of a full-duplex HetNet with decoupled access as a convex geometric programming problem to maximize sum-rate. In addition, they also proposed low-complexity distributed solutions for the association problem.

### 3.2.2   Novelty & Contributions

The main goal of this paper is to investigate the efficacy of decoupled access in a full-duplex two-tier HetNet employing two different frequency bands in each tier i.e., mmWave and microwave. Therefore, a more robust and comprehensive analytical model is derived to analyze the probability

of associations, spectral efficiency, and coverage. The novelty of the derived analytical model is that it accommodates variable transmit powers, different pathloss exponents for different tiers, and accounts for the interference in mmWave networks. Typically, a mmWave network and a microwave network are assumed to be noise limited and interference-limited, respectively. To make the proposed analytical model more robust and comprehensive, it accounts for inter-user interference, inter-cell interference, full-duplex interference, and self-interference due to the full-duplex nature of the network, in both tiers as shown in Fig. 3.1b. To the best of the authors knowledge, this is the first analytical model accommodating all of the aforementioned interference, variable transmit powers, as well as different pathloss exponents for different tiers. The key contributions of this paper are listed as follows.

- The development of full-duplex signal-to-interference-plus-noise-ratio (SINR) model in a two-tier network with decoupled access.
- The developed analytical model takes into account the interference of the mmWave network.
- The development of new analytical expressions of the SINR optimal probability of associations.
- The development of new analytical expressions for the average spectral efficiency of both uplink and downlink transmissions based on the derived SINR model and the probability of associations.
- The development of analytical expressions of the SINR coverage in a network.
- The validation by rigorous simulation of all analytically derived results.
- The comparison of the analytical and simulation results, of a full-duplex two-tier HetNet which employs decoupled access, against its coupled counterpart.
- A comprehensive detailed discussion relating the different system parameters and their implications on the overall network performance is provided

Hence, the proposed analytical model is important for the following reasons:

- To the best of the authors' knowledge, it is the first analytical model that comprehensively encapsulates the characteristics of dense to ultra-dense networks by accommodating all types

of interference and varying transmit powers. Therefore it can be used to study the behavior of UEs and BSs in various deployment scenarios.

- The insights obtained from the outcomes of this paper, regarding crucial analytical performance analysis metrics such as association probabilities, coverage, and spectral efficiency, can allow researchers and wireless communication engineers to quickly evaluate system performance and optimize available parameters in the deployment of future wireless networks.
- The comprehensive nature of the proposed analytical model can help evaluating the performance limits of the network.

### 3.2.3 Organization

The rest of the paper is organized as follows. In Section II, the system model, spatial distributions, propagation assumptions, and cell association criteria are described. In Section III, analytical expressions of the probability of associations, coverage of SINR in a network, and the average spectral efficiency are derived. In Section IV, numerical and simulation results are presented. In addition, an in-depth and detailed discussion on the obtained results and the effect of different system parameters on the performance of the overall network is provided. Finally, Section V concludes the paper.

## 3.3 System Model

### 3.3.1 Spatial distributions

A full-duplex two-tier HetNet is considered where sub-6GHz (i.e., conventional microwave or macro-cell ($Mcell$)) BSs and mmWave (i.e., small-cell ($Scell$)) BSs are modeled according to independent homogeneous Poisson point processes (PPP). All the BSs are uniformly distributed in $\mathbb{R}^2$ in a circular area with a radius $\mu$. $\Phi_k$ denotes the set of points obtained through PPP with density $\lambda_k$, that can be explicitly written as

$$\Phi_k \triangleq \{x_{k,i} \in \mathbb{R}^2 : i \in \mathbb{N}_+\},$$

a) An illustration of the full-duplex two-tier heterogeneous network under consideration

b) An illustration of the decoupled access scenario
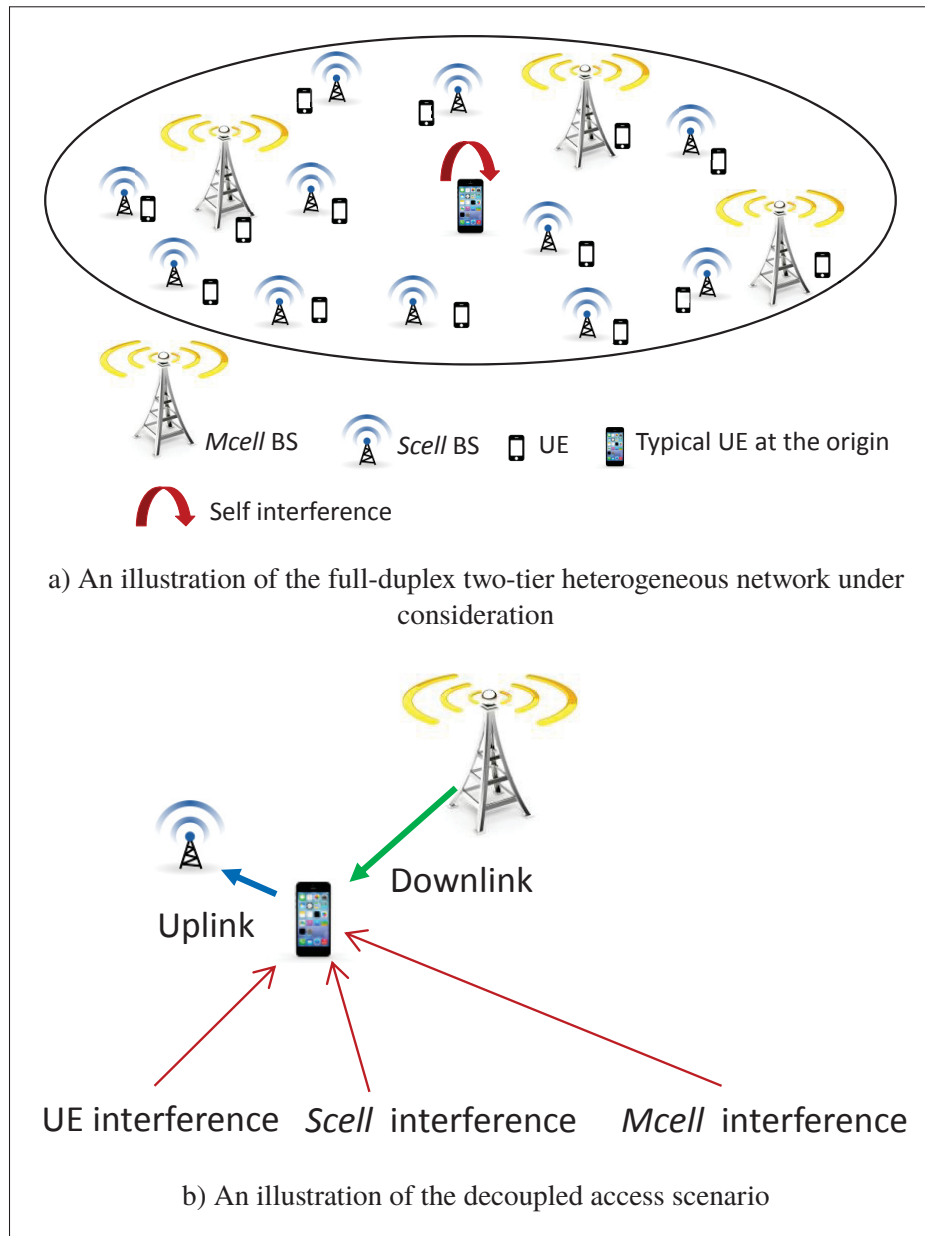
Figure 3.1    System model

where the index $k \in \{M, S\}$ for $Mcell$ and $Scell$ BSs, respectively. Similarly, all the UEs are also modeled according to PPP $\Phi_u$ with density $\lambda_u$, that can also be explicitly written as

$$\Phi_u \overset{\Delta}{=} \{u_j \in \mathbb{R}^2 : j \in \mathbb{N}_+\}.$$

### 3.3.2 Propagation Assumptions

The major assumptions critical to the analytical analysis are listed as follows.

- Since the addition of a node at the origin of the area of concern does not change the distribution of a point process (Chiu *et al.*, 2013), it is assumed that a typical full-duplex UE is located at $u_j = (0,0)$.

- Since in a hybrid BSs' deployment such as the case here, the $Mcell$ BSs will provide an umbrella coverage to all UEs, conversely, $Scell$ BSs will mainly focus on the high capacity links with individual UEs. Therefore, it is assumed that beamforming gains from massive array of antenna elements exist only in the tier of $Scell$ BSs.

- Since microwave and mmWave spectra do not interfere with each other, therefore it is assumed that there is no inter-tier interference.

- Since typically UE density $\lambda_u$ is much greater than the BS density $\lambda_k$ (i.e., $\lambda_u >> \lambda_k$) (Zhang *et al.*, 2017; Elshaer *et al.*, 2014, 2016; Sattar *et al.*, 2019), it is assumed that there exists at least one UE in the association region of every BS as shown in Fig. 3.1a.

- It is assumed that the network can have different fractions of full-duplex and half-duplex BSs i.e., the PPP $\Phi_k$ of BSs can have different number of full-duplex and half-duplex BSs. Similarly, the PPP $\Phi_u$ of UEs can also have different number of full-duplex and half-duplex UEs.

- It is assumed that each BS has enough orthogonal resources to serve all the UEs in its association region. Thus two UEs tagged to one BS can not interfere with each other, i.e., interference can only come from the UEs associated with the other BSs and from the other BSs using the same resources.

- It is assumed that both microwave and mmWave communication links are subjected to Rayleigh fading. It is worth mentioning that, in principle, more general fading distributions can be assumed such as Nakagami (Andrews *et al.*, 2017), but this additional complexity in analytical expressions does not provide any new design insights. The rationale behind this is the fact that performance trends are kind of robust to the underlying fading distribution as far as the employed fading distribution has distance-dependent channel components

(Saha & Dhillon, 2019). Therefore, the Rayleigh distribution's well-established mathematical tractability makes it a key ingredient in the analysis of mmWave systems as well (Singh *et al.*, 2015).

### 3.3.3 Full-Duplex SINR Model & Cell Association Criteria

To make the association criteria SINR optimal, a typical UE associates with a BS in uplink at $x* \in \Phi_l$, where $l \in \{S, M\}$ if and only if

$$
\begin{aligned}
\text{SINR}_{\text{UL},l}(x*) \quad & \geq \quad \text{SINR}_{\text{UL},k}(x_i), \\
& \quad \forall k \in \{S, M\}.
\end{aligned}
\tag{3.1}
$$

Similarly, a typical UE associates with a BS in downlink at $x* \in \Phi_l$ if and only if

$$
\begin{aligned}
\text{SINR}_{\text{DL},l}(x*) \quad & \geq \quad \text{SINR}_{\text{DL},k}(x_i), \\
& \quad \forall k \in \{S, M\}.
\end{aligned}
\tag{3.2}
$$

Moreover, based on the aforementioned propagation assumptions and the system model, the uplink/downlink SINRs of both tiers take the following form

$$
\begin{aligned}
\text{SINR}_{\text{UL},M} \quad &= \quad \frac{Q_M G_M h_{0,x*} ||x*||^{-\alpha_M}}{I_{\text{UL},M} + \epsilon_0 P_M + \sigma_M^2}, \\
\text{SINR}_{\text{DL},M} \quad &= \quad \frac{P_M G_M h_{x*,0} ||x*||^{-\alpha_M}}{I_{\text{DL},M} + \epsilon_* Q_M + \sigma_M^2}, \\
\text{SINR}_{\text{UL},S} \quad &= \quad \frac{Q_S G_S h_{0,x*} ||x*||^{-\alpha_S}}{I_{\text{UL},S} + \epsilon_0 P_S + \sigma_S^2}, \\
\text{SINR}_{\text{DL},S} \quad &= \quad \frac{P_S G_S h_{x*,0} ||x*||^{-\alpha_S}}{I_{\text{DL},S} + \epsilon_* Q_S + \sigma_S^2},
\end{aligned}
\tag{3.3}
$$

where, $P_k$ and $Q_k$ are the transmit powers for downlink and uplink transmission links, respectively, for the $k$th tier of BSs. $\sigma_k^2$, $h$, and $\alpha_k$ denote the noise variance for the UE-$kcell$ BS communication link, small scale fading power gain and path loss exponent, respectively. $\epsilon_0(\epsilon_*)$ is the self-interference suppression factor of BS (UE) and $I_{\text{UL},k}(I_{\text{DL},k})$ is the interference in uplink (downlink) UE-$kcell$ BS communication link.

It is worth mentioning that the self-interference in a full-duplex communication system is characterised by the presence of transceiver non-linearity, whose power is not ideally proportional to the transmit power. Though the recent progress in self-interference cancellation techniques have enabled the mitigation of this interference to within acceptable levels through a combination of passive interference mitigation, and active cancellation in both the analog and digital domains (Sabharwal, Schniter, Guo, Bliss, Rangarajan & Wichman, 2014; Hong, Brand, Choi, Jain, Mehlman, Katti & Levis, 2014; Everett, Sahai & Sabharwal, 2014). Therefore most of the research works investigating the performance of full-duplex communication either assume perfect self-interference cancellation (Mahmood, Berardinelli, Tavares & Mogensen, 2015; Goyal, Liu, Panwar, Yang, DiFazio & Bala, 2014; Xie & Zhang, 2014), or consider the self-interference to be mitigated to a noise floor like level (Tong & Haenggi, 2015; Riihonen, Werner & Wichman, 2011). Moreover, even for the case of millimeter-wave communication, recently the authors in (Roberts, Jain & Vishwanath, 2020) proposed a method to mitigate self-interference to the level of ideal full-duplex communication system. Therefore, the adopted self-interference model is not ideal, but still effectively emulates the existence of self-interference in the full-duplex communication system under consideration.

In a full-duplex network interference comes from UEs and also from other BS in both uplink and downlink. Therefore, the total interference can be formulated as two separate summations over two independent Poisson point processes.

$$I_{\mathrm{UL},k} = I_{x,k}^{\mathrm{UL}} + I_{u,k}^{\mathrm{UL}}$$

$$= \sum_{i:x_{k,i}\in\Phi_{k,FD}\setminus x*} \frac{P_k h_{k,i}}{||x*-x_{k,i}||^{\alpha_k}} + \sum_{j:u_{k,j}\in\Phi_{Iu,k}} \frac{Q_k g_{k,j}}{||x*-u_{k,j}||^{\alpha_k}}, \tag{3.4}$$

$$I_{\mathrm{DL},k} = I_{x,k}^{\mathrm{DL}} + I_{u,k}^{\mathrm{DL}}$$

$$= \sum_{i:x_{k,i}\in\Phi_k\setminus x*} \frac{P_k \widehat{h}_{k,i}}{||x_{k,i}||^{\alpha_k}} + \sum_{j:u_{k,j}\in\Phi_{I_{u,FD},k}} \frac{Q_k \widehat{g}_{k,j}}{||u_{k,j}||^{\alpha_k}}, \tag{3.5}$$

where $I_{x,k}^{\mathrm{UL}}(I_{x,k}^{\mathrm{DL}})$ and $I_{u,k}^{\mathrm{UL}}(I_{u,k}^{\mathrm{DL}})$ denote the interference from other BSs and UEs, respectively, in UL(DL). $\Phi_{k,FD}$ is the PPP of full-duplex BSs in the $k$th tier which can be generated by thinning $\Phi_k$, $\Phi_{I_u,k}$ is the PPP of interfering UEs tagged to the $k$th tier BSs which can be generated by thinning $\Phi_u$, and $\Phi_{I_{u,FD},k}$ is the PPP of full-duplex interfering UEs tagged to the $k$th tier BSs which can also be generated by thinning $\Phi_u$. $h_{k,i}(\widehat{h}_{k,i})$ and $g_{k,j}(\widehat{g}_{k,j})$ are the channel gains from interfering BSs to a typical UE and from interfering UEs to a typical UE's tagged BS, respectively, in UL(DL). Moreover, Table 3.1 lists the definitions and notations of the main variables, symbols, and functions used in this paper.

## 3.4 Performance Analysis

In this section, we derive all the necessary ingredients required to evaluate the performance of the proposed system model.

### 3.4.1 Association probabilities

To understand the UEs behavior in the cell association phase, we start by deriving the cell association probabilities for all the possible association cases with respect to the criteria defined in Section 3.3.3.

Table 3.1    Notations of variables, symbols, and parameters

| Symbol | Definition | Symbol | Definition |
|---|---|---|---|
| $\Phi_k$ | PPP of $k$th tier of BSs | $\Phi_u$ | PPP of UEs |
| $x_{k,i}$ | Coordinates of BS $i$ in $k$th tier | $u_j$ | Coordinates of UE $j$ |
| $\lambda_k$ | Density of BSs in $k$th tier | $\lambda_u$ | Density of UEs |
| $Q_k$ | Transmit power of UEs tagged to BS in $k$th tier | $P_k$ | Transmit power of BS in $k$th tier |
| $G_k$ | Antenna gain of $k$th tier of BS | $h_{0,x*}$ | Channel gain from typical UE at the origin to its tagged BS |
| $h_{x*,0}$ | Channel gain from a BS to a typical UE at the origin | $\epsilon_0(\epsilon_*)$ | Self-interference suppression factor of BS(UE) |
| $\sigma_k^2$ | Noise variance | $I_{\text{UL},k}$ ($I_{\text{DL},k}$) | Interference in uplink (downlink) UE-$kcell$ BS communication link. |
| $\Phi_{k,FD}$ | Set of $k$th tier of full-duplex BSs | $\Phi_{I_u,k}$ | Set of interfering UEs tagged to $k$th tier of BSs |
| $\Phi_{I_u,FD,k}$ | Set of full-duplex interfering UEs | $h_{k,i}(\widehat{h}_{k,i})$ | Channel gain from an interfering BS to a typical UE in UL(DL) |
| $g_{k,j}(\widehat{g}_{k,j})$ | Channel gain from an interfering UE to a typical UE's tagged BS in UL(DL) | $\lambda_{I_u,FD,k}$ | Density of full-duplex interfering UEs tagged to BSs in $k$th tier |
| $\lambda_{I_u,k}$ | Density of interfering UEs tagged to BSs in $k$th tier | $\bar{F}_{\text{SINR}_{DL,k}}(z)$ $(\bar{F}_{\text{SINR}_{UL,k}}(z))$ | CCDF of DL(UL) SINR |
| $f_{\text{SINR}_{DL,k}}(z)$ $(f_{\text{SINR}_{UL,k}}(z))$ | PDF of DL(UL) SINR | $_2F_1[.,.,.;.]$ | Gauss hypergeometric function |
| $r, y$ | variables used in the numerical integration to represent distance between UE and BS | $z$ | variable used in numerical integration to represent SINR threshold. |

- **Case 1**: Downlink BS = $Mcell$ BS
- **Case 2**: Downlink BS = $Scell$ BS
- **Case 3**: Uplink BS = $Mcell$ BS
- **Case 4**: Uplink BS = $Scell$ BS

We denote $\text{Pr}_{DL,M}$, $\text{Pr}_{DL,S}$, $\text{Pr}_{UL,M}$, and $\text{Pr}_{UL,S}$ as the probability of Case 1, 2, 3, and 4, respectively. To derive these association probabilities based on the SINR optimal criteria mentioned in Section 3.3.3, first the complementary cumulative distribution function (CCDF)

and the probability density function (PDF) of their respective SINRs are derived in the following four Lemmas.

**Lemma 3.1.** *The* $\text{SINR}_{DL,k}$ *CCDF which is required to numerically evaluate the downlink cell association probabilities is mathematically formulated in (3.6).*

$$
\bar{F}_{\text{SINR}_{DL,k}}(z)
$$

$$
= \int_{r>0}^{\infty} 2\pi r \lambda_k \exp(-\pi \lambda_k r^2) \exp\left( \frac{-zr^{\alpha_k}}{P_k G_k}(\epsilon_* Q_k + \sigma_k^2) \right)
$$

$$
\times \exp\left( -2\pi \lambda_k \frac{r^{2-\alpha_k}}{(\alpha_k - 2)} \frac{zr^{\alpha_k} P_k}{P_k G_k} {}_2F_1\left[ 1, 1 - \frac{2}{\alpha_k}, 2 - \frac{2}{\alpha_k}; \frac{-zP_k}{P_k G_k} \right] \right)
$$

$$
\times \exp\left( -2\pi \lambda_{I_u,FD,k} \frac{r^{2-\alpha_k}}{(\alpha_k - 2)} \frac{zr^{\alpha_k} Q_k}{P_k G_k} {}_2F_1\left[ 1, 1 - \frac{2}{\alpha_k}, 2 - \frac{2}{\alpha_k}; \frac{-zQ_k}{P_k G_k} \right] \right) dr.
$$

(3.6)

*Proof.* The development and proof are shown in Appendix II.1. ∎

**Lemma 3.2.** *The PDF of* $\text{SINR}_{DL,k}$ *which is required to numerically evaluate the downlink cell association probabilities is mathematically formulated in (3.7).*

$$f_{\text{SINR}_{DL,k}}(z) = -\int_{y>0}^{\infty} 2\pi y \lambda_k \exp(-\pi\lambda_k y^2)\left[-\frac{y^{\alpha_k}}{P_k G_k}(\epsilon_* Q_k + \sigma_k^2) - 2\pi\lambda_k \frac{y^{2-\alpha_k}}{(\alpha_k-2)}\frac{y^{\alpha_k}P_k}{P_k G_k}\left(1-\frac{2}{\alpha_k}\right)\right.$$

$$\times\left[\frac{1}{\frac{zP_k}{P_k G_k}+1} - {}_2F_1\left[1, 1-\frac{2}{\alpha_k}, 2-\frac{2}{\alpha_k}; \frac{-zP_k}{P_k G_k}\right]\right]$$

$$-2\pi\lambda_k \frac{y^{2-\alpha_k}}{(\alpha_k-2)}\frac{y^{\alpha_k}P_k}{P_k G_k}{}_2F_1\left[1, 1-\frac{2}{\alpha_k}, 2-\frac{2}{\alpha_k}; \frac{-zP_k}{P_k G_k}\right]$$

$$-\left(1-\frac{2}{\alpha_k}\right)\left(2\pi\lambda_{I_u,FD,k}\frac{y^{2-\alpha_k}}{(\alpha_k-2)}\frac{y^{\alpha_k}Q_k}{P_k G_k}\right)\left[\frac{1}{\frac{zQ_k}{P_k G_k}+1} - {}_2F_1\left[1, 1-\frac{2}{\alpha_k}, 2-\frac{2}{\alpha_k}; \frac{-zQ_k}{P_k G_k}\right]\right]$$

$$-\left(2\pi\lambda_{I_u,FD,k}\frac{y^{2-\alpha_k}}{(\alpha_k-2)}\frac{y^{\alpha_k}Q_k}{P_k G_k}\right){}_2F_1\left[1, 1-\frac{2}{\alpha_k}, 2-\frac{2}{\alpha_k}; \frac{-zQ_k}{P_k G_k}\right]\right]$$

$$\times\exp\left(-\frac{zy^{\alpha_k}}{P_k G_k}(\epsilon_* Q_k + \sigma_k^2) - 2\pi\lambda_k\frac{y^{2-\alpha_k}}{(\alpha_k-2)}\frac{zy^{\alpha_k}P_k}{P_k G_k}{}_2F_1\left[1, 1-\frac{2}{\alpha_k}, 2-\frac{2}{\alpha_k}; \frac{-zP_k}{P_k G_k}\right]\right.$$

$$\left.-2\pi\lambda_{I_u,FD,k}\frac{y^{2-\alpha_k}}{(\alpha_k-2)}\frac{zy^{\alpha_k}Q_k}{P_k G_k}{}_2F_1\left[1, 1-\frac{2}{\alpha_k}, 2-\frac{2}{\alpha_k}; \frac{-zQ_k}{P_k G_k}\right]\right)dy.$$

$$(3.7)$$

*Proof.* The development and proof are shown in Appendix II.2. ∎

**Lemma 3.3.** *The* $\text{SINR}_{UL,k}$ *CCDF which is required to numerically evaluate the uplink cell association probabilities is mathematically formulated in (3.8).*

$$\bar{F}_{\text{SINR}_{UL,k}}(z)$$

$$=\int_{r>0}^{\infty} 2\pi r \lambda_k \exp(-\pi\lambda_k r^2)\exp\left(\frac{-zr^{\alpha_k}}{Q_k G_k}(\epsilon_0 P_k + \sigma_k^2)\right)$$

$$\times\exp\left(-2\pi\lambda_{k,FD}\frac{r^{2-\alpha_k}}{(\alpha_k-2)}\frac{zr^{\alpha_k}P_k}{Q_k G_k}{}_2F_1\left[1, 1-\frac{2}{\alpha_k}, 2-\frac{2}{\alpha_k}; \frac{-zP_k}{Q_k G_k}\right]\right)$$

$$\times\exp\left(-2\pi\lambda_{I_u,k}\frac{r^{2-\alpha_k}}{(\alpha_k-2)}\frac{zr^{\alpha_k}Q_k}{Q_k G_k}{}_2F_1\left[1, 1-\frac{2}{\alpha_k}, 2-\frac{2}{\alpha_k}; \frac{-zQ_k}{Q_k G_k}\right]\right)dr.$$

$$(3.8)$$

*Proof.* The proof is similar to that of Lemma 3.1 provided in Appendix II.1. ∎

**Lemma 3.4.** *The PDF of* $\text{SINR}_{UL,k}$ *which is required to numerically evaluate the uplink cell association probabilities is mathematically formulated in (3.9).*

$$
\begin{aligned}
f_{\mathrm{SINR}_{UL,k}}(z) = - \int\limits_{y>0}^{\infty} & 2\pi y \lambda_k \exp(-\pi\lambda_k y^2) \Bigg[ -\frac{y^{\alpha_k}}{Q_k G_k}(\epsilon_0 P_k + \sigma_k^2) - 2\pi\lambda_k \frac{y^{2-\alpha_k}}{(\alpha_k - 2)} \frac{y^{\alpha_k} P_k}{Q_k G_k}\left(1 - \frac{2}{\alpha_k}\right) \\
& \times \left[ \frac{1}{\frac{zP_k}{Q_k G_k} + 1} - {}_2F_1\left[1, 1 - \frac{2}{\alpha_k}, 2 - \frac{2}{\alpha_k}; \frac{-zP_k}{Q_k G_k}\right] \right] \\
& - 2\pi\lambda_k \frac{y^{2-\alpha_k}}{(\alpha_k - 2)} \frac{y^{\alpha_k} P_k}{Q_k G_k} {}_2F_1\left[1, 1 - \frac{2}{\alpha_k}, 2 - \frac{2}{\alpha_k}; \frac{-zP_k}{Q_k G_k}\right] \\
& - \left(1 - \frac{2}{\alpha_k}\right)\left(2\pi\lambda_{I_u,FD,k} \frac{y^{2-\alpha_k}}{(\alpha_k - 2)} \frac{y^{\alpha_k} Q_k}{Q_k G_k}\right) \left[ \frac{1}{\frac{zQ_k}{Q_k G_k} + 1} - {}_2F_1\left[1, 1 - \frac{2}{\alpha_k}, 2 - \frac{2}{\alpha_k}; \frac{-zQ_k}{Q_k G_k}\right] \right] \\
& - \left(2\pi\lambda_{I_u,FD,k} \frac{y^{2-\alpha_k}}{(\alpha_k - 2)} \frac{y^{\alpha_k} Q_k}{Q_k G_k}\right) {}_2F_1\left[1, 1 - \frac{2}{\alpha_k}, 2 - \frac{2}{\alpha_k}; \frac{-zQ_k}{Q_k G_k}\right] \Bigg] \\
& \times \exp\Bigg( -\frac{zy^{\alpha_k}}{Q_k G_k}(\epsilon_0 P_k + \sigma_k^2) - 2\pi\lambda_k \frac{y^{2-\alpha_k}}{(\alpha_k - 2)} \frac{zy^{\alpha_k} P_k}{Q_k G_k} {}_2F_1\left[1, 1 - \frac{2}{\alpha_k}, 2 - \frac{2}{\alpha_k}; \frac{-zP_k}{Q_k G_k}\right] \\
& - 2\pi\lambda_{I_u,FD,k} \frac{y^{2-\alpha_k}}{(\alpha_k - 2)} \frac{zy^{\alpha_k} Q_k}{Q_k G_k} {}_2F_1\left[1, 1 - \frac{2}{\alpha_k}, 2 - \frac{2}{\alpha_k}; \frac{-zQ_k}{Q_k G_k}\right] \Bigg) dy
\end{aligned}
$$

$$(3.9)$$

*Proof.* The proof is similar to that of Lemma 3.2 provided in Appendix II.2. ∎

**Theorem 3.1.** *The association probabilities* $\Pr_{DL,M}$, $\Pr_{DL,S}$, $\Pr_{UL,M}$, *and* $\Pr_{UL,S}$ *for the received SINR optimal criteria mentioned in Section 3.3.3 are derived as follows*

$$
\Pr_{DL,M} = \int\limits_{0}^{\infty} \bar{F}_{\mathrm{SINR}_{DL,M}}(z) f_{\mathrm{SINR}_{DL,S}}(z)\, dz, \tag{3.10}
$$

$$
\Pr_{DL,S} = 1 - \Pr_{DL,M}, \tag{3.11}
$$

*Similarly, the association probabilities* $\Pr_{UL,M}$ *and* $\Pr_{UL,S}$ *can be formulated as follows*

$$\Pr_{UL,M} = \int_0^\infty \bar{F}_{\text{SINR}_{UL,M}}(z) f_{\text{SINR}_{UL,S}}(z) dz, \tag{3.12}$$

$$\Pr_{UL,S} = 1 - \Pr_{UL,M}, \tag{3.13}$$

*Proof.* Following the association criteria mentioned in Section 3.3.3, the association probabilities $\Pr_{DL,M}$ and $\Pr_{UL,M}$ can easily be derived using Lemma 3.1, Lemma 3.2, Lemma 3.3, and Lemma 3.4.

$$\begin{aligned} \Pr_{DL,M} &= \Pr(\text{SINR}_{DL,M} > \text{SINR}_{DL,S}) \\ &= \mathbb{E}_{\text{SINR}_{DL,S}=s}[\bar{F}_{\text{SINR}_{DL,M}}(s)] \\ &= \int_0^\infty \bar{F}_{\text{SINR}_{DL,M}}(z) f_{\text{SINR}_{DL,S}}(z) dz. \end{aligned} \tag{3.14}$$

$$\begin{aligned} \Pr_{UL,M} &= \Pr(\text{SINR}_{UL,M} > \text{SINR}_{UL,S}) \\ &= \mathbb{E}_{\text{SINR}_{UL,S}=s}[\bar{F}_{\text{SINR}_{UL,M}}(s)] \\ &= \int_0^\infty \bar{F}_{\text{SINR}_{UL,M}}(z) f_{\text{SINR}_{UL,S}}(z) dz. \end{aligned} \tag{3.15}$$

Where $\Pr_{DL,S}$ and $\Pr_{UL,S}$ in (3.11) and (3.13), respectively, directly follow from the fact that $\Pr_{DL,M} + \Pr_{DL,S} = 1$ and $\Pr_{UL,M} + \Pr_{UL,S} = 1$. ∎

### 3.4.2 SINR Coverage

In the previous subsection, the SINR CCDF of both downlink and uplink transmission links are derived in Lemma 3.1 and 3.3. Since the SINR CCDF denotes the probability of coverage of its respective tier, therefore using the probability of association of each tier for both downlink and uplink derived in Theorem 3.1, we can compute the total SINR coverage as formulated in the following Corollary.

**Corollary 3.1.** *For both downlink and uplink transmission links, SINR coverage of the full-duplex two-tier network can be expressed as the summation of the SINR CCDF of each tier weighted by their association probabilities.*

$$
\begin{aligned}
&\mathrm{P}_{c,SINR_{DL}}(z) \\
&= \mathrm{Pr}_{DL,M}\bar{F}_{\mathrm{SINR}_{DL,M}}(z) + \mathrm{Pr}_{DL,S}\bar{F}_{\mathrm{SINR}_{DL,S}}(z)
\end{aligned}
\tag{3.16}
$$

$$
\begin{aligned}
&\mathrm{P}_{c,SINR_{UL}}(z) \\
&= \mathrm{Pr}_{UL,M}\bar{F}_{\mathrm{SINR}_{UL,M}}(z) + \mathrm{Pr}_{UL,S}\bar{F}_{\mathrm{SINR}_{UL,S}}(z)
\end{aligned}
\tag{3.17}
$$

### 3.4.3 Average Spectral Efficiency

To calculate the average spectral efficiency of the whole full-duplex HetNet in downlink and uplink transmission, first the average spectral efficiency of both downlink and uplink are derived separately for the $k$th tier in the following Theorem.

**Theorem 3.2.** *The average downlink spectral efficiency for the kth tier can be formulated as the summation of 1) the spectral efficiency of the fraction of time a typical UE chooses to decouple and 2) spectral efficiency of the fraction of time a typical UE chooses to transmit in a conventional way. Since there would not be any self interference when a typical UE chooses to*

*decouple because of the different frequency bands for its downlink and uplink transmission links, therefore in this case $\epsilon_* = 0$.*

$$SE_{DL,k} = |Pr_{DL,k} - Pr_{UL,k}| f_{SE_{DL,k}}(0)$$
$$+ (1 - |Pr_{DL,k} - Pr_{UL,k}|) f_{SE_{DL,k}}(\epsilon_*),$$
(3.18)

*where $f_{SE_{DL,k}}(\epsilon_*)$ is given by*

$$
\begin{aligned}
f_{SE_{DL,k}}(\epsilon_*) = &\int\limits_{z>0}^{\infty} \int\limits_{r>0}^{\infty} 2\pi r \lambda_k \exp(-\pi\lambda_k r^2) \\
&\times \exp\left(\frac{-(\exp(z) - 1)r^{\alpha_k}}{P_k G_k}(\epsilon_* Q_k + \sigma_k^2)\right) \\
&\times \exp\left(-2\pi\lambda_k \frac{r^{2-\alpha_k}}{(\alpha_k - 2)} \frac{(\exp(z) - 1)r^{\alpha_k} P_k}{P_k G_k}\right. \\
&\quad {}_2F_1\left[1, 1 - \frac{2}{\alpha_k}, 2 - \frac{2}{\alpha_k}; \frac{-(\exp(z) - 1)P_k}{P_k G_k}\right]\right) \\
&\times \exp\left(-2\pi\lambda_{I_{u,FD,k}} \frac{r^{2-\alpha_k}}{(\alpha_k - 2)} \frac{(\exp(z) - 1)r^{\alpha_k} Q_k}{P_k G_k}\right. \\
&\quad {}_2F_1\left[1, 1 - \frac{2}{\alpha_k}, 2 - \frac{2}{\alpha_k}; \frac{-(\exp(z) - 1)Q_k}{P_k G_k}\right]\right) dr\, dz.
\end{aligned}
$$
(3.19)

*Similarly, the average uplink spectral efficiency for the kth tier can be formulated as*

$$SE_{UL,k} = |Pr_{DL,k} - Pr_{UL,k}| f_{SE_{UL,k}}(0)$$
$$+ (1 - |Pr_{DL,k} - Pr_{UL,k}|) f_{SE_{UL,k}}(\epsilon_0),$$
(3.20)

*where $f_{SE_{UL,k}}(\epsilon_0)$ is given by*

$$f_{SE_{UL,k}}(\epsilon_0) = \int\limits_{z>0}^{\infty} \int\limits_{r>0}^{\infty} 2\pi r \lambda_k \exp(-\pi\lambda_k r^2)$$

$$\times \exp\left(\frac{-(\exp(z)-1)r^{\alpha_k}}{Q_k G_k}(\epsilon_0 P_k + \sigma_k^2)\right)$$

$$\times \exp\left(-2\pi\lambda_{k,FD}\frac{r^{2-\alpha_k}}{(\alpha_k-2)}\frac{(\exp(z)-1)r^{\alpha_k}P_k}{Q_k G_k}\right.$$

$$\left._2F_1\left[1,1-\frac{2}{\alpha_k},2-\frac{2}{\alpha_k};\frac{-(\exp(z)-1)P_k}{Q_k G_k}\right]\right)$$

$$\times \exp\left(-2\pi\lambda_{I_u,k}\frac{r^{2-\alpha_k}}{(\alpha_k-2)}\frac{(\exp(z)-1)r^{\alpha_k}Q_k}{Q_k G_k}\right.$$

$$\left._2F_1\left[1,1-\frac{2}{\alpha_k},2-\frac{2}{\alpha_k};\frac{-(\exp(z)-1)Q_k}{Q_k G_k}\right]\right)dr\,dz. \tag{3.21}$$

*Proof.* The development and proof are shown in Appendix II.3. ∎

**Corollary 3.2.** *Based on the probability of association in Theorem 3.1 and the spectral efficiency of each tier in Theorem 3.2, the average spectral efficiency of the whole full-duplex HetNet for both uplink and downlink transmissions can be formulated as*

$$SE_{DL} = Pr_{DL,M}SE_{DL,M} + Pr_{DL,S}SE_{DL,S} \tag{3.22}$$

$$SE_{UL} = Pr_{UL,M}SE_{UL,M} + Pr_{UL,S}SE_{UL,S} \tag{3.23}$$

## 3.5 Numerical and Simulation Results

In this section, to highlight the performance insights of the system under consideration, rigorous numerical and simulation results are presented. The analytical results are validated by Monte

Carlo simulations for randomly located UEs and BSs according to their respective densities. It is

assumed that all UEs and BSs can communicate in full-duplex mode unless they are decoupling.

We did system level simulations, where we deployed BSs and UEs in a circular area of radius $\mu$

with the help of tools from stochastic geometry. Then, based on their coordinates, randomly

generated fading coefficients, transmit powers, and antenna gains, we calculated all types of

interferences. All these ingredients help us calculate the SINRs which eventually derive the

association criteria. All the simulation results are obtained by averaging over 10,000 independent

realizations in MATLAB. The default system parameters are selected according to the 3GPP

specifications (3GPP TR 36.942, 2009) and existing research works (Smiljkovikj $et\ al.$, 2015b,a;

Elshaer $et\ al.$, 2016), where their values are listed in Table 3.2.

Table 3.2    System Parameters

| **Parameters** | **Values** |
|---|---|
| $Mcell$ BS transmit power $P_M$ (dBm) | 46 |
| $Scell$ BS transmit power $P_S$ (dBm) | 30 |
| Antenna Gain for $Mcell$ BS $G_M$ (dBi) | 0 |
| Antenna Gain for $Scell$ BS $G_S$ (dBi) | 18 |
| UE's transmit power to $Mcell$ BS $Q_M$ (dBm) | 23 |
| UE's transmit power to $Scell$ BS $Q_S$ (dBm) | 20 |
| Radius of the circular area of simulation $\mu$ (m) | 1500 |
| Pathloss exponent for sub-6GHz tier $\alpha_M$ | 3 |
| Pathloss exponent for millimeter wave tier $\alpha_S$ | 4 |
| Self-interference suppression factor of BS(UE) $\epsilon_*(\epsilon_0)$ | $10^{-5}$ |
| Microwave or sub-6GHz bandwidth $B_M$ (MHz) | 20 |
| mmWave bandwidth $B_S$ (GHz) | 1 |
| Noise power $\sigma_k^2$ | -174 dBm/Hz + $10\log_{10}(B_k)$ + $10dB$ |

### 3.5.1   Association Probabilities

Fig. 3.2a and 3.2b illustrate the association probabilities derived in Theorem 3.1 against the

ratio of $Scell$ to $Mcell$ density for $G_S = 18dBi$ and $G_S = 32dBi$, respectively. It is observed

that there is a close match between the simulation and analytical results, which validates the

analysis. The significant gap between the downlink and uplink association probabilities for both *Scell* and *Mcell* BSs represents the decoupling gain. In other words, this gap defines the decoupled access where UEs prefer to connect with two different BSs for their uplink and doownlink transmissions. Fig. 3.2a shows that almost 10% of the UEs choose to decouple at $\lambda_S/\lambda_M = 40$. Moreover, the decrease in the decoupling gain from 35% for $\lambda_S/\lambda_M = 5$ to 10% for $\lambda_S/\lambda_M = 40$ is due to the fact that as we increase the density of *Scell* BSs, the UEs prefer to connect to *Scell* BSs for both downlink and uplink transmissions due to its antenna gain and close proximity. Fig. 3.2b shows that a higher antenna gain for mmWave BSs significantly reduces the decoupling gain. This stem from the fact that higher antenna gain of mmWave BSs make them SINR optimal for both downlink and uplink transmissions.

Fig. 3.3 illustrates the effect of the number of full-duplex UEs and BSs in a network on the association probabilities. The 100% and 10% in the legend of the figure represent the fraction of the full-duplex UEs and BSs. The full-duplex transmission mode gives birth to two additional interference components. A self-interference and full-duplex interference that comes from the other full-duplex UEs in downlink and the other full-duplex BSs in uplink. Therefore Fig. 3.3 compares the association probabilities of two scenarios: 1) when all the UEs and BSs can communicate in full-duplex mode and 2) when only 10% of them can communicate in full-duplex mode. It is intriguing to see that the additional full-duplex interference does not measurably change or modify the association curves. The rationale behind this is related to the fact that the additional full-duplex interference is only a small fraction of the total interference, therefore, it does not affect the association curves notably. The zoomed-in window in the figure shows the insignificant effect of the additional full-duplex interference on the association curves.

In Fig. 3.4, the association probabilities are plotted for different values of the self-interference suppression factor. Since it is assumed that $\epsilon_0 = \epsilon_*$, therefore the subscript of $\epsilon$ is omitted from the legend of Fig. 3.4. The additional curves are plotted with 50% decrease and 100% increase in the default value of the self-interference suppression factor, i.e. $10^{-5}$. Fig. 3.4 illustrates that the increase or decrease in the self-interference suppression factor does not change the trends of association probabilities in a measurable way. This is because, after suppression, the

self-interference is only a small fraction of the total interference. Moreover, the slight difference in the downlink association probabilities for different values of the self-interference suppression factor is due to the difference of transmit powers of the *Mcell* and *Scell* BSs. Similarly, since the difference between the transmit powers of the UEs for both microwave and millimeter-wave links is no significant, compared to the difference of transmit powers of the *Mcell* and *Scell* BSs, therefore the curves of uplink association probabilities overlap for different values of self-interference suppression factor.

### 3.5.2   SINR Coverage

In this part, SINR coverage analysis is validated by rigorous simulations. Fig. 3.5 shows that the analytical expressions sharply match the corresponding simulation results, which gives us the confidence to use the analysis for further insights in the following results. Fig. 3.6 illustrates the effect of the assumption of a typical noise-limited mmWave network and compares it with the proposed model, which accounts for all kinds of interference for both mmWave and sub-6GHz networks. It can be seen that for a fairly dense mmWave network i.e., $\lambda_S = 200/km^2$, the noise-limited assumption closely matches with the proposed model i.e., SINR $\approx$ SNR. However, as we move into the realm of ultra-dense networks (UDNs) (Xie, Liu, Sheng, Zhang & Li, 2019; Liu, Sheng & Li, 2018) where the density of access points is greater than the density of UEs (Kamel *et al.*, 2016), the typical noise-limited assumption does not remain valid. For example for $\lambda_S = 1000/km^2$ at $z = 30$dB, there is a significant gap of 20% between SNR and SINR coverage. This result not only reaffirms the assumption that the interference in the mmWave network should also be accounted for, specially when moving into the realm of UDN, but also validates the robustness of the proposed model.

### 3.5.3   Spectral Efficiency

Fig. 3.7 compares the spectral efficiency of full-duplex two-tier HetNet with decoupled access with its coupled counterpart for both uplink and downlink separately. It can be seen that decoupled access outperforms its coupled counterpart for a fairly large range of densities. The

rationale behind this gain in spectral efficiency is the BS diversity caused by decoupled access. Moreover, to understand the small bump on the uplink spectral efficiency curve of the decoupled case at $\lambda_S/\lambda_M = 5$, we have to take a look at Fig. 3.2a again. In this context,it is observed that from $\lambda_S/\lambda_M = 1$ to $\lambda_S/\lambda_M = 5$, there is a sharp increase in the association probability of *Scell* BSs, which means more UEs connect with *Scell* BSs. Moreover, since uplink coverage of *Scell* BSs is better than *Mcell* BSs, as shown in Fig. 3.8, therefore in Fig. 3.7 the uplink spectral efficiency curve of decoupled case at $\lambda_S/\lambda_M = 5$ has a sharp bump. Furthermore, the slight decrease in the uplink spectral efficiency curve of the decoupled case from $\lambda_S/\lambda_M = 6$ to $\lambda_S/\lambda_M = 15$ is due to the decrease in the decoupling gain for this range of the ratio of the density of BSs. The rise in the curve afterward is due to the very high association probability of *Scell* BSs. In addition, Fig. 3.9 shows the effect of decoupling on uplink energy efficiency. It can be noted that the average uplink energy efficiency, which is defined as the uplink channel capacity normalized by the UE's transmit power, for the system with decoupled access is always superior to that of the system without decoupling. This is due to the fact that with decoupled access UEs transmits to *Scell* BSs with less transmit power.

Fig. 3.10 illustrates the effect of the number of full-duplex UEs and BSs in a network on the spectral efficiency. The 100%, 50%, and 10% in the legend of the figure represent the fraction of the full-duplex UEs and BSs. Since the downlink transmit power of a BS is always significantly greater than the uplink transmit power of a UE, therefore the added full-duplex interference does not affect the spectral efficiency of downlink measurably. On the other hand, the notable effect of full-duplex interference can be seen on the uplink spectral efficiency.

## 3.6  Conclusions

In this paper, we proposed a comprehensive characterization of a full-duplex two-tier HetNets with decoupled access. Since the future mmWave networks are envisioned to coexist with microwave or sub-6GHz networks, therefore we modeled a HetNet with a tier of microwave BSs and a tier of mmWave BSs. To study the association behavior of UEs in the aforementioned model, we derived the SINR optimal association probabilities and showed the effect of full-duplex

interference on them. It is interesting to note that the added full-duplex interference does not change the association probabilities in a significant way. Unlike the typical convention of noise-limited mmWave network, we accounted for interference and performed a comparative analysis of both assumptions showing that the former become invalid as we move into the realm of UDNs. Finally, we derived the spectral efficiency of both the downlink and uplink separately and compared it with its coupled counterpart. We also showed the effect of full-duplex interference on the spectral efficiency by evaluating HetNets with different fractions of full-duplex UEs and BSs. It is intriguing to see that the effect of added full-duplex interference is rather insignificant on the downlink spectral efficiency and as we move towards a denser mmWave network, its effect on uplink spectral efficiency diminishes too.

a) $G_S = 18\text{dBi}$

b) $G_S = 32\text{dBi}$
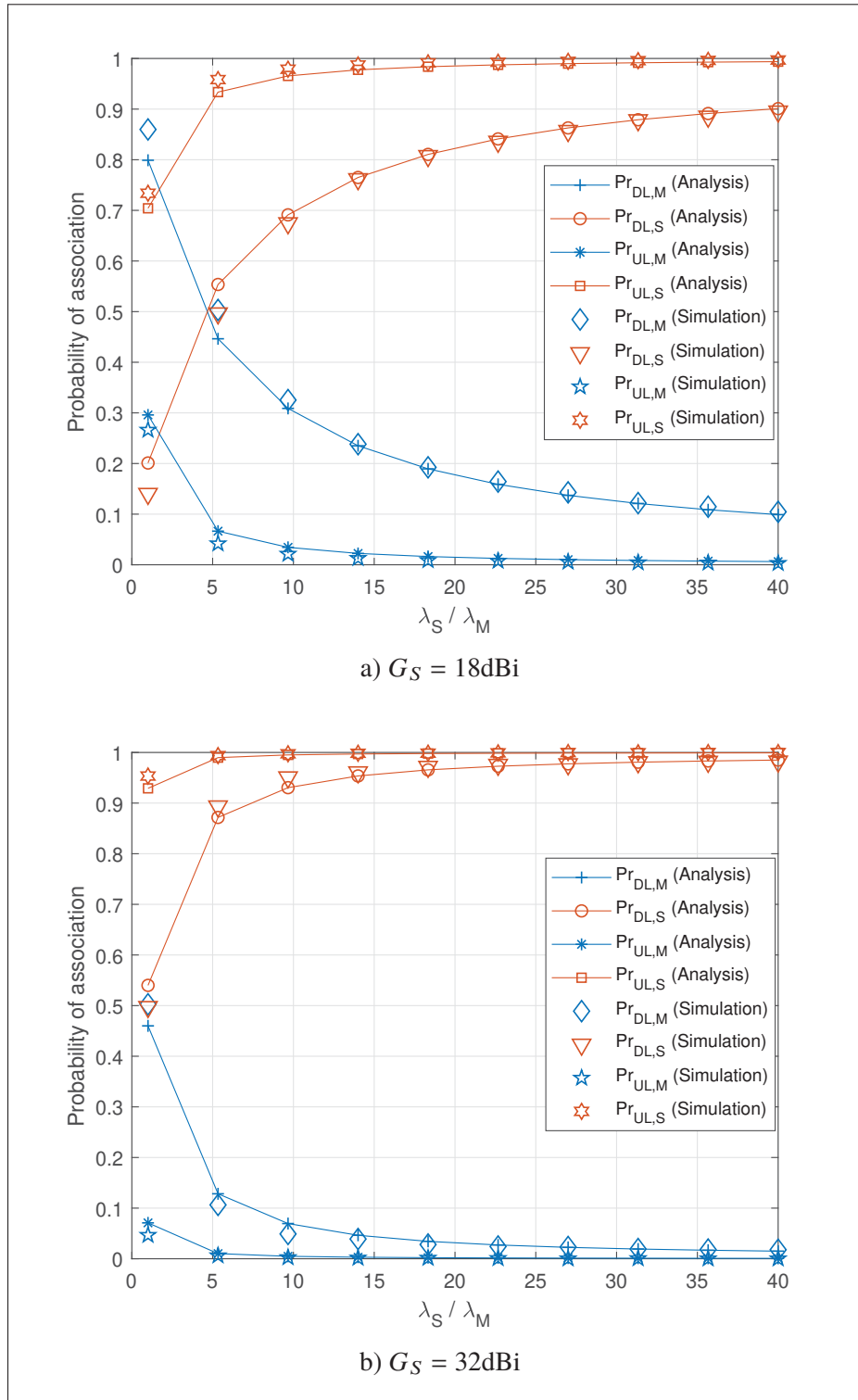
Figure 3.2    Probability of association and validation of analysis
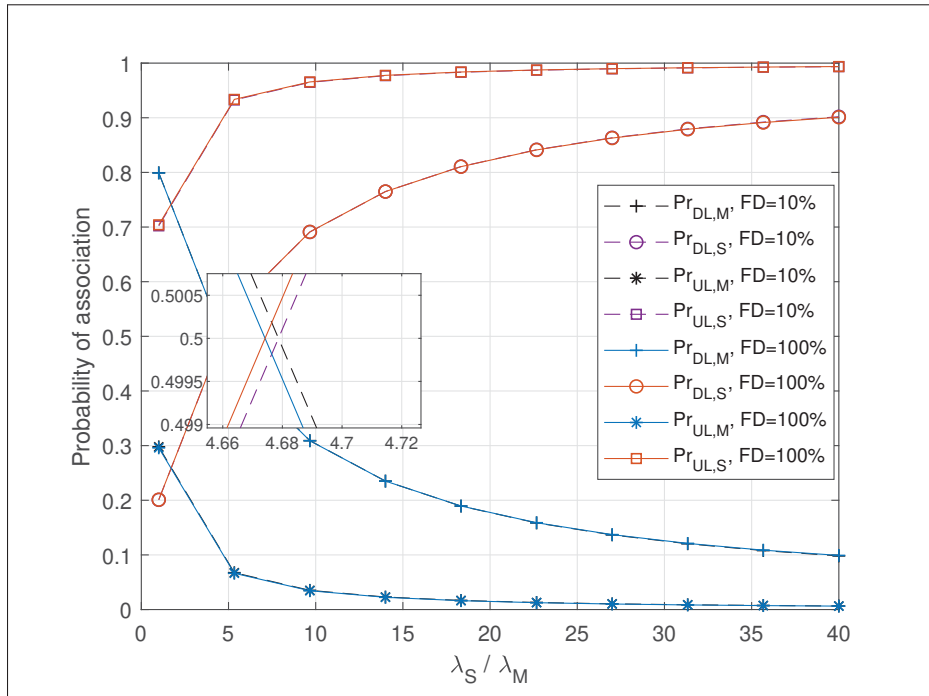
Figure 3.3　Effect of the number of full-duplex UEs and BSs in the network on the probability of association
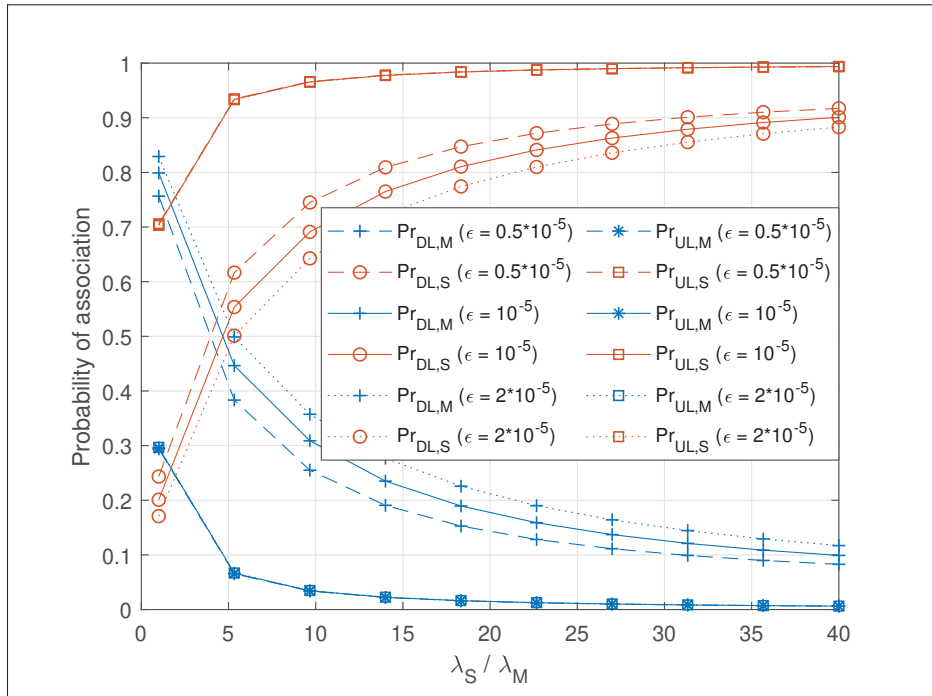
Figure 3.4    Effect of the different levels of self-interference suppression factor on the association probabilities for $G_S = 18$dBi
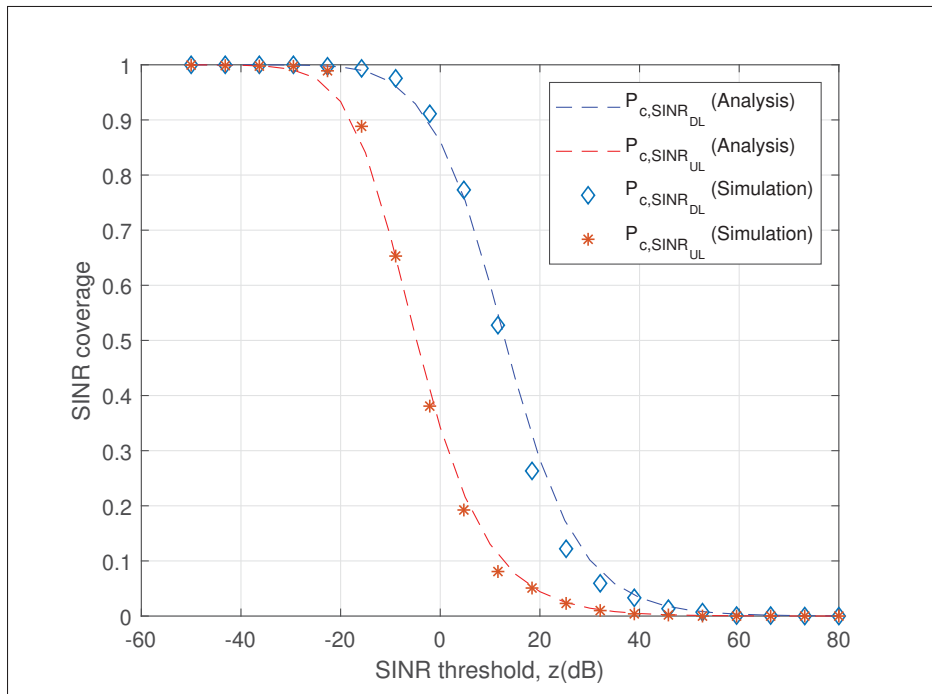


Figure 3.5    SINR coverage for $\lambda_S/\lambda_M = 40$ and validation of analysis
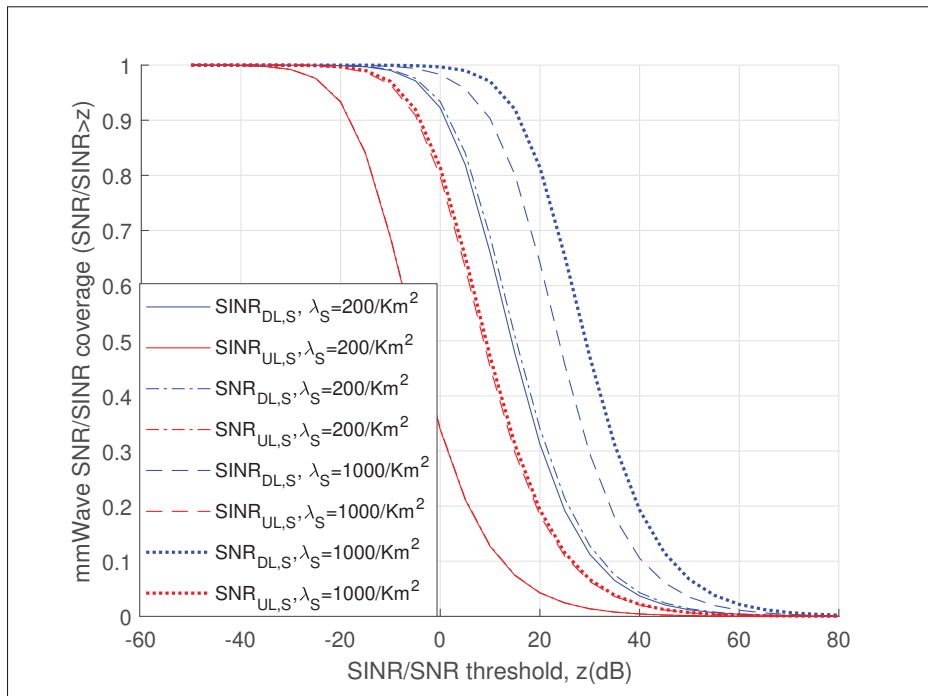
Figure 3.6    Comparative results for the distribution of the
mmWave SINR and SNR
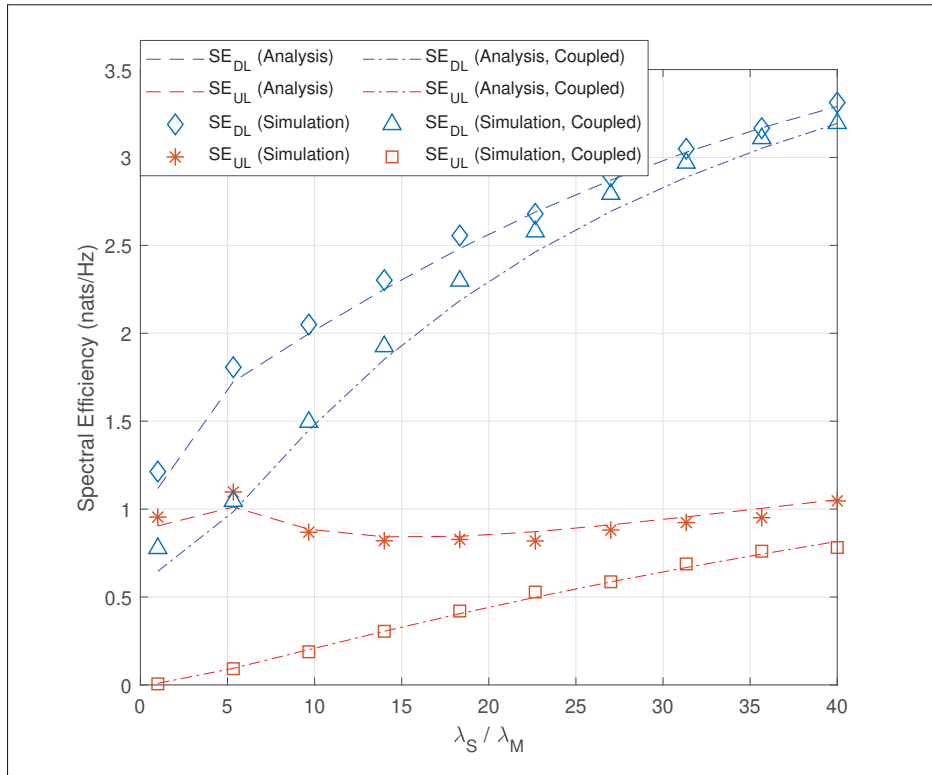
Figure 3.7    Spectral efficiency of decoupled and coupled
full-duplex two tier HetNet and validation of analysis
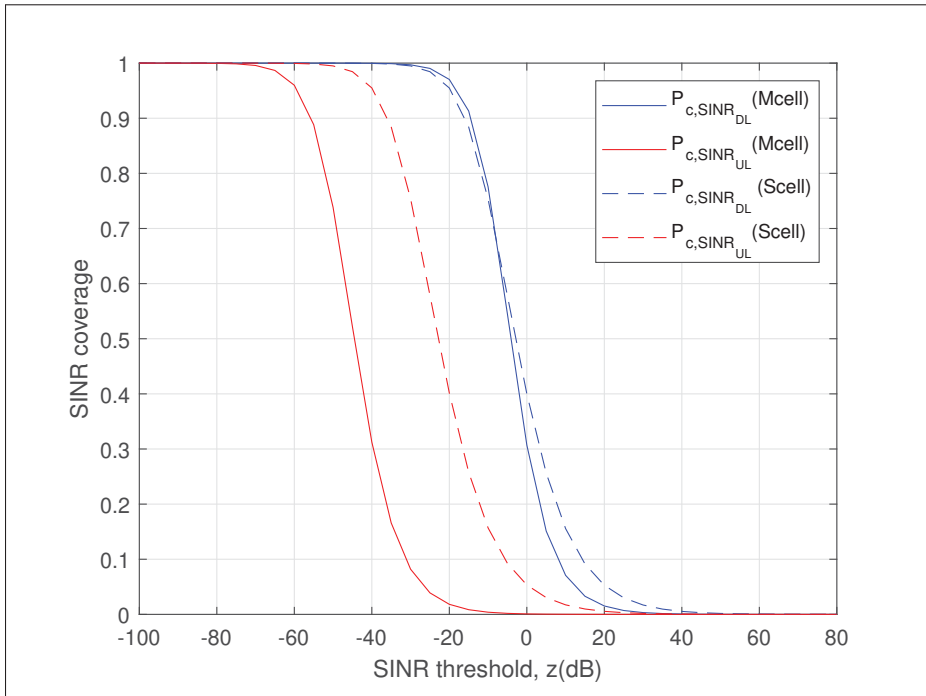
Figure 3.8    SINR coverage of Mcell and Scell BSs for $\lambda_S/\lambda_M = 5$
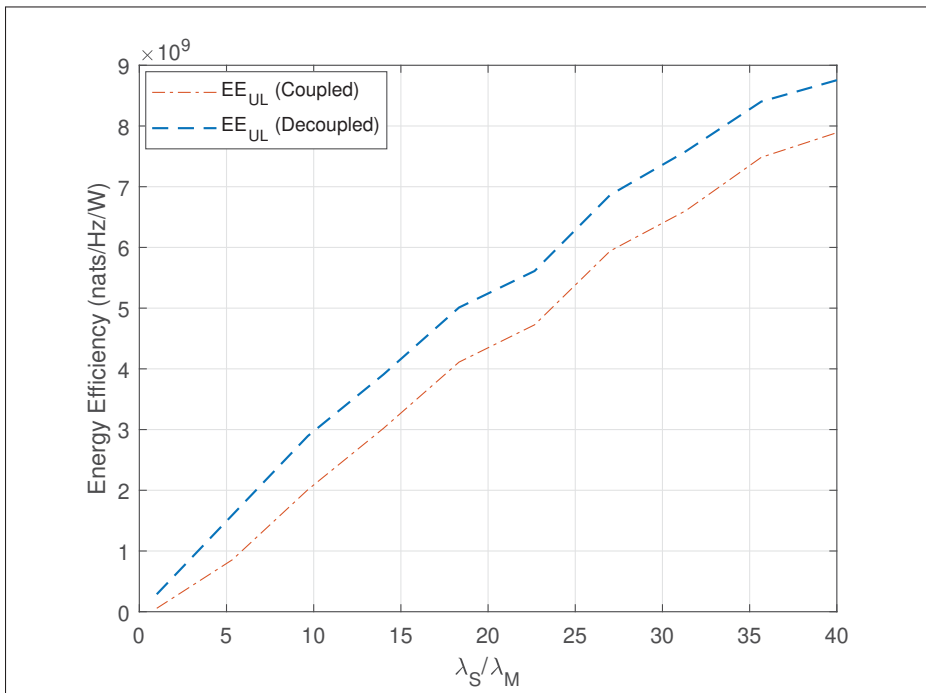


Figure 3.9    Average uplink energy efficiency of decoupled and coupled full-duplex two tier HetNet
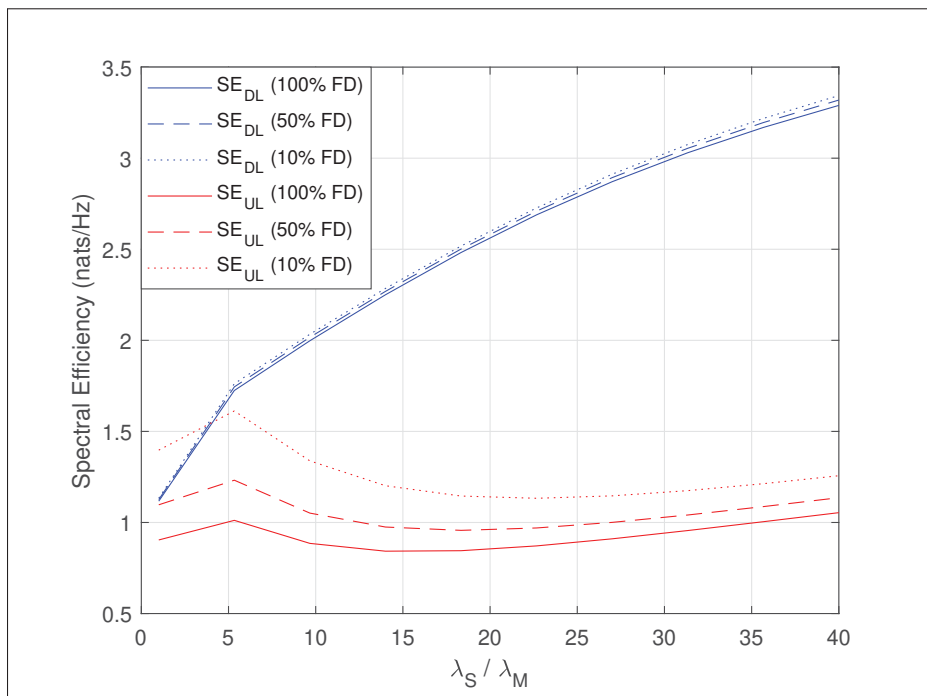
Figure 3.10     Effect of number of full-duplex UEs and BSs in a
network on the spectral efficiency

# CHAPTER 4

# ANTENNA ARRAY GAIN AND CAPACITY IMPROVEMENTS OF ULTRA-WIDEBAND MILLIMETER WAVE SYSTEMS USING A NOVEL ANALOG ARCHITECTURE DESIGN

Zeeshan Sattar[a] , Joao V.C. Evangelista[b] , Georges Kaddoum[c] , Naïm Batani[d]

[a,b,c,d]Department of Electrical Engineering, École de Technologie Supérieure, 1100 Notre-Dame Ouest, Montréal, Québec, Canada H3C 1K3

## 4.1 Abstract

In this letter, we address the issue of beam-squinting encountered in ultra-wideband millimeter wave mobile communication systems. First, the beam-squinting effects on the antenna array gain and the usable bandwidth of these systems are analyzed. The obtained results show that, in ultra-wideband communication systems, beam-squinting causes loss in array gain and limits the achievable capacity. To mitigate these effects, a new analog architecture design, that improves the array gain and the achievable capacity, is proposed. The proposed architecture is most suitable for delay-sensitive or computational power constrained applications and does not require the computation of any compensation matrix in the digital domain. In addition, the exact expression for the array gain of the proposed analog architecture is derived. To further simplify the evaluation of the system performance, an approximated closed-form expression for the array gain is derived. Furthermore, to evaluate the performance of the proposed design, rigorous numerical results concerning different system parameters are provided in this paper.

## 4.2 Introduction

Beam-squinting did not get enough limelight to come on the dissecting table of researchers of mobile communications until recently. The reason for this deliberate neglect was the fact that, so far, almost all mobile communication systems work on narrowband signals, which by

their very nature make the beam-squinting issue negligible. Since the main quest of the next generation of communication systems, i.e., 5G, is to provide seamless coverage, hot-spot high capacity, low end-to-end latency, and massive connectivity; in order to meet these requirements, one of the most promising solutions is the use of extremely high frequencies (EHF) which are commonly known as the millimeter wave (mmWave) band. Since the main attraction in the mmWave band is its large available bandwidth, wideband and ultra-wideband communication systems will become an unavoidable reality in the near future and therefore, beam-squinting cannot be ignored anymore.

Recently, the authors in (Wang *et al.*, 2018a,b) revisited the issue of beam-squinting from the perspective of massive multiple-input multiple-output (MIMO) systems. They highlighted problems specific to wideband massive MIMO systems caused by beam-squinting. In (Li *et al.*, 2018a), the authors proposed a beam squint (BS) compensation method in the digital domain for hybrid precoding. They designed a compensation matrix for hybrid precoding to reduce the impact of the BS. Furthermore, they showed the performance loss of analog precoder with BS compared with the ideal analog precoder. In (Liu & Qiao, 2019), the authors also investigated the BS problem in a millimeter wave communication system using space time coding. They proposed a space-time-block-code (STBC) based beamforming scheme and demonstrated through numerical simulations, that their proposed scheme can compensate for the BS and improve the throughput performance for wideband communication systems in certain cases. Since beam-squinting issue is related to the analog nature of ultra-wideband signals, therefore any compensation in the digital domain can only result in very limited improvements in the array gain and spectral efficiency. The authors in (Liu & Zhu, 2018), adopted a radically different approach to tackle this issue, they proposed to adopt the Rotman lens array as an analog precoder to provide true-time-delay (TTD) and reduce the BS impairment.

In this paper, a novel analog architecture design to mitigate the impact of BS is proposed. The main idea behind the proposed design is to divide a wideband or ultra-wideaband signal into chunks of comparatively narrowband signals using a bank of bandpass filters, followed by an additional phase shift with respect to the centre frequency of each filter. The advantage of our

proposed design is that it does not rely on any compensation in the digital domain or use any specialized components such as a Rotman lens. It is therefore suitable for computational power constrained or delay-sensitive applications (Alsenwi, Tran, Bennis, Kumar Bairagi & Hong, 2019; Vu, Liu, Bennis, Debbah, Latva-aho & Hong, 2017), which do not have the liberty to calculate large compensation matrices in the digital domain. Table 4.1 provides a brief summary along with comments on the key design features of the aforementioned existing approaches to mitigate beam-squinting. The previously proposed methods are either specifically intended for a system employing hybrid precoding or require multiple radio frequency (RF) chains in the transceiver design. In comparison, our proposed design does not have such constraints and can be tailored for the aforementioned scenarios. Therefore to show a fair comparison and following the literature (Li *et al.*, 2018a; Liu & Qiao, 2019), the performance of the proposed design is compared against an ideal system with no BS and a practical system with BS. Hence, this letter addresses the question in ultra-wideband mmWave-enabled massive MIMO systems: *"how to provide an order of magnitude capacity improvement without adding any computational complexity?"*

## 4.3 System Model

In this letter, we consider analog beamforming with one uniform linear array (ULA) antenna of size $N$, where the antenna elements of an array are divided into groups of size $K$. Here, the distance between any two adjacent antenna elements is denoted by $d$. Each antenna element in its group is driven by a phase shifter, where each group of antenna elements are further driven by a bank of bandpass filters of size $L$ and an additional array of phase shifters, as shown in Fig. 4.1. The additional driving elements of an antenna array, i.e., bank of band pass filters and additional phase shifters are there to push the array gain of subcarriers of an ultra-wideband signal towards the angle of arrival (AoA) of their centre frequency. Hence in this paper, a phase correction (PC) factor is introduced to provide the additional phase shift, which consequently minimizes the beam-squinting effect.

Table 4.1    Different approaches to mitigate beam-squinting

| Ref. | Design features | Comments |
|---|---|---|
| (Li *et al.*, 2018a) | • Proposed for hybrid pre-coding.<br>• Compensate beam-squinting in digital domain.<br>• Compensation matrix is a solution of an approximation of a non-convex optimization problem. | For this method, the authors formulated a rate maximisation problem considering frequency-varying analogue precoders, and designed a compensation matrix in the digital domain. This method is basically an improvement to a digital precoder, considering the frequency-dependent analogue precoder for each subcarrier. |
| (Liu & Qiao, 2019) | • STBC based beamforming design.<br>• Transmitted signals are first encoded using a STBC encoder.<br>• Compensate beam-squinting in digital domain. | This method requires a computation of eigen-values and eigen-vectors of a $N \times N$ matrix (here $N$ is the number of transmit antennas). It is well known that the computational complexity of eigen-values and eigen-vectors of an $N \times N$ matrix is $O(N^3)$, therefore the computational complexity grows with the number of transmit antennas. |
| (Liu & Zhu, 2018) | • Two-tier hybrid beamforming.<br>• Rotman-lens based TTD beamformer.<br>• Mitigate beam-squinting in analog domain. | As mentioned in (Vashist, Soni & Singhal, 2014), the design of a Rotman lens that is feasible for all signals with various and continuous directions is not possible due to a limited spatial resolution and discreet beam port (focal point) in the focal point arc. Therefore the authors in (Liu & Zhu, 2018) proposed a Rotman lens based two-tier hybrid precoder, where the first tier provides TTD, the second tier's hybrid precoder compensates for the finite spatial resolution problem of practical lens array. |
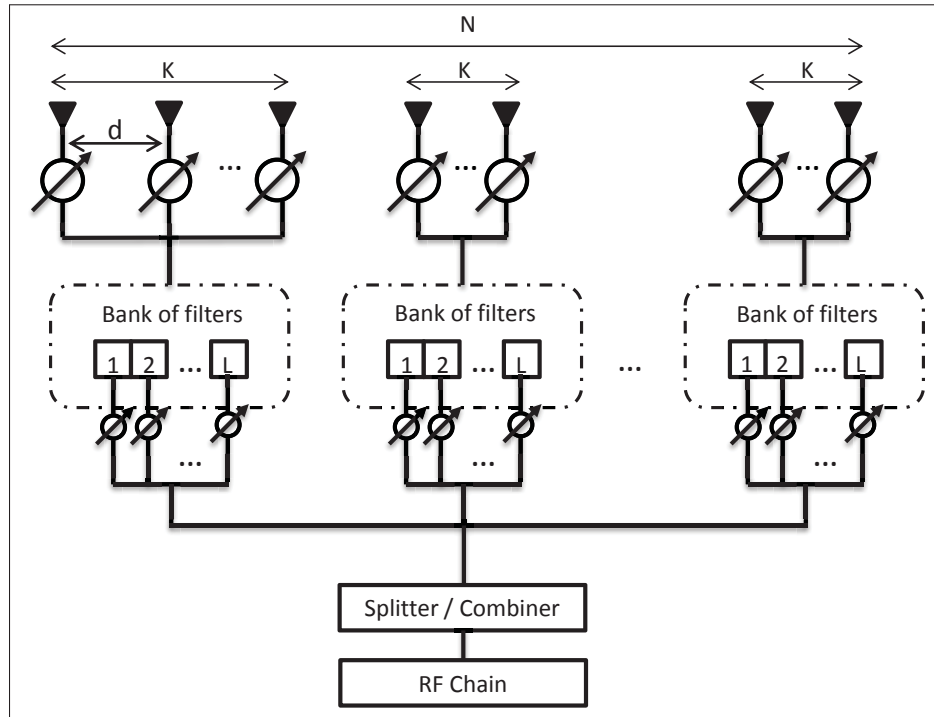
Figure 4.1    System Model

Suppose the signal arriving at the array is $s(t)$, then the received signal vector $\mathbf{y(t)}$ at $N$ antenna elements before the phase shifters is

$$
\begin{aligned}
\mathbf{y}(t) = \Bigg[ s(t), ..., s\left(t - \frac{(n-1)d\sin\theta}{c}\right), \\
..., s\left(t - \frac{(N-1)d\sin\theta}{c}\right) \Bigg]^T .
\end{aligned}
\tag{4.1}
$$

Similarly, its frequency response can be written as

$$
\begin{aligned}
\mathbf{y}(f, \theta) = s(f) \Big[ 1, \exp j(2\pi c^{-1} f d \sin\theta), \\
..., \exp j(2\pi c^{-1} f (n-1)d\sin\theta), \\
..., \exp j(2\pi c^{-1} f (N-1)d\sin\theta) \Big]^T
\end{aligned}
\tag{4.2}
$$

where $\mathbf{y}(f, \theta)$ is a function of the AOA $\theta$, and $\theta \in \{-\frac{\pi}{2}, \frac{\pi}{2}\}$. Define the ULA response vector as

$$
\begin{aligned}
\mathbf{a}(\theta, f) = \big[&1, \exp j(2\pi c^{-1} f d \sin \theta), \\
&..., \exp j(2\pi c^{-1} f(n-1)d \sin \theta), \\
&..., \exp j(2\pi c^{-1} f(N-1)d \sin \theta)\big]^T.
\end{aligned}
\tag{4.3}
$$

The optimal combiner or steering vector for the received signal $\mathbf{y}(f, \theta)$ should be a filter matched to $\mathbf{a}(\theta, f)$ denoted as

$$
\mathbf{w} = \mathbf{a}^H(\theta, f).
\tag{4.4}
$$

Since elements in the matched filter are true time delay devices and they have their own implementation issues, we use phase shifters instead. A phase shifter is typically modeled as a constant phase shift for the whole frequency range it is designed for. Hence, the phase shifter based steering vector with phase shift $\beta_n$ for the $n$th antenna element is written as

$$
\hat{\mathbf{w}} = [\exp j(\beta_1), ..., \exp j(\beta_n), ..., \exp j(\beta_N)].
\tag{4.5}
$$

Following (Balanis, 2016), the array gain of phased array at angle of arrival $\theta$ can be formulated as

$$
\begin{aligned}
g(\hat{\mathbf{w}}, \theta, f) &= \frac{1}{\sqrt{N}} \hat{\mathbf{w}}^H \mathbf{a}(\theta, f) \\
&= \frac{1}{\sqrt{N}} \sum_{n=1}^{N} \exp j(2\pi c^{-1} f(n-1)d \sin \theta - \beta_n).
\end{aligned}
\tag{4.6}
$$

Typically we choose $\beta_n$ with respect to the centre frequency i.e., $f_c$ in our case

$$
\beta_n(\psi) = 2\pi c^{-1} f_c(n-1)d \sin \psi.
\tag{4.7}
$$

Here $\psi$ is the angle of desired beam and inter-antenna element distance $d = \frac{\lambda_c}{2}$. Putting (4.7) into (4.6), we get

$$g(\psi, \theta, \xi_{n_f}) = \frac{1}{\sqrt{N}} \sum_{n=1}^{N} \exp j(\pi(n-1)(\xi_{n_f} \sin \theta - \sin \psi)). \qquad (4.8)$$

Here, $\xi_{n_f}$ is the ratio of subcarrier frequency to the carrier frequency $f_c$ for subcarrier $n_f$.

$$\xi_{n_f} = 1 + \frac{(2n_f - N_f + 1)b_{frac}}{2N_f}. \qquad (4.9)$$

Here $b_{frac} = B/f_c$ is the fractional bandwidth, $n_f \in \{0, 1, ..., N_f - 1\}$, and $N_f$ is the total number of subcarriers.

**Lemma 4.1.** *Following the proposed analog architecture, the array gain with the PC factor $\pi\phi_k(\xi_{n_f})$ is obtained as*

$$g_{pc}(\psi, \theta, n_f) = \frac{1}{\sqrt{N}} \sum_{k=1}^{\frac{N}{K}} \sum_{n=(k-1)K+1}^{Kk} \exp\left(j\pi\left((n-1)x_{n_f} + \phi_k(n_f)\right)\right), \qquad (4.10)$$

*where*

$$x_{n_f} = (\xi_{n_f} \sin \theta - \sin \psi),$$

*and*

$$\phi_k(n_f) = (K(k-1) + c_k)x_{c,n_f}.$$

*Here the variable $c_k$ represents the index of antenna element which drives the subsequent layer of phase shifters within its antenna group of size K, and $x_{c,n_f} = (\xi_{c,n_f} \sin \theta - \sin \psi)\ \forall \xi_{c,n_f}$.*

$\xi_{c,n_f}$ represents the ratio of the centre subcarrier frequency of each bandpass filter to the carrier frequency $f_c$. Hence, the value of $x_{c,n_f}$ remains constant for all the subcarriers of each filter.

*Proof.* The development and proof are shown in Appendix III.1. ∎

In Lemma 4.1, the exact array gain of our proposed model is derived, we can further simplify it into a closed form expression by approximating $c_k$ to a linear function.

**Theorem 4.1.** *If we approximate $c_k$ to a linear function $(k-1)b$, where $b$ is an integer and its value is bounded by $(k-1)b \leq K \; \forall k$ the array gain of the proposed model takes the following form*

$$
\begin{aligned}
\hat{g}_{pc}(\psi, \theta, n_f) = {} & \frac{1}{\sqrt{N}} \frac{\sin(K\pi x/2)}{\sin(\pi\frac{x}{2})} \exp\left(j(K-1)\pi\frac{x}{2}\right) \\
& \times \frac{\sin(\frac{N}{K}\pi(K(x_{n_f} + x_{c,n_f}) + bx_{c,n_f})/2)}{\sin(\pi(K(x_{n_f} + x_{c,n_f}) + bx_{c,n_f})/2)} \\
& \times \exp\left(j\pi(\frac{N}{K} - 1)(K(x_{n_f} + x_{c,n_f}) + bx_{c,n_f})/2\right).
\end{aligned}
\tag{4.11}
$$

*Proof.* The development and proof are shown in Appendix III.2. ∎

**Corollary 4.1.** *Assuming Gaussian signalling (Cover & Thomas, 2012) and following (Tse & Viswanath, 2005), the achievable capacity for the derived array gain in Lemma 4.1 can be expressed as*

$$
C_{pc} = B\frac{1}{N_f} \sum_{n_f=0}^{N_f} \log\left(1 + \frac{P|g_{pc}(\psi, \theta, n_f)|^2}{B\sigma^2}\right)
\tag{4.12}
$$

**Corollary 4.2.** *Similar to Corollary 4.1, the achievable capacity for the array gain derived in Theorem 4.1 can be expressed as*

$$
\hat{C}_{pc} = B\frac{1}{N_f} \sum_{n_f=0}^{N_f} \log\left(1 + \frac{P|\hat{g}_{pc}(\psi, \theta, n_f)|^2}{B\sigma^2}\right)
\tag{4.13}
$$

### 4.4 Numerical Results

In this section, we analyze the performance of the novel proposed architecture. Fig. 4.2 shows the comparison between the array gain of the proposed model with PC (Lemma 4.1 and Theorem 4.1) and the array gain of a typical system with BS. It is observed that the proposed design improves the array gain of the subcarriers on the left and right of the main lobe. For example, at $\xi_{n_f} = 1.03$ and $\xi_{n_f} = 0.97$, the improvement in array gain is approximately 10dB. Hence, in applications where the reliability of the information on all subcarriers are of equal importance or in scenarios where we do not have the liberty to calculate large compensation matrices in the digital domain, the proposed design can provide significant improvement in the array gain that will consequently improve the achievable rate. This improvement in the array gain is a direct result of those additional antenna driving elements, i.e., the bank of bandpass filters and the additional phase shifters.
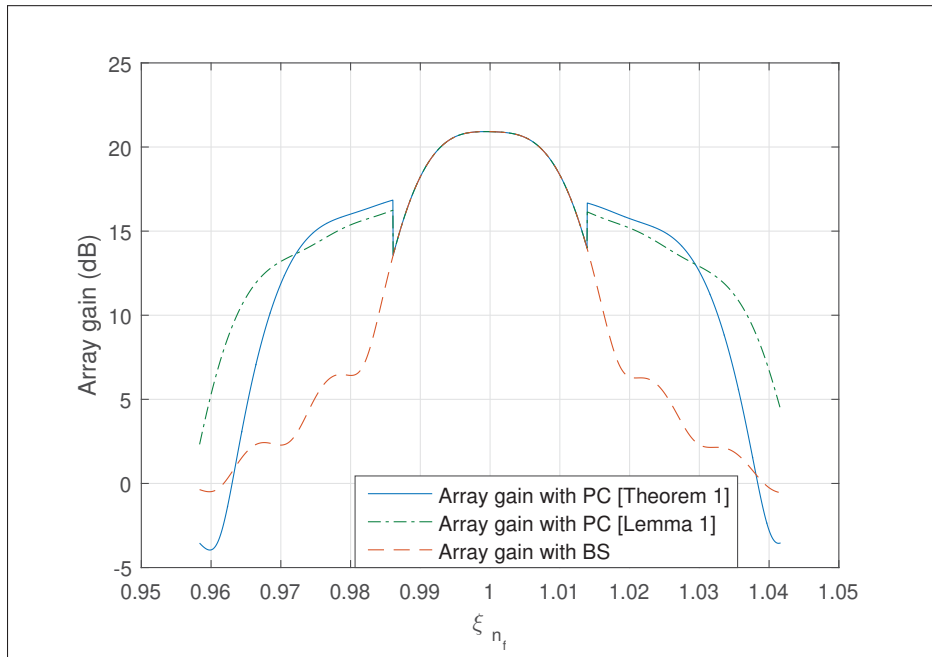


Figure 4.2    Array gain for $f_c = 60$GHz, $N_f = 2048$, $N = 256$, $B = 5$GHz, $\psi = \theta = 0.8$ $K = 64$, $b = 16$, and $L = 3$. The plotted array gain is averaged over the set $\{\theta - 0.1, \theta, \theta + 0.1\}$

In addition to that, Fig. 4.2 also shows the impact of linear approximation of $c_k$ on the array gain by comparing the array gain curves of Lemma 4.1 and Theorem 4.1. It can be observed that the linear approximation of $c_k$ provided in theorem 1 is very tight for a wide range of subcarriers. The effect of this approximation on capacity is illustrated in Fig. 4.3.
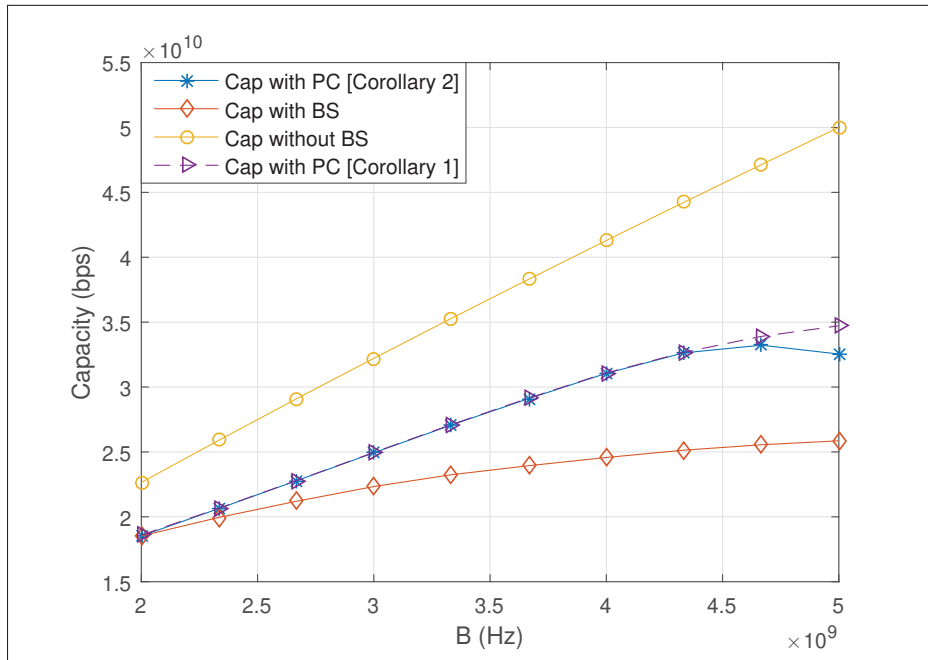


Figure 4.3  Capacity with and without PC for $f_c = 60\text{GHz}$, $N_f = 2048, N = 256, \psi = \theta = 0.8 \; K = 64, b = 16,$ and $L = 3$. The plotted capacity is averaged over the set $\{\theta - 0.1, \theta, \theta + 0.1\}$

Fig. 4.3 compares the capacity of an ideal system with no BS, with BS, and with PC based on the proposed design (Corollary 4.1 and 4.2). All the relevant parameters are listed in the caption. Although gain of the proposed design, approximately 20% at $B = 5\text{GHz}$, is evident from the figure, it is worth mentioning that this capacity gain does not increase linearly with the bandwidth $B$. For example, we notice that the trend of the capacity with PC curve, at around $B = 4\text{GHz}$, starts to flatten and as we move further, it even shows a slightly decreasing trend, at around $B = 4.6\text{GHz}$. The rationale behind this nonlinear gain in capacity is the use of bank of filters of fixed size for all bandwidths (i.e., $L = 3$ used in Fig. 4.3). Moreover, capacity curves of Corollary 1 and Corollary 2 show that the approximation of $c_k$ to a linear function of $b$ is very

tight for a reasonable range of bandwidths and it can be even tighter for larger bandwidths if we optimize $b$ for a given signal bandwidth. For example, the gap between the capacity curves of Corollary 1 and Corollary 2 at $B = 5$GHz can be further reduced if we optimize the value of $b$ for $B = 5$GHz, this point is further elaborated in the discussion of Fig. 4.5. Here, the capacity curve of Corollary 1 is generated using an exhaustive search on $c_k$.

Fig. 4.4 shows the impact of the size of bank of band pass filters on to the capacity of the proposed design. It is noticed that the increase in the size of bank of filters doesn't directly translate into an increase in the capacity. Interestingly, if we look at the capacity curves around $B = 4.5$GHz, we notice that the increase in the size of bank of filters can even reduce the capacity. The rationale behind this non-trivial behavior is that each bandpass filter and its following phase shifter perform the PC with respect to the centre frequency of that bandpass filter. Hence, that constant PC can work negatively for the other subcarriers that lie within that bandpass filter. Therefore, increasing the size of a bank of bandpass filters does not always result in a linear increase in capacity and it should be optimized for a given signal bandwidth.

Fig. 4.5 shows the impact of the parameter $b$ on the capacity. It is evident from the results that its impact is nonlinear for ultra-wide bandwidths. Therefore, just like the size of a bank of filters $L$, it should also be optimized for a given signal bandwidth and desired beam angle to achieve maximum capacity.

## 4.5  Conclusions & future works

In this letter, an analog architecture design to mitigate the issue of beam-squinting in wideband and ultra-wideband communication systems is proposed. We provided a detailed analytical model of the proposed design and illustrated its performance using numerical results. The results show that the significant gain in capacity can be achieved by the proposed design, for a range of signal bandwidths. Moreover, since the proposed design does not require any computation of large compensation matrices in the digital domain, it can be a promising solution for the delay sensitive applications.
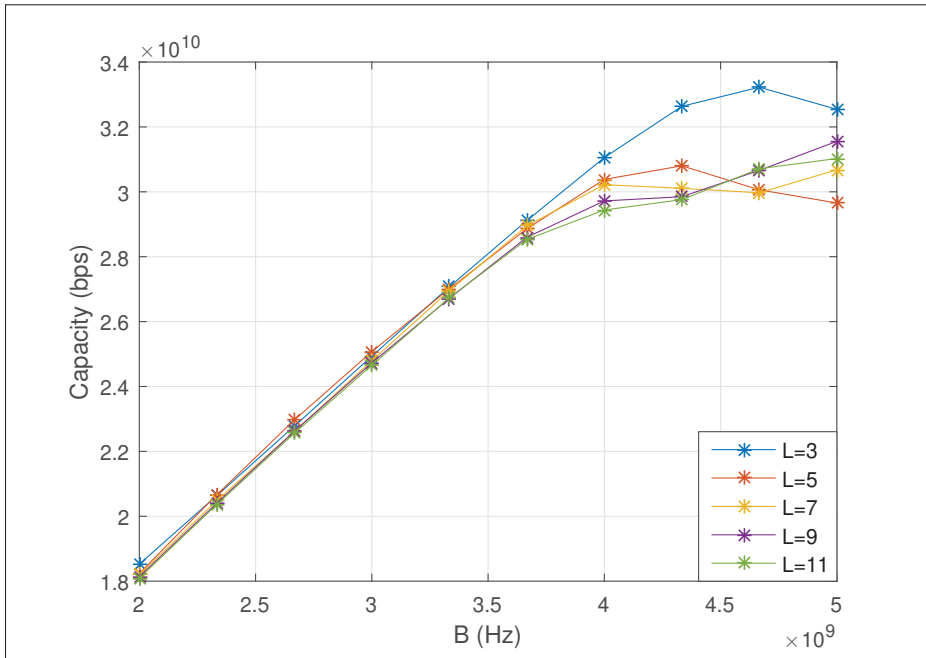
Figure 4.4    Capacity with PC for $f_c = 60$GHz, $N_f = 2048$,
$N = 256$, $\psi = \theta = 0.8 \ K = 64$, and $b = 16$. The plotted capacity
(Corollary 2) is averaged over the set $\{\theta - 0.1, \theta, \theta + 0.1\}$

It is worth mentioning that this work can be extended to find the optimal values of the size of the bank of filters $L$ and $c_k$, which represents the index of antenna element which drives the subsequent layer of phase shifters, for a given signal bandwidth. Also, parameter $b$ which approximates the $c_k$ to a linear function $(k-1)b$ can be optimized for a given signal bandwidth to maximize the array gain and consequently the achievable capacity.
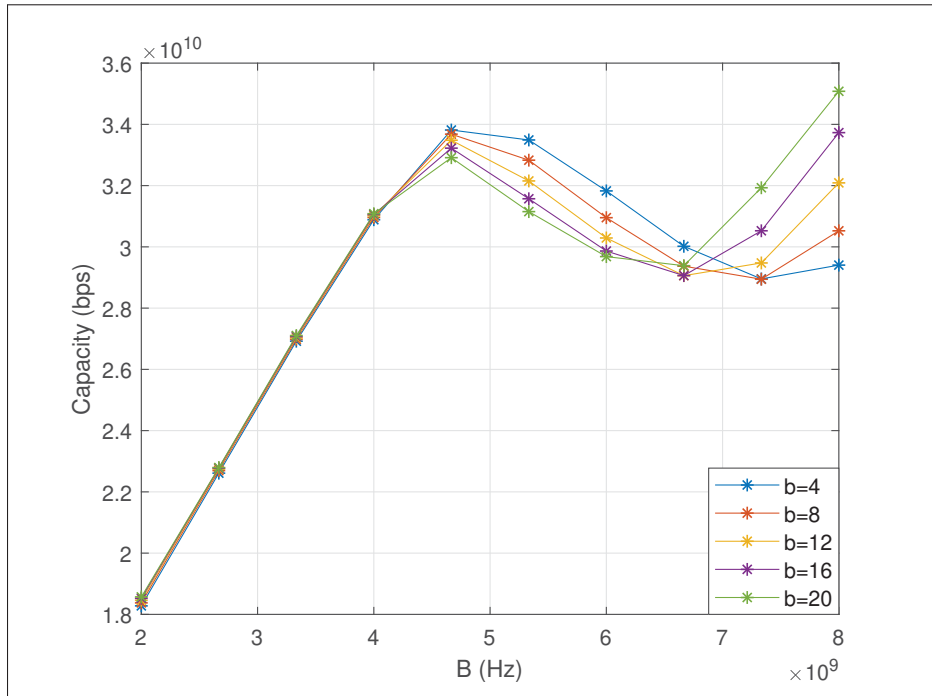
Figure 4.5   Capacity with PC for $f_c = 60$GHz, $N_f = 2048$, $N = 256$, $\psi = \theta = 0.8$ $K = 64$, and $L = 3$. The plotted capacity (Corollary 2) is averaged over the set $\{\theta - 0.1, \theta, \theta + 0.1\}$

# CHAPTER 5

# ANTENNA ARRAY GAIN AND CAPACITY IMPROVEMENTS IN A HYPERSURFACE ASSISTED CONTROLLED ENVIRONMENT

Zeeshan Sattar[a] , Joao V.C. Evangelista[b] , Georges Kaddoum[c] , Naïm Batani[d]

[a,b,c,d]Department of Electrical Engineering, École de Technologie Supérieure, 1100 Notre-Dame Ouest, Montréal, Québec, Canada H3C 1K3

## 5.1 Abstract

This paper highlights the use case of hypersurfaces that can be exploited to mitigate the beam-squinting issue in a millimeter-wave enabled ultra-wideband communication systems. A hypersurface is a software-controlled intelligent surface, which can manipulate impinging signals for the benefit of their intended receiver. Consequently, this paper explores achievable capacity gains by minimizing beam-squinting in a unique programmable environment consisting of hypersurface coated walls and objects. The obtained results show that a transceiver in a hypersurface assisted controlled environment can achieve better performance compared to a more advanced, sophisticated transceiver in a typical environment, i.e., a conventional environment without any hypersurface assistance.

## 5.2 Introduction

hased array antenna systems have diverse applications, including radar, imaging, and communication systems (Mailloux, 2017; Fourikis & Fourikis, 2000; Paramesh, Bishop, Soumyanath & Allstot, 2005). The recent wedlock of large phased array antenna system or massive multiple-input multiple-output (MIMO) and millimeter-Wave (mmWave) only elevated the critical role of massive MIMO in the next generation of communication systems. There is no direct relationship between mmWave and massive MIMO, as a significant amount of research has been done on massive MIMO mainly focused on conventional cellular frequency bands. While massive

MIMO is an option in current cellular bands to provide array and multiplexing gain, it is an unavoidable need or prerequisite to gather enough power at the millimeter-wave spectrum. Since we shrink the area per antenna element as we increase the frequency, we need more antenna elements to gather the same amount of signal power as before. Moreover, small wavelengths of frequencies in the millimeter-wave band made it easier to pack a large number of antenna elements in a compact form. The design of phased array systems is challenging, especially when ultra-wideband communication is required. An important issue that can limit bandwidth in phased array antenna systems is beam-squinting (Wang *et al.*, 2018a,b).

Beam-squinting, in simple words, means that a frequency component $f_0 + \Delta f$ points to $\theta_0 + \Delta\theta$ instead of $\theta_0$ which is the intended beam direction at frequency $f_0$. Since, so far, almost all conventional mobile communication systems operate on narrowband signals, which intrinsically makes the $\Delta\theta$ quite small, thus beam-squinting issues were negligible until recently.

Since one of the main attractions in the mmWave spectrum is its sizeable available bandwidth, wideband and ultra-wideband communication systems will soon become a reality. Therefore, beam-squinting cannot be ignored anymore. In (Wang *et al.*, 2018a,b), the authors highlighted the issue of beam-squinting in prospective communication systems. In (Li *et al.*, 2018a), the authors proposed a hybrid precoding based compensation method in the digital domain to minimize beam-squinting effect. They also evaluated the performance loss of a typical analog precoder with beam-squinting against the ideal analog precoder. In (Liu & Qiao, 2019), the authors investigated the beam-squinting problem in a mmWave communication system using space-time coding. They proposed the idea of a space-time-block-code (STBC) based beamforming. They demonstrated using numerical simulations that their proposed scheme can compensate for the beam-squinting and, in certain cases, elevates the throughput performance for wideband communication systems. Since the beam-squinting issue is intrinsic to the ultra-wideband signals' analog nature, any compensation in the digital domain can only result in minimal improvements in the array gain and spectral efficiency (Sattar, Evangelista, Kaddoum & Batani, 2020). Therefore, the authors in (Sattar *et al.*, 2020) provided a novel analog transceiver architecture to minimize the effect of beam-squinting on the achievable capacity and array gain.

The goal of this paper is to minimize the beam-squinting of an ultra-wideband mmWave enabled communication system in a hypersurface assisted controlled environment (Liaskos, Tsioliaridou, Pitsillides, Ioannidis & Akyildiz, 2018; Liaskos, Nie, Tsioliaridou, Pitsillides, Ioannidis & Akyildiz, 2018). This paper investigates the role of a hypersurface as an array or grid of the dynamic phase shifters, which changes the phase of the impinging signal to improve the array gain and achievable capacity at the receiver. The obtained results are compared against a recently proposed ultra-wideband specific transceiver (Sattar *et al.*, 2020). It is intriguing to learn that a conventional transceiver can achieve better performance in terms of achievable capacity in a hypersurface assisted controlled environment than a more advanced, sophisticated transceiver (Sattar *et al.*, 2020) in a typical environment.

## 5.3 System Model

### 5.3.1 Hypersurfaces: A concept

The concept behind hypersurfaces is to embed software-controlled metamaterials in any surface in the environment (Liaskos, Tsioliaridou, Pitsillides, Akyildiz, Kantartzis, Lalas, Dimitropoulos, Ioannidis, Kafesaki & Soukoulis, 2015). Therefore, in a hypersurface-assisted controlled environment, the wireless environment's electromagnetic behavior can be tailored to the requirements of the mobile devices within it. Similarly, the outdoor settings can also be controlled by coating traffic lights, polls, facades of the sky-scrappers with hypersurface metamaterials. This concept of a programmable wireless environment has the potential to elevate the performance of wireless communication systems notably.

### 5.3.2 A hypersurface deployment scenario

Fig. 5.1 shows an illustration of the hypersurface assisted controlled programmable wireless environment, where a hypersurface plays the role of the dynamic phase shifters by providing phase shifts $\pi\phi_{HS}(n_f)$ at different frequency components of the impinging signal. It is worth mentioning that the design of such frequency-selective hypersurfaces is not new, for example,
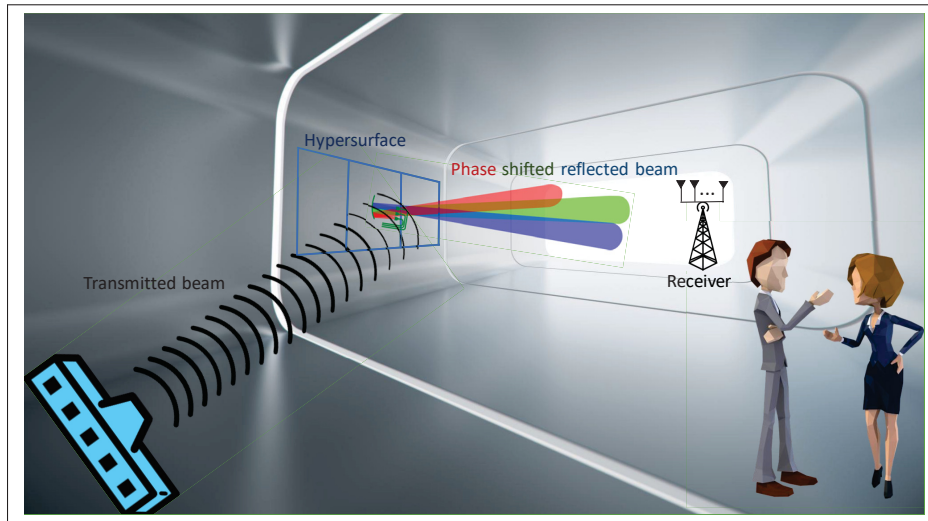
Figure 5.1    Illustration of the hypersurface assisted controlled
programmable wireless environment concept

their usage has been studied in dual-band reflective arrays (Tayebi, Tang, Paladhi, Udpa, Udpa & Rothwell, 2015), antenna covering surfaces, frequency-selective absorbers and, in general, to perform spectral filtering in both microwave and optical ranges through the design of metasurfaces with extremely dispersive reflection or transmission properties (Glybovski, Tretyakov, Belov, Kivshar & Simovski, 2016). In addition, more recently, the authors in (Dardari & Massari, 2020) also proposed the idea of using frequency-dependent properties of metaprism to control the reflection of the signal by steering it for the benefit of its intended receiver.

A hypersurface assisted controlled environment is a novel concept of programmable environment where hypersurface coated walls and objects interact with impinging signals to manipulate them for the benefit of mobile devices within it, in real-time, based on the re-configurable software commands. In Fig. 5.1, a transmitted beam interacts with a hypersurface coated wall, which treats the impinging ultra-wideband signal as consecutive chunks of narrowband signals and it further adds a phase correction factor $\pi\phi_{HS}(n_f)$ to each chunk with respect to its center frequency. Since the main issue of beam-squinting is that a frequency component $f_0 + \Delta f$ points to $\theta_0 + \Delta\theta$ instead of $\theta_0$, which is the intended beam direction at frequency

$f_0$, then this phase correction factor helps the array gains of subcarriers of an ultra-wideband signal to align themselves with their centre frequency $f_0$ by reducing the effect of $\Delta\theta$. In addition, it is worth mentioning that the whole premise of the aforementioned use case of hypersurface assisted controlled environment is to highlight that the complexities of controlling and manipulating signals can be pushed towards a more intelligent wireless environment while keeping the transceiver designs simple and conventional.

### 5.3.3 The receiver architecture
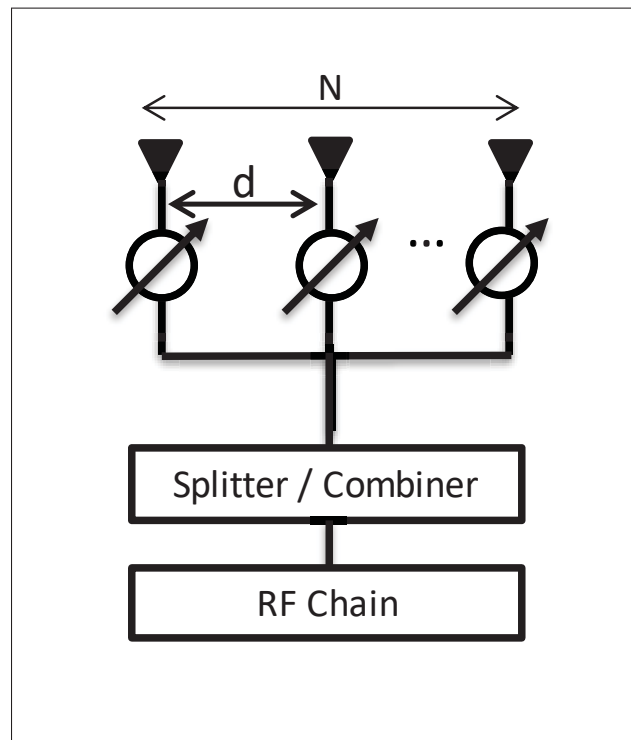


Figure 5.2    Receiver architecture

In this paper, analog beamforming with one uniform linear array (ULA) antenna of size $N$ is considered at the receiver. Here, the distance between any two adjacent antenna elements is denoted by $d$, and each antenna element is driven by a phase shifter, as shown in Fig.5.2.

Suppose the signal arriving at the receiver array is $s(t)$, then the received signal vector $\mathbf{y}(t, \theta)$ at the $N$ antenna elements before the phase shifters is

$$\mathbf{y}(t, \theta) = \left[ s(t), ..., s\left(t - \frac{(n-1)d \sin \theta}{c}\right), ..., s\left(t - \frac{(N-1)d \sin \theta}{c}\right) \right]^T. \tag{5.1}$$

Here $[.]^T$ and $c$ denote the transpose of a vector and speed of light, respectively. Similarly, its frequency response can be written as

$$\mathbf{y}(f, \theta) = s(f) \left[ 1, \exp j(2\pi c^{-1} f d \sin \theta), ..., \exp j(2\pi c^{-1} f(n-1)d \sin \theta), \right.$$
$$\left. ..., \exp j(2\pi c^{-1} f(N-1)d \sin \theta) \right]^T \tag{5.2}$$

where $\mathbf{y}(f, \theta)$ is a function of the angle of arrival $\theta$, and $\theta \in \{-\frac{\pi}{2}, \frac{\pi}{2}\}$. Define the ULA response vector as

$$\mathbf{a}(\theta, f) = \left[ 1, \exp j(2\pi c^{-1} f d \sin \theta), ..., \exp j(2\pi c^{-1} f(n-1)d \sin \theta), \right.$$
$$\left. ..., \exp j(2\pi c^{-1} f(N-1)d \sin \theta) \right]^T. \tag{5.3}$$

The optimal combiner or steering vector for the received signal $\mathbf{y}(f, \theta)$ is a matched filter denoted as

$$\mathbf{w} = \mathbf{a}^H(\theta, f). \tag{5.4}$$

Since elements in the matched filter are true-time-delay devices with their implementation issues, then phase shifters are typically used instead. A phase shifter is typically modeled as a constant phase shift for the whole frequency range it is designed for. Hence, the phase shifter based steering vector with phase shift $\beta_n$ for the $n$th antenna element is written as

$$\hat{\mathbf{w}} = \left[ \exp j(\beta_1), ..., \exp j(\beta_n), ..., \exp j(\beta_N) \right]. \tag{5.5}$$

Following Balanis (2016), the array gain of the phased array at angle of arrival $\theta$ can be formulated as

$$
\begin{aligned}
g(\hat{\mathbf{w}}, \theta, f) &= \frac{1}{\sqrt{N}} \hat{\mathbf{w}}^H \mathbf{a}(\theta, f) \\
&= \frac{1}{\sqrt{N}} \sum_{n=1}^{N} \exp j(2\pi c^{-1} f(n-1) d \sin\theta - \beta_n).
\end{aligned}
\tag{5.6}
$$

### 5.3.4   Performance analysis

In this subsection the array gain and the achievable capacity at the receiver are derived for the hypersurface assisted controlled programmable wireless environment illustrated in Fig. 5.1.

**Theorem 5.1.** *The array gain at the receiver in this hypersurface assisted controlled programmable wireless environment with phase correction factor $\pi\phi_{HS}(n_f)$ can be formulated as*

$$
g_{\phi_{HS}}(\psi, \theta, \xi_{n_f}) = \frac{1}{\sqrt{N}} \frac{\sin(N\pi[x_{n_f} + \phi_{HS}(n_f)]/2)}{\sin(\pi[x_{n_f} + \phi_{HS}(n_f)]/2)} \exp j\left(\pi[x_{n_f} + \phi_{HS}(n_f)]\frac{N-1}{2}\right), \tag{5.7}
$$

*where $x_{n_f} = (\xi_{n_f} \sin\theta - \sin\psi)$, $\psi$ is the angle of desired the beam, $\xi_{n_f}$ is the ratio of subcarrier frequency to the carrier frequency $f_c$ for subcarrier $n_f$.*

$$
\xi_{n_f} = 1 + \frac{(2n_f - N_f + 1)b_{frac}}{2N_f}.
$$

*Here $b_{frac} = B/f_c$ is the fractional bandwidth, $n_f \in \{0, 1, ..., N_f - 1\}$, and $N_f$ is the total number of subcarriers.*

*Proof.* From (5.6) we know the array gain of the phased array at angle of arrival $\theta$, adding a phase correction factor $\pi\phi_{HS}(f)$ to yeilds

$$g(\hat{\mathbf{w}}, \theta, f) = \frac{1}{\sqrt{N}} \sum_{n=1}^{N} \exp j\left(\pi(n-1)(2c^{-1}fd\sin\theta + \phi_{HS}(f)) - \beta_n\right). \tag{5.8}$$

Since we typically choose $\beta_n$ with respect to the centre frequency $f_c$, consequently $d = \frac{\lambda_c}{2}$ in this case. Hence, $\beta_n$ takes the following form

$$\beta_n(\psi) = 2\pi c^{-1} f_c(n-1)d\sin\psi. \tag{5.9}$$

Putting (5.9) into (5.8), we get

$$g_{\phi_{HS}}(\psi, \theta, \xi_{n_f}) = \frac{1}{\sqrt{N}} \sum_{n=1}^{N} \exp j\left(\pi(n-1)[(\xi_{n_f}\sin\theta - \sin\psi) + \phi_{HS}(n_f)]\right). \tag{5.10}$$

Let's denote $x_{n_f} = (\xi_{n_f}\sin\theta - \sin\psi)$. Now using the identity of sum of complex exponential functions, given as follows

$$\sum_{n=0}^{N-1} \exp j(nx) = \frac{\sin(\frac{1}{2}Nx)}{\sin(\frac{1}{2}x)} \cdot \exp j(x\frac{N-1}{2}), \tag{5.11}$$

we can solve the summation in (5.10) in closed form, as given in (5.7). This concludes the proof. ■

Moreover, for the aforementioned array gain, assuming Gaussian signalling (Cover & Thomas, 2012), the achievable capacity can be expressed as follows (Tse & Viswanath, 2005)

$$C_{\phi_{HS}} = B\frac{1}{N_f} \sum_{n_f=0}^{N_f} \log\left(1 + \frac{P_r|g_{\phi_{HS}}(\psi,\theta,n_f)|^2}{B\sigma^2}\right) \tag{5.12}$$

where $P_r = P_t|h|^2L^{-\alpha}$ is the total received power. $P_t$, $h$, $L^{-\alpha}$ are the transmitted power, channel coefficient, and pathloss, respectively. Moreover, $B$ and $\sigma^2$ are bandwidth and noise variance, respectively.

## 5.4 Numerical Results

This section presents the performance analyses of the hypersurface assisted controlled environment, as illustrated in Fig. 5.1. Fig. 5.3 shows a comparison between the received array gain of the proposed model, a typical received array gain with beam-squint (BS), and a received array again for the transceiver design proposed in (Sattar *et al.*, 2020). To show a fair comparison with (Sattar *et al.*, 2020), the phase shifts $\pi\phi_{HS}(n_f)$ are designed accordingly. For example, the additional phase shifts are only added on the extreme left (i.e., 1 to 512) and extreme right (i.e., 1536 to 2048) quarter of the subcarriers, with respect to the center frequency of each quarter. The significant improvement in array gain can be seen on the left and right sides of the main lobe. For example, at $\xi_{n_f} = 1.03$ and $\xi_{n_f} = 0.97$, the improvement in array gain is approximately 20dB over the typical array gain with BS. Similarly, at $\xi_{n_f} = 1.03$ and $\xi_{n_f} = 0.97$ the improvement in array gain is approximately 10dB over the array gain in (Sattar *et al.*, 2020).

Fig. 5.4 compares the achievable capacity of an ideal system with no BS, a typical system with BS, the system in (Sattar *et al.*, 2020), and the system under consideration. It is intriguing to see that a typical receiver performs notably better in a hypersurface assisted controlled environment compared to a more sophisticated transceiver (Sattar *et al.*, 2020) in a typical environment. It is worth mentioning that even better performance can be achieved by carefully optimizing $\pi\phi_{HS}(n_f)$.
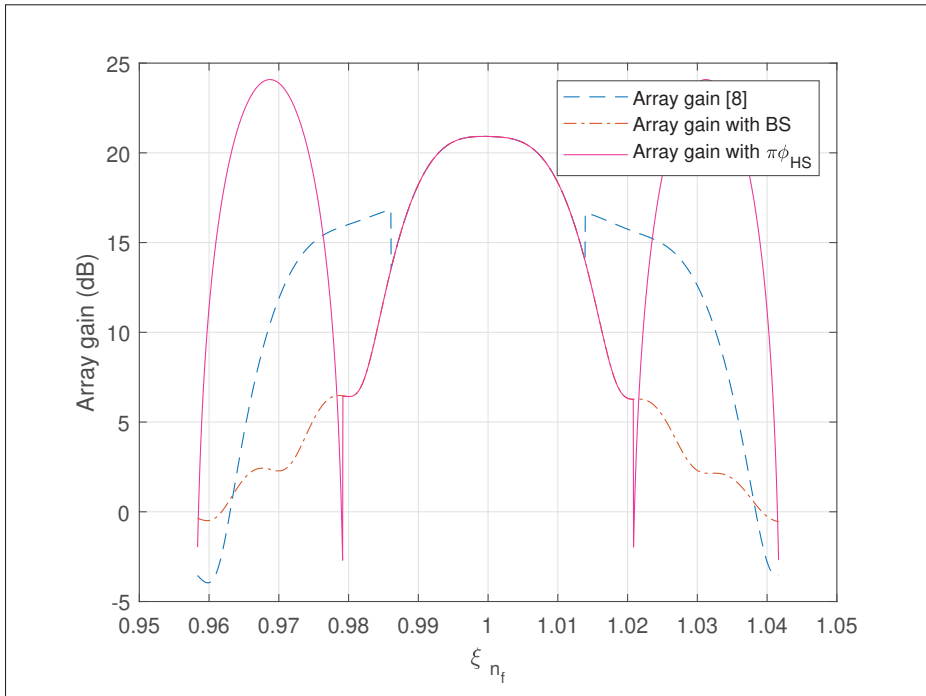
Figure 5.3    Array Gain for $f_c = 60$GHz, $N_f = 2048$, $N = 256$, $B = 5$GHz, $\psi = \theta = 0.8$. The plotted array gain is averaged over the set $\{\theta - 0.1, \theta, \theta + 0.1\}$

## 5.5    Conclusions

In this paper, a use case of hypersurface assisted controlled environment is discussed. The obtained results show that significant improvements in the array gain and the achievable capacity of the ultra-wideband systems can be obtained by carefully tuning the hypersurface assisted environment. Moreover, it is intriguing to see that even a simple transceiver can achieve better performance than a more advanced transceiver in a hypersurface assisted controlled environment. This result highlighted that future handheld wireless communication devices can opt for simple designs, and the complexities of controlling and taming the signals would be pushed towards a more intelligent wireless environment.
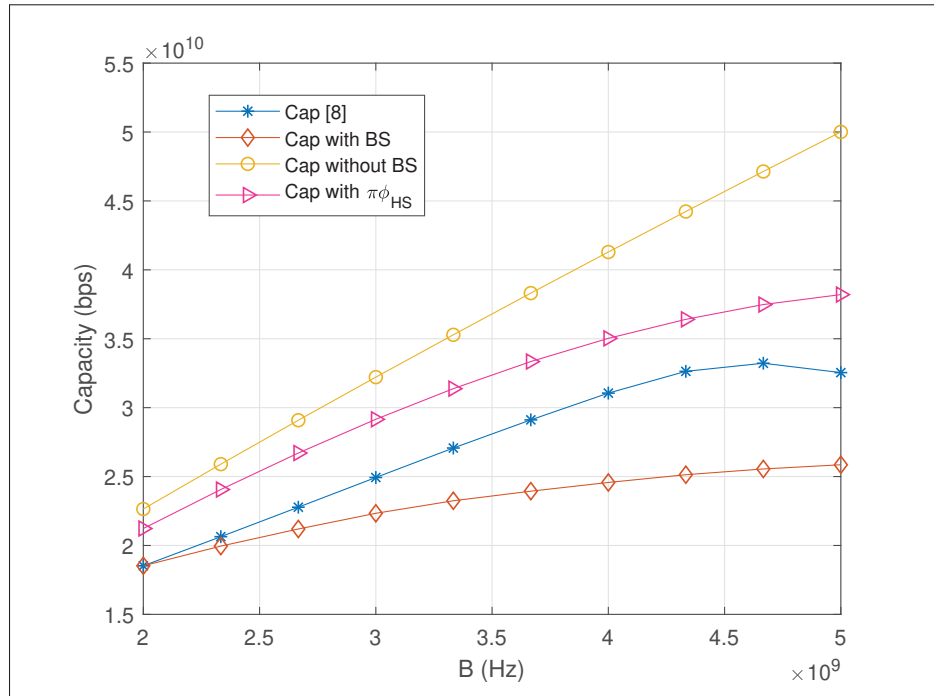
Figure 5.4　Capacity for $f_c = 60$GHz, $N_f = 2048$, $N = 256$, $\psi = \theta = 0.8$, $\frac{P_r}{\sigma^2} = 20 \times 10^9$. The plotted capacity is averaged over the set $\{\theta - 0.1, \theta, \theta + 0.1\}$

# CONCLUSION AND RECOMMENDATIONS

## 6.1 Conclusions

A utopia is an imaginary concept of a perfect world. In contrast, the concept of wireless utopia is not so imaginary. In wireless communications, the utopian wireless network is a concept where many different technologies will come together to assist each other in providing seamless service to the connected devices.

In this thesis we studied, investigated, analyzed, and proposed novel designs for the two ingredients of the aforementioned wireless utopian network, i.e., (i) two-tier HetNet where UEs have the liberty to choose different BSs for uplink and downlink transmissions and (ii) ultra-wideband communications where the available bandwidth is immense.

In chapter two, we did a comparative analysis of decoupled and coupled access modes. We constructed a half-duplex two-tier HetNet employing sub-6Ghz and millimeter-wave, where BSs of both tiers are modeled as independent PPP. Our analytical and simulation results validate each other and illustrate the effect of decoupled access on distance distributions of serving BSs and average spectral efficiency. We observed that although decoupling can improve the uplink spectral efficiency, yet that improvement is rather small from a system-level point of view. Therefore, whether decoupled access is a viable option for the next generation of communication systems depends only on a comprehensive cost analysis of control signals overhead.

In chapter three, we proposed a comprehensive characterization of full-duplex two-tier HetNets with decoupled access. To study the association behavior of UEs in the aforementioned model, we derived the SINR optimal association probabilities and showed the effect of full-duplex interference on them. It is interesting to note that the added full-duplex interference does not change the association probabilities in a significant way. Unlike the typical convention of noise-limited mmWave network, we accounted for interference and performed a comparative

analysis of both assumptions showing that the former becomes invalid as we move into the realm of UDNs. Finally, we derived the spectral efficiency of both the downlink and uplink separately and compared them with their coupled counterpart. We also showed the effect of full-duplex interference on the spectral efficiency by evaluating HetNets with different fractions of full-duplex UEs and BSs. It is intriguing to see that the effect of added full-duplex interference is rather insignificant on the downlink spectral efficiency, and as we move towards a denser mmWave network, its effect on uplink spectral efficiency diminishes too.

In chapter four, an analog architecture design to mitigate the issue of beam-squinting in wideband and ultra-wideband communication systems was proposed. We provided a detailed analytical model of the proposed design and illustrated its performance using numerical results. The results show that a significant gain in capacity can be achieved by the proposed design for a range of signal bandwidths. Moreover, since the proposed design does not require any computation of large compensation matrices in the digital domain, it can be a promising solution for the delay sensitive applications. Moreover, in chapter five, a use case of hypersurface assisted controlled environment was discussed. The obtained results show that significant improvements in the array gain and the achievable capacity of the ultra-wideband systems can be obtained by carefully tuning the hypersurface assisted environment. In addition, it is intriguing to see that even a simple transceiver can achieve better performance than a more advanced transceiver, proposed in chapter four, in a hypersurface assisted controlled environment. This result highlighted that future handheld wireless communication devices can opt for simple designs, and the complexities of controlling and taming the signals would be pushed towards a more intelligent wireless environment.

## 6.2   Future work

Based on the literature review and the research outcomes of this Ph.D. thesis, following future research directions could be worth investigating.

### 6.2.1 UDNs and the concept of doubly massive MIMO

The concept of UDN is one of the expected outcomes of the network densification paradigm. However, due to the lack of standardization, the scientific community is still arguing on its definition. Since in this thesis, chapters 2 and 3 both provide very detailed analytical models of practical HetNets from a system-level point of view, this work can be extended to link level. The basic idea is to find a trade-off between the increase in the number of small cell BSs and the number of antenna elements on small cell BSs. Since so far all the proposed designs and the link-level performance analysis of UDN only have been done for the cases where small cell BSs are only equipped with a single antenna, this kind of system model and its analysis could be the first work in the direction of the application of doubly massive MIMO (Buzzi & D'Andrea, 2016) in UDN.

The aforementioned design idea with a massive number of antenna elements on each access point may sound trivial, but from a pragmatic point of view, it raises some very critical questions, for example:

- How many antenna elements would be good enough for small cell access points?
- Why should we increase the number of antenna elements on each small cell access point rather than increase the density of single antenna access points?
- How can we find a trade-off between the density of small cell access points and a massive number of antenna elements on each access point?
- How can a massive number of antenna elements help us decrease the interference in a UDN?

#### 6.2.1.1 Prospective methodology

- The tools from stochastic geometry could be used to generate two kinds of UDN.
  1. A typical UDN with single antenna access points.
  2. A novel design of the UDN with a massive number of antenna elements on each access point.

- An optimization problem to minimize the inter-cell and intra-cell interference in a UDN could be formulated. This problem could be formulated as a function of the density of small cell access points and the massive number of antenna elements. A trade-off could be found between the density of small cell access points and the massive number of antenna elements.

- A link-level analysis on the diversity versus directivity gain could be done for a point to point communication case of doubly massive MIMO. It could also be further extended to the analysis of the backhaul transmission link.

- The channel estimation in doubly massive MIMO is also a challenging task, though the assumption of the parametric channel model can simplify this problem as the number of parameters to be estimated does not scale with the product of antenna elements at the transmitter and the receiver ($N_t \times N_r$). Therefore the design and analysis of efficient channel estimation schemes specific to the aforementioned UDN model could be done.

- The investigation and comparative analysis of the aforementioned UDN model with existing work in two scenarios could be done.
  1. Backhauling i.e., the link between small cell access points and macro BS.

  2. Access network i.e., the link between UE and small cell access points.

- Backhauling
  1. The optimization of a nonlinear cost function (capacity, ergodic sum-rate, or the probability of outage) over a set of discrete variables (access point locations or number of antenna elements) could be formulated.

  2. Generally, the computational cost to obtain the optimal solution of the aforementioned optimization problems is prohibitive, as the problems are NP-hard. Thus, various sub-optimal and low complexity algorithms, using mixed integer nonlinear programming techniques, could be proposed.

- Access Network
  1. In the access network, an optimization problem to minimize the interference, specifically of cell edge UEs could be formulated.

2. An investigation on the trade-off of increasing the number of small cell access points and increasing the number of antenna elements on small cell access points could also be done.

- We are addressing the issues of doubly massive MIMO as we are assuming a large number of antennas on both macro BS and on small cell access points. Unlike sub-6GHz communications, millimeter-wave does not enjoy the rich scattering environment, which leads to a channel matrix with i.i.d. entries. Therefore in the case of millimeter-wave communications, channel rank is independent of the number of antennas and depends on the scene geometry, which results in correlated entries in the channel matrix.

- To address this correlation, an investigation on the compact antenna arrays with inter-element distance less than $\lambda/2$ for small cell access points could also be done.

### 6.2.2 Re-configurable intelligent surfaces for mmWave-enabled ultra-wide communications

Imagine a world where your environment become programmable in a way that it can change its interaction with electromagnetic waves with respect to the software command or configuration, offering unprecedented advantages to the users. For example, the authors in (Liaskos *et al.*, 2018) presented a very intuitive scenario, as depicted in Fig. 6.1.

"In the example of Fig. 6.1, user A expresses a need for security against eavesdropping. The programmable environment, in collaboration with the user devices, sets an improbable "air-path" that avoids all other users, hindering eavesdropping. Users B, C, and D express no requirement, and are automatically treated by a global environment policy instead, which dictates the optimization of their data transfer rates. This can be attained by negating cross-interference and a minute crafting of the received power delay profile (PDP), i.e., ensuring that all received wave echoes get constructively superposed at the devices. User F is observed to be inactive and–according to his preferences–has his device remotely charged by receiving a very focused
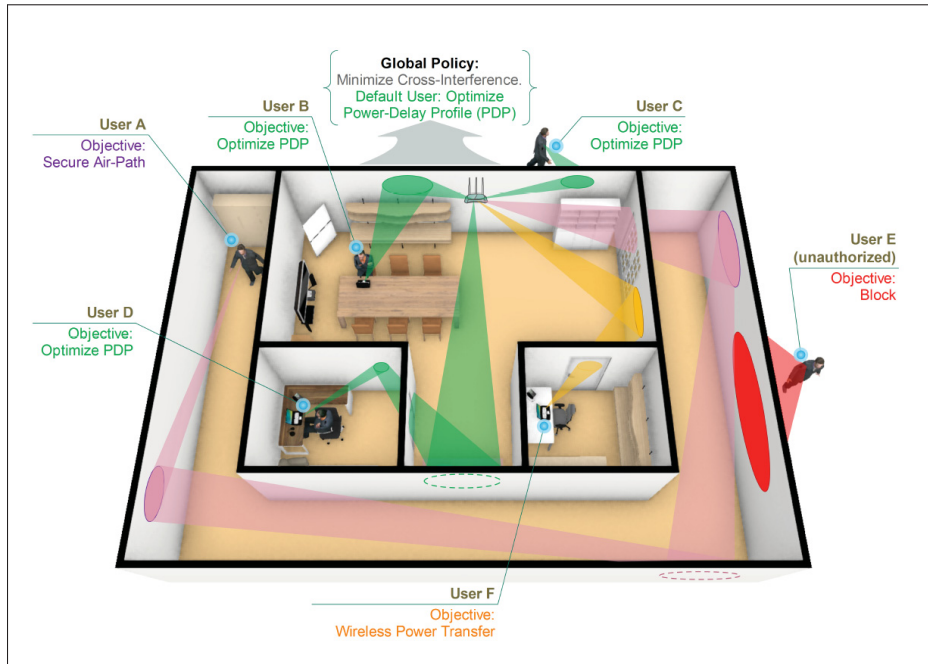
Figure 6.1    Illustration of the programmable wireless environment concept.  The electromagnetic behavior of walls is programmatically changed to exemplary maximize data rates (green use-cases), wireless power transfer (orange use-case), negate eavesdropping (purple use-case) and provide electromagnetic shielding (red use-case)
Taken from Liaskos *et al.* (2018)

energy beam.  Finally, user E fails to pass the network's access policies (e.g., unauthorized physical device address), and is blocked by the environment.  This can be accomplished by absorbing his emissions, potentially using the harvested energy to a constructive use."(Liaskos *et al.*, 2018)

In other words, we are talking about an environment where an easily programmable interface abstracts the underlying complexities of the wireless propagation.  Essentially, the environment composed of re-configurable intelligent surfaces would work as a router, which can change the impinging signals on the electromagnetic level.

Since the problem addressed in chapter 4, i.e., beam-squinting, is intrinsic to the electromagnetic behavior of the impinging signals, it can be mitigated by the aforementioned environment composed of re-configurable intelligent surfaces. For example, it is worth investigating how an intelligent environment can provide phase shifts to the particular frequency components of an ultra-wideband signal to mitigate the beam-squinting effect. Some initial results on this subject are presented in chapter 5.

## APPENDIX OF CHAPTER 2

### 1. Proof of Lemma 2.1

Using (2.4) and (2.5), we can express the probabilistic expression of (2.7) in the form shown in (A I-1).

$$
\begin{aligned}
\Pr(\text{Case1}) &= 2\pi\lambda_S \int_0^\infty \left(1 - \exp\left(-\pi\lambda_M \left(\frac{Q_M}{Q_S}\right)^{\frac{2}{\alpha_M}} x^{\frac{2\alpha_S}{\alpha_M}}\right)\right) \exp\left(-\pi\lambda_S x^2\right) x \, dx \\
&= 1 - 2\pi\lambda_S \int_0^\infty \left(\exp\left(-\pi\lambda_M \left(\frac{Q_M}{Q_S}\right)^{\frac{2}{\alpha_M}} x^{\frac{2\alpha_S}{\alpha_M}}\right)\right) \exp\left(-\pi\lambda_S x^2\right) x \, dx. \quad \text{(A I-1)}
\end{aligned}
$$

Since, the integral given in (A I-1) is over the product of two exponentials with different powers of variable $x$, there is no straightforward way to solve this integral. Therefore, we use the theory of Fox's H-function to express this integral in closed form.

$$
\begin{aligned}
\Pr(\text{Case1}) &\overset{(a)}{=} 1 - 2\pi\lambda_S \int_0^\infty \left(\frac{1}{2}\frac{\alpha_M}{\alpha_S} H_{0,1}^{1,0}\left[\xi_1 x \,\middle|\, \begin{array}{c} (-,-) \\ (0, \frac{1}{2}\frac{\alpha_M}{\alpha_S}) \end{array}\right] \right. \\
&\qquad \left. \cdot \frac{1}{2} H_{0,1}^{1,0}\left[\xi_2 x \,\middle|\, \begin{array}{c} (-,-) \\ (0, \frac{1}{2}) \end{array}\right] x\right) dx \qquad\qquad \text{(A I-2)} \\
&\overset{(b)}{=} 1 - \frac{1}{2}\frac{\alpha_M}{\alpha_S} H_{1,1}^{1,1}\left[z_1 \,\middle|\, \begin{array}{c} (0, \frac{1}{2}) \\ (0, \frac{1}{2}\frac{\alpha_M}{\alpha_S}) \end{array}\right].
\end{aligned}
$$

In (A I-2), (a) is a direct result of equation (2.9.4) in (Kilbas, 2004); (b) follows from Theorem 2.9 in (Kilbas, 2004), here, $\xi_1 = \left(\sqrt{\pi\lambda_M}\right)^{\frac{\alpha_M}{\alpha_S}} \left(\frac{Q_M}{Q_S}\right)^{\frac{1}{\alpha_S}}$ and $\xi_2 = \left(\sqrt{\pi\lambda_S}\right)$.

Similarly, the proofs of lemma 2.2 and 2.3 can be obtained by following the same steps as adopted here.

## 2. Proof of Lemma 2.4

The distance of all the UEs connected to a *Mcell* BS in the association case 1 satisfies $(X_M^{-\alpha_M} > \frac{\bar{Q}_S}{\bar{Q}_M} X_S^{-\alpha_S})$. Therefore, the complementary CDF of the distance of UEs to their serving BS is formulated as

$$
\begin{aligned}
F_{X_M|\text{Case1}}^c &= \Pr\left(X_M > x | X_S > \left(\frac{\bar{Q}_S}{\bar{Q}_M}\right)^{\frac{1}{\alpha_S}} X_M^{\frac{\alpha_M}{\alpha_S}}\right) \\
&= \frac{\Pr\left(X_M > x; X_S > \left(\frac{\bar{Q}_S}{\bar{Q}_M}\right)^{\frac{1}{\alpha_S}} X_M^{\frac{\alpha_M}{\alpha_S}}\right)}{\Pr(\text{Case1})} \\
&= \frac{\int\limits_x^\infty \exp\left(-\pi\lambda_S \left(\frac{\bar{Q}_S}{\bar{Q}_M}\right)^{\frac{2}{\alpha_S}} X_M^{\frac{2\alpha_M}{\alpha_S}}\right) \cdot f_{X_M}(x_M) dx_M}{\Pr(\text{Case1})}.
\end{aligned}
\tag{A I-3}
$$

Where $\Pr(\text{Case 1})$ and $f_{X_M}$ are given in equations (2.15) and (2.4), respectively. The cdf of the distance to the serving BS for the association case 1 is $F_{X_M|\text{Case1}} = 1 - F_{X_M|\text{Case1}}^c$, and by simply differentiating this cdf, we derive the pdf of the distance to the serving BS for the association case 1.

Similarly, proofs of lemma 2.5 and 2.6 can be obtained following the same steps.

## 3. Proof of Theorem 2.1

Following the approach adopted in (Andrews *et al.*, 2011), the average user rate $\tau \overset{\Delta}{=} W\mathbf{E}[\ln(1 + \text{SINR})]$. Here we derive the average user rates, uplink and downlink separately, for the cell association case 2. Same steps can be followed to derive the average user rate expressions

for the other two cases where

$$
\begin{aligned}
\tau_{\text{UL,Case2}} \quad &\overset{\triangle}{=} \quad W_S \mathbf{E}\left[\ln\left(1 + \text{SNR}_{\text{UL},S}(x)\right)\right] \\
&\overset{(c)}{=} \quad W_S \int\limits_{x>0} \int\limits_{t>0} \left(\exp\left(-\frac{x^{\alpha_S}\left(\exp(t) - 1\right)}{\bar{Q}_S}\right) \right. \\
&\qquad\qquad\qquad\qquad\qquad \left. \cdot f_{X_S|\text{Case2}}\right) dt \, dx,
\end{aligned}
\tag{A I-4}
$$

(c) comes from following the same steps as given in the proof of Theorem 3 in Appendix C of (Andrews *et al.*, 2011). To further solve the integrals of (A I-4), we first change the order of integrals. The rationale behind this change is to exploit the properties of Fox's H-function and obtain the result in form of bivariate Fox's H-function.

$$
\begin{aligned}
\tau_{\text{UL,Case2}} \quad &= \quad W_S \int\limits_{t>0} \int\limits_{x>0} \exp\left(-\frac{x^{\alpha_S}\left(\exp(t) - 1\right)}{\bar{Q}_S}\right) \\
&\qquad\qquad\qquad\qquad\qquad \cdot f_{X_S|\text{Case2}} \, dx \, dt \\
&\overset{(d)}{=} \quad W_S \int\limits_{t>0} \int\limits_{x>0} \frac{1}{\alpha_S} H_{0,1}^{1,0}\left[\xi_{\text{UL},S}x \,\middle|\, \begin{matrix} (-,-) \\ \left(0, \frac{1}{\alpha_S}\right) \end{matrix} \right] \\
&\qquad\qquad\qquad\qquad\qquad \cdot f_{X_S|\text{Case2}} \, dx \, dt,
\end{aligned}
\tag{A I-5}
$$

where $\xi_{\text{UL},S} = \dfrac{(\exp(t)-1)^{\frac{1}{\alpha_S}}}{\bar{Q}_S^{\frac{1}{\alpha_S}}}$ and (d) follows from eq. (2.9.4) in (Kilbas, 2004). Similarly, we can write the exponential terms in the PDF $f_{X_S|\text{Case2}}$ in the form of Fox's H-function as expressed in (A I-6). Then, using the result of an integral involving the product of three Fox's H-function provided in (Mittal & Gupta, 1972), which concludes the proof of $\tau_{\text{UL,Case2}}$. The proof of $\tau_{\text{DL,Case2}}$ also follows the same steps except the fact that now we have to accommodate interference in our expression too. It is assumed that all the communication within each *Mcell* is based on orthogonal resources, therefore, only inter cell interference is accounted. It is also assumed that each *Mcell* has at least one active UE which causes interference to its neighboring cells.

$$\tau_{\text{UL}|\text{Case2}} = W_S \int\limits_{t>0} \int\limits_{x>0} 2\pi\lambda_S x \frac{1}{\alpha_S} H_{0,1}^{1,0}\left[\xi_{\text{UL},S}x \,\middle|\, \begin{matrix}(-,-)\\\left(0,\frac{1}{\alpha_S}\right)\end{matrix}\right] \cdot \left(\frac{1}{2}\frac{\alpha_M}{\alpha_S} H_{0,1}^{1,0}\left[\xi_1 x \,\middle|\, \begin{matrix}(-,-)\\\left(0,\frac{1}{2}\frac{\alpha_M}{\alpha_S}\right)\end{matrix}\right]\right.$$

$$\left.-\frac{1}{2}\frac{\alpha_M}{\alpha_S} H_{0,1}^{1,0}\left[\xi_3 x \,\middle|\, \begin{matrix}(-,-)\\\left(0,\frac{1}{2}\frac{\alpha_M}{\alpha_S}\right)\end{matrix}\right]\right) \cdot \frac{1}{2} H_{0,1}^{1,0}\left[\xi_2 x \,\middle|\, \begin{matrix}(-,-)\\\left(0,\frac{1}{2}\right)\end{matrix}\right] \, dx \, dt.$$

$$\text{(A I-6)}$$

$$\tau_{\text{DL},\text{Case2}} \overset{\Delta}{=} W_M \left[\ln\left(1 + \text{SINR}_{\text{DL},M}(x)\right)\right]$$

$$\overset{(e)}{=} W_M \int\limits_{t>0}\int\limits_{x>0} \exp\left(-\frac{x^{\alpha_M}\left(\exp(t)-1\right)}{\bar{P}_M}\right)$$

$$\cdot \mathbf{E}\left[\exp\left(-\frac{x^{\alpha_M}\left(\exp(t)-1\right)I_{\text{DL},M}}{\bar{P}_M}\right)\right]$$

$$\cdot f_{X_M|\text{Case2}} \, dx \, dt, \qquad \text{(A I-7)}$$

where (e) again follows the similar steps as listed in the proof of Theorem 3 in Appendix C of (Andrews *et al.*, 2011). In the (A I-7), the expected value of the interference term can be modeled as a Laplace function, hence it can be formulated as follows

$$\mathbf{E}\left[\exp\left(-\frac{x^{\alpha_M}\left(\exp(t)-1\right)I_{\text{DL},M}}{\bar{P}_M}\right)\right] \overset{(f)}{=} \mathbf{E}\left[\exp\left(-\frac{x^{\alpha_M}\left(\exp(t)-1\right)\sum\limits_{v\in\Phi_{\text{IU}}} I_{\text{IU},v}}{\bar{P}_M}\right)\right]$$

$$\overset{(g)}{=} \mathbf{E}\left[\prod_{v\in\Phi_{\text{IU}}} \exp\left(-\frac{x^{\alpha_M}\left(\exp(t)-1\right)I_{\text{IU},v}}{\bar{P}_M}\right)\right]$$

$$\overset{(h)}{=} \exp\left(-2\pi\lambda_{\text{IU}}\right.$$

$$\left.\cdot \int\limits_{y>0}\left(1 - \frac{1}{1 + \left(\frac{x^{\alpha_M}\left(\exp(t)-1\right)}{\bar{P}_M}\right)\bar{P}_M y^{-\alpha_M}}\right) y \, dy\right)$$

$$\overset{(i)}{=} \exp\left(-\pi\lambda_{\text{IU}}x^2(\exp(t)-1)^{\frac{2}{\alpha^M}}\frac{2}{\alpha^M}\right.$$

$$\left.\cdot\int\limits_{(\exp(t)-1)^{-1}}^{\infty}\frac{u^{\frac{2}{\alpha^M}-1}}{1+u}du\right)$$

$$\overset{(j)}{=} \exp\left(-\pi\lambda_{\text{IU}}x^2 G(t)\right), \qquad\qquad\qquad\text{(A I-8)}$$

where (f) is simply the expectation over the distance between a typical UE and its interferers; (g) follows from the simple fact that channel between the interferers and a typical UE is i.i.d. and it is independent from the point process of interferers $\phi_{\text{IU}}$; (h) follows from the probability generating functional (Chiu *et al.*, 2013) of the PPP, which states that $\mathbf{E}\left[\prod\limits_{x\in\Phi}f(x)\right] = \exp\left(-\lambda\int_{\mathbb{R}^2}(1-f(x))\,dx\right)$; (i) is a result of some trivial mathematical manipulation and change of variable. In (j), we solve the inner integral over $u$ by using the eq. given in section 3.194 of (Mittal & Gupta, 1972), where the $G(t)$ is defined in (A I-9).

$$G(t) = (\exp(t)-1)^{\frac{2}{\alpha^M}}\frac{2}{\alpha^M}\left(\frac{(\exp(t)-1)^{1-\frac{2}{\alpha^M}}}{1-\frac{2}{\alpha^M}}{}_2F_1\left[1,1-\frac{2}{\alpha^M};2-\frac{2}{\alpha^M};\frac{-1}{(\exp(t)-1)^{-1}}\right]\right)$$

$$\text{(A I-9)}$$

Similar to the steps adopted in the proof of $\tau_{\text{UL,Case2}}$, we can replace the exponential terms in the expression of $\tau_{\text{DL,Case2}}$ with their respective Fox's H-function as formulated in (A I-10). Then, again using the result of an integral involving the product of three Fox's H-function provided in (Mittal & Gupta, 1972), we concludes the proof of $\tau_{\text{DL,Case2}}$.

$$\tau_{\text{DL|Case2}} = W_M\int\limits_{t>0}\int\limits_{x>0}2\pi\lambda_M x\frac{1}{\alpha_M}\text{H}_{0,1}^{1,0}\left[\xi_{\text{DL},M}x\,\bigg|\,\begin{matrix}(-,-)\\(0,\frac{1}{\alpha_M})\end{matrix}\right]\cdot\left(\frac{1}{2}\frac{\alpha_S}{\alpha_M}\text{H}_{0,1}^{1,0}\left[\xi_4 x\,\bigg|\,\begin{matrix}(-,-)\\(0,\frac{1}{2}\frac{\alpha_S}{\alpha_M})\end{matrix}\right]\right)$$

$$-\frac{1}{2}\frac{\alpha_S}{\alpha_M}\mathrm{H}_{0,1}^{1,0}\left[\xi_6 x \left| \begin{matrix} (-,-) \\ \left(0,\frac{1}{2}\frac{\alpha_S}{\alpha_M}\right) \end{matrix} \right.\right]\right) \cdot \frac{1}{2}\mathrm{H}_{0,1}^{1,0}\left[\xi_5 x \left| \begin{matrix} (-,-) \\ \left(0,\frac{1}{2}\right) \end{matrix} \right.\right] dx\, dt.$$

<div align="right">(A I-10)</div>

## 4.  Structure of bivariate Fox's H-function

In this section of the paper, the structure of the bivariate Fox's H-function is defined in (A I-11).

$$\hat{\mathrm{H}}(k;x,y) \; = \; \mathrm{H}\left[ \begin{pmatrix} \begin{pmatrix} 0 & 1 \\ 1 & 0 \end{pmatrix} & \begin{pmatrix} 1-2\beta_k;\beta_k,\beta_k \\ -;-,- \end{pmatrix} \\[6pt] \begin{pmatrix} 1 & 0 \\ 0 & 1 \end{pmatrix} & \begin{pmatrix} -- \\ 0,\beta_{k+1} \end{pmatrix} & (x,y) \\[6pt] \begin{pmatrix} 1 & 0 \\ 0 & 1 \end{pmatrix} & \begin{pmatrix} -- \\ 0,\beta_{k+2} \end{pmatrix} \end{pmatrix} \right]$$

<div align="right">(A I-11)</div>

## APPENDIX OF CHAPTER 3

### 1. Proof of Lemma 3.1

Conditioning on the serving BS at distance $r$ from the typical UE, the CCDF of the received SINR can be written as

$$
\begin{aligned}
\bar{F}_{\text{SINR}_{DL,k}}(z) &= \mathbb{E}_r\left[\text{SINR}_{DL,k} > z|r\right] \\
&\overset{(a)}{=} \int_{r>0}^{\infty} 2\pi r \lambda_k \exp(-\pi\lambda_k r^2) \Pr(\text{SINR}_{DL,k} > z)dr \\
&= \int_{r>0}^{\infty} 2\pi r \lambda_k \exp(-\pi\lambda_k r^2) \\
&\qquad\qquad \times \Pr\left(h_{x*,0} > \frac{(I_{\text{DL},k} + \epsilon_* Q_k + \sigma_k^2)r^{\alpha_k}z}{P_k G_k}\right)dr,
\end{aligned}
\tag{A II-1}
$$

where (a) follows from the fact that the PDF of the distance $r$ by the null probability of a 2D PPP (Chiu $et\ al.$, 2013) is given by

$$
f_r(r) = 2\pi\lambda_k r \exp(-\pi\lambda_k r^2), \quad r \geq 0.
$$

Using the assumption that $h_{x*,0} \sim \exp(1)$, the coverage probability can be written as

$$\Pr\left(h_{x*,0} > \frac{(I_{\mathrm{DL},k} + \epsilon_* Q_k + \sigma_k^2) r^{\alpha_k} z}{P_k G_k}\right)$$

$$= \exp\left(\frac{-zr^{\alpha_k}}{P_k G_k}(\epsilon_* Q_k + \sigma_k^2)\right) \mathbb{E}_{I_{DL,k}}\left[\exp\left(\frac{-zr^{\alpha_k}}{P_k G_k} I_{DL,k}\right)\right] \qquad \text{(A II-2)}$$

$$\overset{(b)}{=} \exp\left(\frac{-zr^{\alpha_k}}{P_k G_k}(\epsilon_* Q_k + \sigma_k^2)\right) \mathcal{L}_{I_{DL,k}}\left(\frac{zr^{\alpha_k}}{P_k G_k}\right),$$

where (b) simply follows from the fact that $\mathcal{L}_Z(s) \overset{\Delta}{=} \mathbb{E}[\exp(-sZ)]$ for $s > 0$ is the Laplace transform of a non-negative random variable Z.

$$\mathcal{L}_{I_{DL,k}}\left(\frac{zr^{\alpha_k}}{P_k G_k}\right) \overset{(c)}{=} \mathbb{E}_{I_{DL,k}}\left[\frac{-zr^{\alpha_k}}{P_k G_k}(I_{x,k}^{\mathrm{DL}} + I_{u,k}^{\mathrm{DL}})\right]$$

$$\overset{(d)}{=} \mathbb{E}\left[\frac{-zr^{\alpha_k}}{P_k G_k} I_{x,k}^{\mathrm{DL}}\right] \mathbb{E}\left[\frac{-zr^{\alpha_k}}{P_k G_k} I_{u,k}^{\mathrm{DL}}\right], \qquad \text{(A II-3)}$$

where (d) follows from the fact that the total downlink interference is the summation over two independent point processes as formulated in (3.5).

$$\mathbb{E}\left[\frac{-zr^{\alpha_k}}{P_k G_k} I_{x,k}^{\mathrm{DL}}\right] \overset{(e)}{=} \exp\left(-2\pi\lambda_k \frac{r^{2-\alpha_k}}{(\alpha_k - 2)} \frac{zr^{\alpha_k} P_k}{P_k G_k}\right.$$

$$\left. {}_2F_1\left[1, 1 - \frac{2}{\alpha_k}, 2 - \frac{2}{\alpha_k}; \frac{-zP_k}{P_k G_k}\right]\right),$$

$$\mathbb{E}\left[\frac{-zr^{\alpha_k}}{P_k G_k} I_{u,k}^{\mathrm{DL}}\right] \overset{(f)}{=} \exp\left(-2\pi\lambda_{I_u,FD,k} \frac{r^{2-\alpha_k}}{(\alpha_k - 2)} \frac{zr^{\alpha_k} Q_k}{P_k G_k}\right.$$

$$\left. {}_2F_1\left[1, 1 - \frac{2}{\alpha_k}, 2 - \frac{2}{\alpha_k}; \frac{-zQ_k}{P_k G_k}\right]\right),$$

where (e) and (f) follow the same steps as mentioned in the proof of Theorem 1 in Appendix C of (Sattar *et al.*, 2019) and the equality given in section 3.194 of (Gradshteyn & Ryzhik, 2014). This concludes the proof.

## 2.  Proof of Lemma 3.2

Since a PDF of a function is simply the derivative of its CDF, we can write $f_{\text{SINR}_{DL,k}}(z)$ as follows

$$
\begin{aligned}
f_{\text{SINR}_{DL,k}}(z) &= \frac{d}{dz}\left(1 - \bar{F}_{\text{SINR}_{DL,k}}(z)\right) \\
&= -\frac{d}{dz}\left(\bar{F}_{\text{SINR}_{DL,k}}(z)\right).
\end{aligned}
\tag{A II-5}
$$

Since $\bar{F}_{\text{SINR}_{DL,k}}(z)$ involves the product of three exponential functions having the differentiable variable $z$ in their arguments, therefore its derivative can easily be solved using the typical product rule of derivatives. Moreover, the differentiation of the Gauss hyergeometric function (Olver, Lozier, Boisvert & Clark, 2010) involves the following equality

$$
\begin{aligned}
&\frac{d}{dz}\left({}_2F_1[1, 1-c, 2-c, -dz]\right) \\
&= \frac{(1-c)\left(\frac{1}{dz+1} - {}_2F_1[1, 1-c, 2-c; -dz]\right)}{z}.
\end{aligned}
\tag{A II-6}
$$

Now using (A II-6) and the typical product rule of derivatives yields (3.7), which concludes the proof.

## 3. Proof of Theorem 3.2

In Theorem 3.2, (3.18) and (3.20) define the total spectral efficiency of the donwlink and uplink transmission links, respectively. Both (3.18) and(3.20) are the summation of 1) the spectral efficiency for the fraction of time a typical UE chooses to decouple and 2) the spectral efficiency for the fraction of time a typical UE chooses to transmit in conventional way. Since the derivation of $f_{SE_{DL,k}}(\epsilon_*)$ and $f_{SE_{UL,k}}(\epsilon_0)$ involves similar steps, only the detailed derivation of $f_{SE_{DL,k}}(\epsilon_*)$ is provided here.

$$f_{SE_{DL,k}}(\epsilon_*) \triangleq \mathbb{E}\left[\ln(1 + \text{SINR}_{DL,k})\right]$$

$$\overset{(g)}{=} \int_{z>0}^{\infty} \int_{r>0}^{\infty} 2\pi r \lambda_k \exp(-\pi\lambda_k r^2)$$

$$\times \Pr(\text{SINR}_{DL,k} > \exp(z) - 1)drdz, \qquad\qquad \text{(A II-7)}$$

$$\overset{(h)}{=} \int_{z>0}^{\infty} \int_{r>0}^{\infty} 2\pi r \lambda_k \exp(-\pi\lambda_k r^2)$$

$$\times \Pr\left(h_{x*,0} > \frac{(I_{\text{DL},k} + \epsilon_* Q_k + \sigma_k^2)r^{\alpha_k}(\exp(z) - 1)}{P_k G_k}\right)drdz.$$

Using the fact that $h_{x*,0} \sim \exp(1)$, the $\Pr(h_{x*,0} > \frac{(I_{\text{DL},k} + \epsilon_* Q_k + \sigma_k^2)r^{\alpha_k}(\exp(z)-1)}{P_k G_k})$ can be written as

$$\Pr\left(h_{x*,0} > \frac{(I_{\text{DL},k} + \epsilon_* Q_k + \sigma_k^2)r^{\alpha_k}(\exp(z) - 1)}{P_k G_k}\right)$$

$$= \exp\left(\frac{-(\exp(z) - 1)r^{\alpha_k}}{P_k G_k}(\epsilon_* Q_k + \sigma_k^2)\right)$$

$$\times \mathbb{E}_{I_{DL,k}}\left[\exp\left(\frac{-(\exp(z) - 1)r^{\alpha_k}}{P_k G_k} I_{DL,k}\right)\right], \qquad\qquad \text{(A II-8)}$$

$$\overset{(i)}{=} \exp\left(\frac{-(\exp(z) - 1)r^{\alpha_k}}{P_k G_k}(\epsilon_* Q_k + \sigma_k^2)\right)$$

$$\times \mathcal{L}_{I_{DL,k}}\left(\frac{(\exp(z) - 1)r^{\alpha_k}}{P_k G_k}\right),$$

where (i) follows from the fact that $\mathcal{L}_Z(s) \triangleq \mathbb{E}(\exp(-sZ))$ for $s > 0$ is the Laplace transform of a non-negative random variable Z. Moreover $\mathcal{L}_{I_{DL,k}}\left(\frac{(\exp(z)-1)r^{\alpha_k}}{P_k G_k}\right)$ can be written as follows

$$\mathcal{L}_{I_{DL,k}}\left(\frac{(\exp(z) - 1)r^{\alpha_k}}{P_k G_k}\right)$$

$$\overset{(j)}{=} \mathbb{E}\left[\frac{-(\exp(z) - 1)r^{\alpha_k}}{P_k G_k}I_{x,k}^{DL}\right]\mathbb{E}\left[\frac{-(\exp(z) - 1)r^{\alpha_k}}{P_k G_k}I_{u,k}^{DL}\right], \qquad \text{(A II-9)}$$

where (j) follows from the fact that the total downlink interference is the summation over two independent Poisson point processes. In addition, following (A II-4), the two expectations over the interference point processes in (A II-9) can be formulated as

$$\mathbb{E}\left[\frac{-(\exp(z) - 1)r^{\alpha_k}}{P_k G_k}I_{x,k}^{DL}\right]$$

$$= \exp\left(-2\pi\lambda_k \frac{r^{2-\alpha_k}}{(\alpha_k - 2)}\frac{(\exp(z) - 1)r^{\alpha_k}P_k}{P_k G_k}\right.$$

$$\left. {}_2F_1\left[1, 1 - \frac{2}{\alpha_k}, 2 - \frac{2}{\alpha_k}; \frac{-(\exp(z) - 1)P_k}{P_k G_k}\right]\right),$$

$$\mathbb{E}\left[\frac{-(\exp(z) - 1)r^{\alpha_k}}{P_k G_k}I_{u,k}^{DL}\right] \qquad \text{(A II-10)}$$

$$= \exp\left(-2\pi\lambda_{I_{u,FD},k} \frac{r^{2-\alpha_k}}{(\alpha_k - 2)}\frac{(\exp(z) - 1)r^{\alpha_k}Q_k}{P_k G_k}\right.$$

$$\left. {}_2F_1\left[1, 1 - \frac{2}{\alpha_k}, 2 - \frac{2}{\alpha_k}; \frac{-(\exp(z) - 1)Q_k}{P_k G_k}\right]\right).$$

This concludes the proof.

# APPENDIX III

## APPENDIX OF CHAPTER 4

### 1.   Proof of Lemma 4.1

Lemma 4.1 follows from (4.8).  The addition of $\phi_k(n_f) = (K(k-1) + c_k)x_{c,n_f}$ inside the exponential function works as a PC factor which compensates for the possible BS. Here, $c_k$ represents the index of antenna element which drives the subsequent layer of phase shifters within its antenna group of size $K$. Since each PC factor is driven by its own group of a bank of filters and phase shifters, we divide the summation over all antenna elements $\sum\limits_{n=1}^{N}$ into step by step summation over each antenna group of size $K$.

### 2.   Proof of Theorem 4.1

The proof of Theorem 4.1 uses the following identity of sum of complex exponential functions

$$\sum_{n=0}^{N-1} \exp j(nx) = \frac{\sin(\frac{1}{2}Nx)}{\sin(\frac{1}{2}x)} \cdot \exp j(x\frac{N-1}{2}). \qquad \text{(A III-1)}$$

In (4.10) lets first denote $m = n - (Kk - K)$, this change of variable changes the limits of the inner summation of (4.10) into the simple $\sum\limits_{m=1}^{K}$ which can be solved in closed form using (A III-1).  Second, lets approximate $c_k$ to a linear function $(k-1)b$, here $b$ is an integer bounded by the antenna group size $K$. Now, similar to the inner summation, the outer summation is solved using (A III-1). This concludes the proof.

# AUTHOR'S PUBLICATIONS

During the course of his Ph.D. research, the author contributed to the following published and submitted research articles.

Dawa, M., Kaddoum, G. & Sattar, Z. (2017). A generalized lower bound on the Bit-Error-Rate of DCSK Systems over multi-path rayleigh fading channels. *IEEE Transactions on Circuits and Systems II: Express Briefs*, 65(3), 321–325.

Evangelista, J. V. C., Sattar, Z., Kaddoum, G. & Chaaban, A. (2019). Fairness and Sum-Rate Maximization via Joint Subcarrier and Power Allocation in Uplink SCMA Transmission. *IEEE Transactions on Wireless Communications*, 18(12), 5855–5867. doi: 10.1109/TWC.2019.2939820.

Evangelista, J. V., Sattar, Z. & Kaddoum, G. (2019). Analysis of Contention-Based SCMA in mMTC Networks. *2019 IEEE Latin-American Conference on Communications (LATINCOM)*, pp. 1–6.

Sattar, Z., Evangelista, J. V. C., Kaddoum, G. & Batani, N. (2019a). Spectral Efficiency Analysis of the Decoupled Access for Downlink and Uplink in Two-Tier Network. *IEEE Transactions on Vehicular Technology*, 68(5), 4871-4883. doi: 10.1109/TVT.2019.2905785.

Sattar, Z., Evangelista, J. V. C., Kaddoum, G. & Batani, N. (2019b). Antenna Array Gain and Capacity improvements of Ultra-Wideband Millimeter Wave Systems using a Novel Analog Architecture Design. *IEEE Wireless Communications Letters*, 9(3), 289–293. doi: 10.1109/LWC.2019.2952862.

Sattar, Z., Evangelista, J. V. C., Kaddoum, G. & Batani, N. (2021). Antenna Array Gain and Capacity improvements in a Hypersurface assisted Controlled Environment. *submitted to IEEE ICC*.

Sattar, Z., de Carvalho Evangelista, J. V., Kaddoum, G. & Batani, N. (2017). Analysis of the cell association for decoupled wireless access in a two tier network. *Proceedings of IEEE International Symposium on Personal, Indoor and Mobile Radio Communications (PIMRC)*.

Sattar, Z., Evangelista, J. V. D. C., Kaddoum, G. & Batani, N. (2020). Full-Duplex Two-Tier Heterogeneous Network With Decoupled Access: Cell Association, Coverage, and Spectral Efficiency Analysis. *IEEE Access*, 8, 172982–172995.

# BIBLIOGRAPHY

3GPP TR 36.942. (2009). *LTE; Evolved Universal Terrestrial Radio Access (E-UTRA); Radio Frequency (RF) system scenarios*.

Adhikari, P. (2008). Understanding millimeter wave wireless communication. *Loea Corporation*.

Akdeniz, M. R., Liu, Y., Samimi, M. K., Sun, S., Rangan, S., Rappaport, T. S. & Erkip, E. (2014). Millimeter wave channel modeling and cellular capacity evaluation. *IEEE J. Sel. Areas Commun.*, 32(6), 1164–1179.

Alsenwi, M., Tran, N. H., Bennis, M., Kumar Bairagi, A. & Hong, C. S. (2019). eMBB-URLLC Resource Slicing: A Risk-Sensitive Approach. *IEEE Commun. Lett.*, 23(4), 740-743. doi: 10.1109/LCOMM.2019.2900044.

Andrews, J. G. (2013). Seven ways that HetNets are a cellular paradigm shift. *IEEE Commun. Mag.*, 51(3), 136–144.

Andrews, J. G., Baccelli, F. & Ganti, R. K. (2011). A tractable approach to coverage and rate in cellular networks. *IEEE Trans. Commun.*, 59(11), 3122–3134.

Andrews, J. G., Claussen, H., Dohler, M., Rangan, S. & Reed, M. C. (2012). Femtocells: Past, present, and future. *IEEE J. Sel. Areas Commun.*, 30(3), 497–508.

Andrews, J. G., Buzzi, S., Choi, W., Hanly, S. V., Lozano, A., Soong, A. C. & Zhang, J. C. (2014). What will 5G be? *IEEE J. Sel. Areas Commun.*, 32(6), 1065–1082.

Andrews, J. G., Bai, T., Kulkarni, M. N., Alkhateeb, A., Gupta, A. K. & Heath, R. W. (2017). Modeling and analyzing millimeter wave cellular systems. *IEEE Trans. Commun.*, 65(1), 403–430.

Ansari, I. S., Yilmaz, F. & Alouini, M.-S. (2013). On the Sum of Squared eta-$\mu$ Random Variates with Application to the Performance of Wireless Communication Systems. *Proc. IEEE 77th Vehicular Technology Conference (VTC Spring)*, pp. 1–6.

Aravanis, A., Pascual-Iserte, A. & Munoz-Medina, O. (2018). Closed-Form Capacity Bounds for Downlink and Uplink Decoupling. *Proc.22nd International ITG Workshop on Smart Antennas*, pp. 1–5.

Bai, T., Vaze, R. & Heath, R. W. (2014). Analysis of blockage effects on urban cellular networks. 13(9), 5070–5083.

Balanis, C. A. (2016). *Antenna theory: analysis and design*. John wiley & sons.

Bethanabhotla, D., Bursalioglu, O. Y., Papadopoulos, H. C. & Caire, G. (2016). Optimal User-Cell Association for Massive MIMO Wireless Networks. 15(3), 1835-1850. doi: 10.1109/TWC.2015.2496942.

Boccardi, F., Heath, R. W., Lozano, A., Marzetta, T. L. & Popovski, P. (2014). Five disruptive technology directions for 5G. *IEEE Commun. Mag.*, 52(2), 74–80.

Boccardi, F., Andrews, J., Elshaer, H., Dohler, M., Parkvall, S., Popovski, P. & Singh, S. (2016). Why to decouple the uplink and downlink in cellular networks and how to do it. *IEEE Commun. Mag.*, 54(3), 110–117.

Buzzi, S. & D'Andrea, C. (2016). Doubly massive mmWave MIMO systems: Using very large antenna arrays at both transmitter and receiver. *Proc. IEEE Global Commun. Conf. (GLOBECOM)*, pp. 1–6.

Błaszczyszyn, B., Karray, M. K. & Keeler, H. P. (2013, April). Using Poisson processes to model lattice cellular networks. *Proc. IEEE INFOCOM*, pp. 773-781.

Cai, M. (2018). *Modeling and mitigating beam squint in millimeter wave wireless communication*. (Ph.D. thesis, University of Notre Dame).

Chandrasekhar, V., Kountouris, M. & Andrews, J. G. (2009). Coverage in multi-antenna two-tier networks. *IEEE Trans. Wireless Commun.*, 8(10).

Chavarria-Reyes, E., Akyildiz, I. F. & Fadel, E. (2015). Energy Consumption Analysis and Minimization in Multi-Layer Heterogeneous Wireless Systems. *IEEE Trans. Mobile Comput.*, 14(12), 2474-2487. doi: 10.1109/TMC.2015.2393352.

Chiu, S. N., Stoyan, D., Kendall, W. S. & Mecke, J. (2013). *Stochastic geometry and its applications*. John Wiley & Sons.

Colombi, D., Thors, B. & Törnevik, C. Implications of EMF exposure limits on output power levels for 5G devices above 6 GHz. *IEEE Antennas Wireless Propag. Lett.*, 14, 1247–1249.

Cover, T. M. & Thomas, J. A. (2012). *Elements of information theory*. John Wiley & Sons.

Dardari, D. & Massari, D. (2020). Using MetaPrisms for Performance Improvement in Wireless Communications. *arXiv preprint arXiv:2003.13505*.

Dhillon, H. S., Ganti, R. K., Baccelli, F. & Andrews, J. G. (2012). Modeling and analysis of K-tier downlink heterogeneous cellular networks. *IEEE J. Sel. Areas Commun.*, 30(3), 550–560.

Di Renzo, M. (2015). Stochastic geometry modeling and analysis of multi-tier millimeter wave cellular networks. *IEEE Trans. Wireless Commun.*, 14(9), 5038–5057.

Ding, M., López-Pérez, D., Mao, G., Wang, P. & Lin, Z. (2015). Will the area spectral efficiency monotonically grow as small cells go dense? *Proc. IEEE Global Commun. Conf. (GLOBECOM)*, pp. 1–7.

El Ayach, O., Rajagopal, S., Abu-Surra, S., Pi, Z. & Heath, R. W. (2014). Spatially sparse precoding in millimeter wave MIMO systems. *IEEE Trans. Wireless Commun.*, 13(3), 1499–1513.

Elshaer, H., Boccardi, F., Dohler, M. & Irmer, R. (2014). Downlink and uplink decoupling: A disruptive architectural design for 5G networks. *Proc. IEEE Global Commun. Conf. (GLOBECOM)*, pp. 1798–1803.

Elshaer, H., Kulkarni, M. N., Boccardi, F., Andrews, J. G. & Dohler, M. (2016). Downlink and uplink cell association with traditional macrocells and millimeter wave small cells. *IEEE Trans. Wireless Commun.*, 15(9), 6244–6258.

Everett, E., Sahai, A. & Sabharwal, A. (2014). Passive self-interference suppression for full-duplex infrastructure nodes. *IEEE Trans. Wireless Commun.*, 13(2), 680–694.

Ferrand, P., Amara, M., Valentin, S. & Guillaud, M. (2016). Trends and challenges in wireless channel modeling for evolving radio access. *IEEE Commun. Mag.*, 54(7), 93–99.

Fourikis, N. & Fourikis, N. (2000). *Advanced array systems, applications and RF technologies*. Academic Press.

Fox, C. (1961). The G and H functions as symmetrical Fourier kernels. *Transactions of the American Mathematical Society*, 98(3), 395–429.

Gao, X., Dai, L., Han, S., Chih-Lin, I. & Heath, R. W. (2016). Energy-efficient hybrid analog and digital precoding for mmWave MIMO systems with large antenna arrays. *IEEE J. Sel. Areas Commun.*, 34(4), 998–1009.

Gapeyenko, M., Samuylov, A., Gerasimenko, M., Moltchanov, D., Singh, S., Aryafar, E., Yeh, S.-p., Himayat, N., Andreev, S. & Koucheryavy, Y. (2016). Analysis of human-body blockage in urban millimeter-wave cellular communications. *Proc. IEEE International Conference on Communications (ICC)*, pp. 1–7.

Ge, X., Yang, B., Ye, J., Mao, G., Wang, C.-X. & Han, T. (2015). Spatial spectrum and energy efficiency of random cellular networks. *IEEE Transactions on Communications*, 63(3), 1019–1030.

Ge, X., Tu, S., Mao, G., Wang, C.-X. & Han, T. (2016). 5G ultra-dense cellular networks. *IEEE Wireless Communications*, 23(1), 72–79.

Ghosh, A. (2016). The 5G mmWave Radio Revolution. *Microwave J.*, 59(9).

Glybovski, S. B., Tretyakov, S. A., Belov, P. A., Kivshar, Y. S. & Simovski, C. R. (2016). Metasurfaces: From microwaves to visible. *Physics reports*, 634, 1–72.

Goyal, S., Liu, P., Panwar, S., Yang, R., DiFazio, R. A. & Bala, E. (2014). Full duplex operation for small cells. *arXiv preprint arXiv:1412.8708*.

Gradshteyn, I. S. & Ryzhik, I. M. (2014). *Table of integrals, series, and products*. Academic press.

Han, S., Chih-Lin, I., Xu, Z. & Rowell, C. (2015). Large-scale antenna systems with hybrid analog and digital beamforming for millimeter wave 5G. *IEEE Commun. Mag.*, 53(1), 186–194.

Haneda, K., Zhang, J., Tan, L., Liu, G., Zheng, Y., Asplund, H., Li, J., Wang, Y., Steer, D., Li, C. et al. (2016). 5G 3GPP-like channel models for outdoor urban microcellular and macrocellular environments. *Proc. IEEE Vehicular Tech. Conf. (VTC Spring)*, pp. 1–7.

Heath, R. W., Gonzalez-Prelcic, N., Rangan, S., Roh, W. & Sayeed, A. M. (2016). An overview of signal processing techniques for millimeter wave MIMO systems. *IEEE J. Sel. Topics Signal Process.*, 10(3), 436–453.

Hong, S., Brand, J., Choi, J. I., Jain, M., Mehlman, J., Katti, S. & Levis, P. (2014). Applications of self-interference cancellation in 5G and beyond. *IEEE Commun. Mag.*, 52(2), 114–121.

Hoydis, J., Ten Brink, S. & Debbah, M. (2013). Massive MIMO in the UL/DL of cellular networks: How many antennas do we need? *IEEE J. Sel. Areas Commun.*, 31(2), 160–171.

Hu, R. Q. & Qian, Y. (2014). An energy efficient and spectrum efficient wireless heterogeneous network framework for 5G systems. *IEEE Commun. Mag.*, 52(5), 94-101. doi: 10.1109/M-COM.2014.6815898.

Intelligence, G. (2014). Understanding 5G: Perspectives on future technological advancements in mobile. *White paper*, 1–26.

Jeong, Y., Shin, H. & Win, M. Z. (2015). H-Transforms for Wireless Communication. *IEEE Trans. Inf. Theory*, 61(7), 3773-3809. doi: 10.1109/TIT.2015.2433264.

Jo, H.-S., Sang, Y. J., Xia, P. & Andrews, J. G. (2012). Heterogeneous cellular networks with flexible cell association: A comprehensive downlink SINR analysis. *IEEE Trans. Wireless Commun.*, 11(10), 3484–3495.

Kamel, M., Hamouda, W. & Youssef, A. (2016). Ultra-Dense Networks: A Survey. *IEEE Commun. Surveys Tuts.*, 18(4), 2522-2545. doi: 10.1109/COMST.2016.2571730.

Kilbas, A. A. (2004). *H-transforms: Theory and Applications*. CRC Press.

Kim, J. & Lee, I. (2015). 802.11 WLAN: history and new enabling MIMO techniques for next generation standards. *IEEE Commun. Mag.*, 53(3), 134–140.

Kong, L., Kaddoum, G. & da Costa, D. B. (2018a). Cascaded $\alpha - \mu$ ; Fading Channels: Reliability and Security Analysis. *IEEE Access*, early access. doi: 10.1109/ACCESS.2018.2833423.

Kong, L., Kaddoum, G. & Vuppala, S. (2018b, May). On Secrecy Analysis for D2D Networks over $\alpha - \mu$ Fading Channels with Randomly Distributed Eavesdroppers. *Proc. IEEE ICC Workshop 5G-Security*. doi: 10.1109/VTCFall.2016.7881216.

Kong, L. (2019). *Wireless networks physical layer security: modeling and performance characterization*. (Ph.D. thesis, École de technologie supérieure).

Kulkarni, M. N., Singh, S. & Andrews, J. G. (2014). Coverage and rate trends in dense urban mmWave cellular networks. *Proc. Global Communications Conference (GLOBECOM)*, pp. 3809–3814.

Li, G., Zhao, H. & Hui, H. (2018a). Beam squint compensation for hybrid precoding in millimetre-wave communication systems. *Electronics Letters*, 54(14), 905–907.

Li, R., Luo, K., Jiang, T. & Jin, S. (2018b). Uplink Spectral Efficiency Analysis of Decoupled Access in Multiuser MIMO HetNets. *IEEE Trans. Veh. Technol.*, 67(5), 4289–4302.

Liao, W. C., Hong, M. & Luo, Z. Q. (2014, May). Max-min network flow and resource allocation for backhaul constrained heterogeneous wireless networks. *2014 IEEE Int. Conf. on Acoustics, Speech and Signal Processing (ICASSP)*, pp. 845-849. doi: 10.1109/ICASSP.2014.6853716.

Liaskos, C., Nie, S., Tsioliaridou, A., Pitsillides, A., Ioannidis, S. & Akyildiz, I. (2018). A New Wireless Communication Paradigm through Software-Controlled Metasurfaces. *IEEE Commun. Mag.*, 56(9), 162-169.

Liaskos, C., Tsioliaridou, A., Pitsillides, A., Akyildiz, I. F., Kantartzis, N. V., Lalas, A. X., Dimitropoulos, X., Ioannidis, S., Kafesaki, M. & Soukoulis, C. (2015). Design and development of software defined metamaterials for nanonetworks. *IEEE Circuits Syst. Mag.*, 15(4), 12–25.

Liaskos, C., Tsioliaridou, A., Pitsillides, A., Ioannidis, S. & Akyildiz, I. (2018). Using any surface to realize a new paradigm for wireless communications. *Communications of the ACM*, 61(11), 30–33.

Liu, B. & Zhu, H. (2018). Rotman lens-based two-tier hybrid beamforming for wideband mmWave MIMO-OFDM system with beam squint. *EURASIP Journal on Wireless Communications and Networking*, 2018(1), 267.

Liu, C.-H. & Hu, H.-M. (2018). Full-Duplex Heterogeneous Networks with Decoupled User Association: Rate Analysis and Traffic Scheduling. *IEEE Trans. Commun.*, 67(3), 2084–2100.

Liu, D., Chen, Y., Chai, K. K. & Zhang, T. (2014a, May). Joint Uplink and Downlink User Association for Energy-Efficient HetNets Using Nash Bargaining Solution. *2014 IEEE 79th Vehicular Technology Conf.*, pp. 1-5. doi: 10.1109/VTCSpring.2014.7022970.

Liu, D., Chen, Y., Chai, K. K. & Zhang, T. (2014b, Jan.). Nash bargaining solution based user association optimization in HetNets. *2014 IEEE 11th Consumer Communications and Networking Conf. (CCNC)*, pp. 587-592. doi: 10.1109/CCNC.2014.6866631.

Liu, D., Chen, Y., Chai, K. K., Zhang, T. & Elkashlan, M. (2014c). Opportunistic User Association for Multi-Service HetNets Using Nash Bargaining Solution. *IEEE Commun. Lett.*, 18(3), 463-466. doi: 10.1109/LCOMM.2014.012314.140090.

Liu, D., Wang, L., Chen, Y., Elkashlan, M., Wong, K. K., Schober, R. & Hanzo, L. (2016). User Association in 5G Networks: A Survey and an Outlook. *IEEE Commun. Surveys Tuts.*, 18(2), 1018-1044.

Liu, J., Sheng, M. & Li, J. (2018). Improving Network Capacity Scaling Law in Ultra-Dense Small Cell Networks. *IEEE Trans. Wireless Commun.*, 17(9), 6218-6230. doi: 10.1109/TWC.2018.2856766.

Liu, X. & Qiao, D. (2019). Space-Time Block Coding-Based Beamforming for Beam Squint Compensation. *IEEE Wireless Commun. Lett.*, 8(1), 241–244.

López-Pérez, D., Ding, M., Claussen, H. & Jafari, A. H. (2015). Towards 1 Gbps/UE in cellular systems: Understanding ultra-dense small cell deployments. *IEEE Commun. Surveys Tuts.*, 17(4), 2078–2101.

Mahmood, N. H., Berardinelli, G., Tavares, F. M. & Mogensen, P. (2015). On the potential of full duplex communication in 5G small cell networks. *Proc. 2015 IEEE 81st Vehicular Technology Conference (VTC Spring)*, pp. 1–5.

Mailloux, R. J. (2017). *Phased array antenna handbook*. Artech house.

Mathai, A. M. & Saxena, R. K. (1978). The H function with applications in statistics and other disciplines.

Mathai, A. M., Saxena, R. K. & Haubold, H. J. (2009). *The H-function: theory and applications*. Springer Science & Business Media.

Méndez-Rial, R., Rusu, C., Alkhateeb, A., González-Prelcic, N. & Heath, R. W. (2015). Channel estimation and hybrid combining for mmWave: Phase shifters or switches? *Proc. Information Theory and Applications Workshop (ITA)*, pp. 90–97.

Méndez-Rial, R., Rusu, C., González-Prelcic, N., Alkhateeb, A. & Heath, R. W. (2016). Hybrid MIMO architectures for millimeter wave communications: Phase shifters or switches? *IEEE Access*, 4, 247–267.

Mittal, P. & Gupta, K. (1972). An integral involving generalized function of two variables. *Proceedings of the Indian academy of sciences-section A*, 75(3), 117–123.

Ogden, C. L., Fryar, C. D., Carroll, M. D. & Flegal, K. M. (2004). *Mean body weight, height, and body mass index: United States 1960-2002*. Department of Health and Human Services, Centers for Disease Control and Prevention, National Center for Health Statistics Washington, DC.

Olver, F. W., Lozier, D. W., Boisvert, R. F. & Clark, C. W. (2010). *NIST handbook of mathematical functions hardback and CD-ROM*. Cambridge university press.

Paramesh, J., Bishop, R., Soumyanath, K. & Allstot, D. J. (2005). A four-antenna receiver in 90-nm CMOS for beamforming and spatial diversity. *IEEE J. Solid-State Circuits*, 40(12), 2515–2524.

Peppas, K. P. (2012). A new formula for the average bit error probability of dual-hop amplify-and-forward relaying systems over generalized shadowed fading channels. 1(2), 85–88.

Peppas, K. P., Lazarakis, F., Alexandridis, A. & Dangakis, K. (2012). Simple, accurate formula for the average bit error probability of multiple-input multiple-output free-space optical links over negative exponential turbulence channels. *Optics letters*, 37(15), 3243–3245.

Pi, Z. & Khan, F. (2011). An introduction to millimeter-wave mobile broadband systems. *IEEE Commun. Mag.*, 49(6).

Rangan, S., Rappaport, T. S. & Erkip, E. (2014). Millimeter-wave cellular wireless networks: Potentials and challenges. *Proceedings of the IEEE*, 102(3), 366–385.

Rappaport, T. S., Sun, S., Mayzus, R., Zhao, H., Azar, Y., Wang, K., Wong, G. N., Schulz, J. K., Samimi, M. & Gutierrez, F. (2013). Millimeter wave mobile communications for 5G cellular: It will work! *IEEE access*, 1, 335–349.

Riihonen, T., Werner, S. & Wichman, R. (2011). Hybrid full-duplex/half-duplex relaying with transmit power adaptation. *IEEE Trans. Wireless Commun.*, 10(9), 3074–3085.

Roberts, I. P., Jain, H. B. & Vishwanath, S. (2020). Equipping Millimeter-Wave Full-Duplex with Analog Self-Interference Cancellation. *arXiv preprint arXiv:2002.02127*.

Rusek, F., Persson, D., Lau, B. K., Larsson, E. G., Marzetta, T. L., Edfors, O. & Tufvesson, F. (2013). Scaling up MIMO: Opportunities and challenges with very large arrays. *IEEE Signal*

*Process. Mag.*, 30(1), 40–60.

Sabharwal, A., Schniter, P., Guo, D., Bliss, D. W., Rangarajan, S. & Wichman, R. (2014). In-band full-duplex wireless: Challenges and opportunities. *IEEE J. Sel. Areas Commun.*, 32(9), 1637–1652.

Saha, C. & Dhillon, H. S. (2019). Millimeter Wave Integrated Access and Backhaul in 5G: Performance Analysis and Design Insights. *IEEE J. Sel. Areas Commun.*

Sattar, Z., Evangelista, J. V., Kaddoum, G. & Batani, N. (2017). Analysis of the cell association for decoupled wireless access in a two tier network. *Proc. IEEE 28th annual international symposium on personal, indoor, and mobile radio communications (PIMRC)*, pp. 1–6.

Sattar, Z., Evangelista, J. V., Kaddoum, G. & Batani, N. (2019). Spectral efficiency analysis of the decoupled access for downlink and uplink in two-tier network. *IEEE Trans. Veh. Technol.*, 68(5), 4871–4883.

Sattar, Z., Evangelista, J. V., Kaddoum, G. & Batani, N. (2020). Antenna Array Gain and Capacity improvements of Ultra-Wideband Millimeter Wave Systems using a Novel Analog Architecture Design. *IEEE Wireless Commun. Lett.*, 9(3), 289-293.

Sekander, S., Tabassum, H. & Hossain, E. (2016). Decoupled uplink-downlink user association in multi-tier full-duplex cellular networks: A two-sided matching game. *IEEE Trans. Mobile Comput.*, 16(10), 2778–2791.

Shi, M., Yang, K., Xing, C. & Fan, R. (2018). Decoupled Heterogeneous Networks With Millimeter Wave Small Cells. *IEEE Trans. Wireless Commun.*, 17(9), 5871–5884.

Shokri-Ghadikolaei, H. & Fischione, C. (2016). The transitional behavior of interference in millimeter wave networks and its impact on medium access control. *IEEE Trans. Commun.*, 64(2), 723–740.

Singh, S., Dhillon, H. S. & Andrews, J. G. (2013). Offloading in heterogeneous networks: Modeling, analysis, and design insights. 12(5), 2484–2497.

Singh, S., Kulkarni, M. N., Ghosh, A. & Andrews, J. G. (2015). Tractable model for rate in self-backhauled millimeter wave cellular networks. *IEEE J. Sel. Areas Commun.*, 33(10), 2196–2211.

Singh, S., Mudumbai, R. & Madhow, U. (2011). Interference analysis for highly directional 60-GHz mesh networks: The case for rethinking medium access control. *IEEE/ACM Trans. Netw.*, 19(5), 1513–1527.

Smiljkovikj, K., Gavrilovska, L. & Popovski, P. (2015a). Efficiency analysis of downlink and uplink decoupling in heterogeneous networks. *Proc. IEEE International Conf. on Commun.*

*Workshop (ICCW)*, pp. 125–130.

Smiljkovikj, K., Popovski, P. & Gavrilovska, L. (2015b). Analysis of the decoupled access for downlink and uplink in wireless heterogeneous networks. *IEEE Wireless Commun. Lett.*, 4(2), 173–176.

Su, L., Yang, C., Xu, Z. & Molisch, A. F. (2013, May). Energy-efficient downlink transmission with base station closing in small cell networks. *2013 IEEE Int. Conf. on Acoustics, Speech and Signal Processing*, pp. 4784-4788.

Sudarshan, P., Mehta, N. B., Molisch, A. F. & Zhang, J. (2006). Channel statistics-based RF pre-processing with antenna selection. *IEEE Trans. Wireless Commun.*, 5(12).

Tayebi, A., Tang, J., Paladhi, P. R., Udpa, L., Udpa, S. S. & Rothwell, E. J. (2015). Dynamic beam shaping using a dual-band electronically tunable reflectarray antenna. *IEEE Trans. Antennas Propag.*, 63(10), 4534–4539.

Tong, Z. & Haenggi, M. (2015). Throughput analysis for wireless networks with full-duplex radios. *Proc. 2015 IEEE Wireless Communications and Networking Conference (WCNC)*, pp. 717–722.

Tse, D. & Viswanath, P. (2005). *Fundamentals of wireless communication*. Cambridge university press.

Vashist, S., Soni, M. & Singhal, P. (2014). A review on the development of Rotman lens antenna. *Chinese Journal of Engineering*, 2014, 1-9.

Venkateswaran, V. & van der Veen, A.-J. (2010). Analog beamforming in MIMO communications with phase shift networks and online channel estimation. *IEEE Trans. Signal Process.*, 58(8), 4131–4143.

Vu, T. K., Liu, C., Bennis, M., Debbah, M., Latva-aho, M. & Hong, C. S. (2017). Ultra-Reliable and Low Latency Communication in mmWave-Enabled Massive MIMO Networks. *IEEE Commun. Lett.*, 21(9), 2041-2044. doi: 10.1109/LCOMM.2017.2705148.

Wang, B., Gao, F., Jin, S., Lin, H. & Li, G. Y. (2018a). Spatial-and frequency-wideband effects in millimeter-wave massive MIMO systems. *IEEE Trans. Signal Process.*, 66(13), 3393–3406.

Wang, B., Gao, F., Jin, S., Lin, H., Li, G. Y., Sun, S. & Rappaport, T. S. (2018b). Spatial-wideband effect in massive MIMO with application in mmWave systems. *IEEE Commun. Mag.*, (99), 1–8.

Xiao, M., Mumtaz, S., Huang, Y., Dai, L., Li, Y., Matthaiou, M., Karagiannidis, G. K., Björnson, E., Yang, K., Chih-Lin, I. et al. (2017). Millimeter wave communications for future mobile networks. *IEEE J. Sel. Areas Commun.*, 35(9), 1909–1935.

Xie, X. & Zhang, X. (2014). Does full-duplex double the capacity of wireless networks? *Proc. INFOCOM 2014-IEEE Conference on Computer Communications*, pp. 253–261.

Xie, Z., Liu, J., Sheng, M., Zhang, Y. & Li, J. (2019, May). Effect of Interference Correlation on the Performance of Ultra-Dense Networks. *IEEE International Conference on Communications (ICC)*, pp. 1-7. doi: 10.1109/ICC.2019.8761808.

Yang, B., Mao, G., Ding, M., Ge, X. & Tao, X. (2018). Dense Small Cell Networks: From Noise-Limited to Dense Interference-Limited. *IEEE Trans. Veh. Technol.*, 67(5), 4262–4277.

Yilmaz, F. & Alouini, M.-S. (2009). Product of the powers of generalized Nakagami-m variates and performance of cascaded fading channels. *Proc. IEEE Global telecommunications conference (GLOBECOM)*, pp. 1–8.

Zhang, L., Nie, W., Feng, G., Zheng, F.-C. & Qin, S. (2017). Uplink Performance Improvement by Decoupling Uplink/Downlink Access in HetNets. *IEEE Trans. Veh. Technol.*, 66(8), 6862–6876.

Zhang, X., Molisch, A. F. & Kung, S.-Y. (2005). Variable-phase-shift-based RF-baseband codesign for MIMO antenna selection. *IEEE Trans. Signal Process.*, 53(11), 4091–4103.

Zhu, H., Wang, S. & Chen, D. (2012, Dec.). Energy-efficient user association for heterogenous cloud cellular networks. *2012 IEEE Globecom Workshops*, pp. 273-278. doi: 10.1109/GLO-COMW.2012.6477582.